Environmentally induced development of pulmonary monocyte-derived alveolar macrophages is controlled by Apolipoprotein E and Dectin-1

Dissertation

zur

Erlangung des Doktorgrades (Dr. rer. nat.)

der

Mathematisch-Naturwissenschaftlichen Fakultät

der

Rheinischen Friedrich-Wilhelms-Universität Bonn

vorgelegt von

Hannah Theobald

aus

Saarlouis

Bonn, Juni 2024

Angefertigt mit Genehmigung der Mathematisch-Naturwissenschaftlichen Fakultät
der Rheinischen Friedrich-Wilhelms-Universität Bonn

Gutachter/Betreuer: Prof. Dr. Andreas Schlitzer
Gutachter: PD Dr. Marc Beyer

Tag der Promotion: 29.01.2025
Erscheinungsjahr: 2025

Contents

Preliminary remarks

I hereby declare that I wrote the present dissertation using only the sources indicated in the text and with no assistance of third parties. The text of this thesis is in parts expressed as first-person plural form according to common practices in English scientific writing. All experiments in this study have been designed and performed by myself, with contributions to the shown data from the following people or institutions:

- Single-cell RNA sequencing experiment was performed in collaboration with the Schultze and Beyer lab and PRECISE (DZNE, Bonn), data analysis performed by Dr. Jiangyan Yu
- *Legionella* infection experiments were performed in collaboration with Dr. Federica Piattini of the Kopf lab (ETH Zurich, Switzerland)
- Broncho-alveolar lung organoid experiments were perfomed in collaboration with Anna-Lena Ament of the Vazquez-Armendariz lab (LIMES Institute, Bonn)
- Histological stainings were performed by Dr. David Bejarano
- *In vitro* phagocytosis experiments were conducted by Hannah Hayer under my supervision
- Other members of the Schlitzer lab, especially Dr. Jessica Haub and Dr. David Bejarano, contributed to the sample preparation and data acquisition of mouse experiments

Part of this work has been published in:
Theobald H. *et al.* (2024): Apolipoprotein E controls Dectin-1-dependent development of monocyte-derived alveolar macrophages upon pulmonary β-glucan-induced inflammatory adaptation. *Nature Immunology* 25, 994–1006. https://doi.org/10.1038/s41590-024-01830-z

Summary

The lung is one of the largest barrier tissues of our body, and is constantly exposed to the environment. By inhaling, the lungs do not only take up oxygen, which is crucial for cellular respiration, but also a plethora of pathogens and particulate matter from ambient air. Adaptation of pulmonary mononuclear phagocytes to these inhaled external stressors ensures the host's fitness by increased pathogen clearance and tissue resilience. However, how the pulmonary immune system integrates this exposure to the environment on a cellular and molecular level remains elusive. B-Glucan, a naturally occurring polysaccharide of fungal cell walls, is abundant in ambient air and has been linked to low-grade inflammation and innate immune training. In this thesis, we aim to investigate the effect of an acute or chronic β-glucan exposure on the murine pulmonary myeloid cell compartment and how this environmental adaptation is regulated on a cellular and molecular level. Single-cell transcriptomic and flow cytometric analyses revealed a CCR2-dependent recruitment of monocyte-derived $CD11b^+$ alveolar macrophages (AM) to the alveolar space up to 21 days after exposure. Furthermore, the β-glucan mediated recruitment of $CD11b^+$ AM to the alveolar space is dependent on the Dectin-1 – CARD9 signaling axis. $CD11b^+$ AM expressed high levels of genes previously linked to a lipid-associated inflammatory monocyte-derived macrophage signature, such as *Apoe*, *Cd63*, *Spp1*, *Gpnmb* and *Trem2*, and were therefore termed $ApoE^+CD11b^+$ AM. Upon *ex vivo* restimulation with Lipopolysaccharide (LPS), $ApoE^+CD11b^+$ AM secreted increased levels of interleukin-6 (IL-6) compared to *bona fide* AM. Transfer of $ApoE^+CD11b^+$ AM to naïve mice preserved the increased IL-6 secretion indicating that the functional rewiring is taking place on the macrophage level. Myeloid cell-specific ApoE ablation impeded $CD11b^+$ AM survival between day 3 to day 7 after β-glucan exposure by promoting excessive cholesterol accumulation. Further experiments showed a specific accumulation of cholesterol in the endoplasmic reticulum (ER) in ApoE-deficient $CD11b^+$ AM, thus inhibiting autocrine M-CSF secretion into the alveolar space and lastly promoting cell death. Functionally, the β-glucan mediated environmental adaptation increased the phagocytic capacity of AM and thereby reduced the bacterial burden in an acute *Legionella pneumophila* infection. Furthermore, the β-glucan mediated environmental adaptation ameliorated fibrosis severity in an organoid model *in vitro*. Repetitive exposure to β-glucan increased the cellular abundance of $ApoE^+CD11b^+$ AM compared to a single exposure without introducing major changes in other immune cell populations. Collectively, we provide evidence of a macrophage-centric tissue-specific adaptation mechanism improving host fitness and resilience via integration of low-grade inflammation eliciting environmental cues.

Abbreviations

Abbreviation	Name
AEC	Alveolar epithelial cell
AKT	Protein kinase B
AM	Alveolar macrophage
ANOVA	Analysis of variance
ApoE	Apolipoprotein E
BAL(F)	Broncho-alveolar lavage (fluid)
BALO	Broncho-alveolar lung organoid
BCL10	B cell lymphoma 10
Bhlh40	Basic helix-loop-helix family member E40
BM	Bone marrow
BODIPY	Boron-dipyrromethene
C1q	Complement component 1q
CARD9	Caspase recruitment domain-containing protein 9
CCR2	C-C chemokine receptor type 2
CD	Cluster of differentiation
cDC	Conventional dendritic cell
CFU	Colony forming unit
Clec7a	C-type lectin domain family 7 member A
cMOP	Common monocyte progenitor
CODEX	Co-detection by indexing
CR3	Complement receptor 3
CSF-1	Colony stimulating factor 1
CSF-1R	Colony stimulating factor 1 receptor
Cxcl12	C-X-C motif chemokine 12
DC	Dendritic cell
DNA	Deoxyribonucleic acid
EEA1	Early endosome antigen 1
Egr2	Early growth response protein 2
ELISA	Enzyme-linked immunosorbent assay
ER	Endoplasmic reticulum
ERK	Extracellular response kinase
FACS	Fluorescence-activated cell sorting
Fcna	Ficolin A
Folr2	Folate receptor 2
GM-CSF	Granulocyte-macrophage colony-stimulating factor
GMP	Granulocyte-monocyte progenitor
Gpnmb	Transmembrane glycoprotein NMB
HDL, LDL and VLDL	High-, low- and very low-density lipoproteins
hemITAM	Hemi-immunoreceptor tyrosine-based activation motif
HIF-1α	hypoxia inducible factor α
IL-6	Interleukin-6
IM	Interstitial macrophage
IRF5	Interferon regulatory factor 5
ISG	Interferon stimulated genes
Itgam	Integrin α M
Itgax	Integrin alpha X
ko	Knockout
LAMP1	Lysosomal-associated membrane protein 1
LDLR	Low-density lipoprotein receptor

Abbreviation	Name
LPS	Lipopolysaccharide
LRP1	Low-density lipoprotein receptor-related protein 1
Lxr	liver-X-receptor
Lyve-1	Lymphatic vessel endothelial hyaluronan receptor 1
MafB	Musculoaponeurotic fibrosarcoma oncogene homolog B
MALT1	Mucosa associated lymphoid tissue 1
Marco	Macrophage receptor with collagenous structure
MCP-1	Monocyte chemoattractant protein 1
M-CSF	Macrophage colony stimulating factor
MerTk	MER tyrosine kinase
MHC	Major histocompatibility complex
moAM	Monocyte-derived alveolar macrophage
Mrc1	Mannose receptor 1
mTOR	Mammalian target of rapamycin
NFAT	Nuclear factor of activated T cells
NF-κB	Nuclear factor kappa-light-chain-enhancer of activated B cells
NK cell	Natural killer cell
OCT	Optimal cutting temperature
PAMP	Pathogen-associated molecular patterns
PBS	Phosphate buffered saline
PI3K	Phosphoinositide 3 kinase
Plaur	Plasminogen activator, urokinase receptor
PLCγ2	Phosphatidylinositol-specific phospholipase Cγ2
pMac	Macrophage progenitor
PPARγ	Peroxisome proliferator-activated receptor γ
PRR	Pattern recognition receptor
Raf-1	V-raf-leukemia viral oncogene 1
RNA	Ribonucleic acid
ROS	Reactive oxygen species
S. aureus	*Staphylococcus aureus*
S. pneumoniae	*Streptococcus pneumoniae*
scRNA seq	Single-cell RNA sequencing
SD	Standard deviation
SiglecF	Sialic acid binding Ig-like lectin F
SMA	Smooth muscle actin
Spp1	Secreted phosphoprotein 1
SSC	Side scattered light
Syk	Spleen tyrosine kinase
TCR-β	T cell receptor beta chain
TGF-β	Transforming growth factor beta
Tim4	T-cell immunoglobulin and mucin domain containing 4
TLR	Toll-like receptor
TNF-α	Tumor necrosis factor α
trAM	Tissue-resident alveolar macrophage
Trem2	Triggering receptor expressed on myeloid cells 2
TUNEL	Terminal deoxynucleotidyl transferase dUTP nick end labeling
UMAP	Uniform manifold approximation and projection
us	Unstimulated
WT	Wildtype

I. Introduction

I.I. Lung: Function, architecture and immune cell composition

I.I.I. Function and architecture of the lung

The respiratory system consists of the upper and lower airways that ensure efficient filtering and uptake of air into the lungs. From the upper airways, the air flows into the trachea, which has a thick wall made of cartilage and smooth muscles, to conduct air down the bronchial tree of the lung. The bronchial tree splits up into two main branches and each of these branches can be further subdivided into lobes and lobules. Within these lobes, dichotomous branching of the airways from the bronchioles into the alveoli decreases the velocity of aspirated air and increases the surface for gas exchange (1). The delicate 0.3 µm thin interface of the alveoli consists of type I and II alveolar epithelial cells (AEC) (1, 2). Type I AEC make up for 95% of the lining of the respiratory zone, while type II AEC are less numerous, sit at the junctions of alveolar septa and produce surfactant. The alveolar epithelium acts as a closed barrier with tight junctions between epithelial cells to prevent leakage of molecules and pathogens. Close contact of the alveolar epithelium with the capillary endothelium of blood vessels ensures a rapid oxygen and carbon dioxide diffusion. “Leaky” junctions between the endothelial cells of the capillaries facilitate molecule exchange between the blood stream and the lung interstitium, the space between the alveolar epithelium and the capillary endothelium (1).

To ensure homeostasis during gas exchange, the lung has to overcome two challenges: defence against the environment and the mechanical stress on the tissue while being inflated (1). Uptake of oxygen from the environment renders the lung susceptible to pollutants and pathogens present in the $1x10^4$ litres of ambient air inhaled daily (2). The respiratory surface of the lung is covered in mucus and surfactant produced by goblet cells and type II AEC forming a mucociliary clearance system together with the ciliated epithelium to remove incoming pollutants and pathogens (1). Excessive production and the inability to clear mucus results in the loss of organ function and oxygen uptake (3). Additionally, regular inflation of the lung causes mechanical stress on the thin epithelium leading to constant need for tissue repair (1). Innate phagocytes like monocytes, macrophages and dendritic cells (DCs) are therefore an integral component of the pulmonary immune system to ensure efficient and rapid clearance of mucus, dead cells and pathogens to re-establish tissue homeostasis (2). This has to be tightly regulated and balanced as overshooting immune responses could damage the delicate alveolocapillary interface (2).

I.I.II. Immune cell composition of the lung

The antigen-rich environment of the lung shapes the composition of tissue-resident innate and adaptive immune cells (4). The innate myeloid compartment of pulmonary immune cells consists of macrophages, monocytes, granulocytes and DCs (5). At the air-exposed interface, alveolar macrophages (AM) form the first line of cellular defence constantly patrolling the luminal side of the alveoli and phagocytosing pathogens, mucus and dead cells (2, 6). Epithelial cells and AM rapidly secrete pro-inflammatory mediators like monocyte chemoattractant protein 1 (MCP-1) attracting neutrophils and monocytes for host defence during inflammation and infection (7, 8). Moreover, it has become evident that monocytes and neutrophils also fulfil homeostatic functions (9–11). In particular, monocytes show a broad heterogeneity in terms of phenotype and location that goes beyond the identification of classical, migratory Ly6c^{+} and non-classical, patrolling Ly6c^{low} monocytes (10). Due to their plasticity, monocytes can be found in all compartments of the lung and give rise to monocyte-derived interstitial macrophages (IM) or AM in steady state and inflammation (10, 12, 13). IM on the other hand are exclusively found in the interstitium, where at least two known subpopulations guard the interstitial space and the vasculature (14). DCs are located in the interstitial space and sit closely attached to the epithelial lining performing luminal sampling with their dendrites (15). Upon uptake for foreign antigens, they can rapidly induce adaptive immune responses via migration to lymphatic vessels in close proximity to the alveoli and capillaries (1). Pulmonary DCs can be separated into conventional DC type 1 and 2 (cDC1, cDC2) and newly discovered DC3 (16, 17). Each of these subtypes sits at specific locations and induces different T cell activation and polarization programs to modulate the adaptative response according to the type of the invading pathogen (18–20). Besides lymphocytes patrolling through the lymph vessels and interacting with the local DC network, the lung also harbours a plethora of tissue-resident lymphoid cells. Innate lymphoid cells (ILC), natural killer (NK) cells, regulatory T cells and γδT cells are the most prominent populations in the lung, completing a functionally specialized network shaped by its exposure to the environment (4).

I.II. Macrophages: General overview

The classification of macrophages has been extensively discussed in the last decade due to their dynamic heterogeneity in regards to origin, phenotype and function. Developmentally, macrophages established during embryogenesis are considered tissue-resident, while the ones that stem from adult bone marrow are monocyte-derived. During prenatal development, macrophage progenitors (pMac) of the yolk sac colonize the embryo as early as embryonic development day 9 and further differentiate into tissue-resident macrophages that are integral

to all organs (21, 22). The core functions of tissue-resident macrophages are efferocytosis, non-opsonic and receptor-dependent phagocytosis and complement system activation. Each of these core function is established by expression of genes like *Timd4* and *Mertk* for efferocytosis, *Cd36, Clec7a* and *Mrc1* for non-opsonic phagocytosis, a variety of Fc receptor genes and *Itgam* for receptor-dependent phagocytosis and *C1qb* and *C1qc* for complement activation (21). After seeding different tissues, macrophages acquire a tissue-specific transcriptional profile on top of their core function profiles to establish their identity and fulfil their homeostatic and immune sentinel function (23). Tissue-resident macrophages usually maintain their population by self-renewal with no or low input of hematopoetic stem cell-derived monocytes. However, distinct macrophage populations across the body require input of monocytes during post-natal tissue maturation and some populations are even exclusively dependent on constant replenishment by monocytes (13, 24). Both embryonically and adult-derived macrophages are able to co-exist in the same tissue and contribute to tissue function during steady state and inflammation (23). A recent publication identified three macrophage populations across organs: embryonically derived long-lived $Tim4^{+}Lyve\text{-}1^{+}Folr2^{+}$ macrophages, monocyte-derived short-lived $CCR2^{+}$ macrophages and $MHCII^{hi}$ macrophages with mixed origin and longevity (25). The following chapters will be focused on macrophage heterogeneity, origin and function in the murine lung.

I.II.I. Alveolar macrophages

AM are the most abundant macrophage subtype in the lung, although only one AM can be found in every third alveolus (6). They can rapidly migrate from one alveolus to another by squeezing through the pores of Kohn that interconnect the alveoli to effero- or phagocytose cellular debris and foreign particles (26). To maintain homeostasis, AM efferocytose apoptotic cells and surfactant via Marco and Axl in an immunologically silent way without triggering inflammation (27, 28). When AM reach their maximal phagocytic capacity limit, they can induce inflammation by secretion of pro-inflammatory cytokines like TNF-α and IL-1β to locally recruit monocytes and granulocytes (29, 30). AM also secrete immunoregulatory cytokines like TGF-β to resolve inflammation and protect the alveolar epithelium from damage (31). AM are categorized into tissue-resident or monocyte-derived AM according to their ontogeny. Tissue-resident AM (trAM) stem from fetal monocytes that reach the niche in response to the actin binding protein L-plastin to colonize the alveoli (32). Postnatal differentiation of fetal monocytes into AM is dependent on granulocyte-macrophage colony stimulating factor (GM-CSF) secreted by type II AEC (33, 34) and TGF-β (35). GM-CSF signalling in combination with epithelial derived and autocrine TGF-β triggers expression of peroxisome proliferator-activated receptor γ (PPARγ), one of the major transcription factors for macrophage development (31,

36). Other transcription factors like Egr2, Bhlh40 and Bhlh41 and MafB ensure their self-renewal and identity (21, 37, 38) (**Figure 1**).

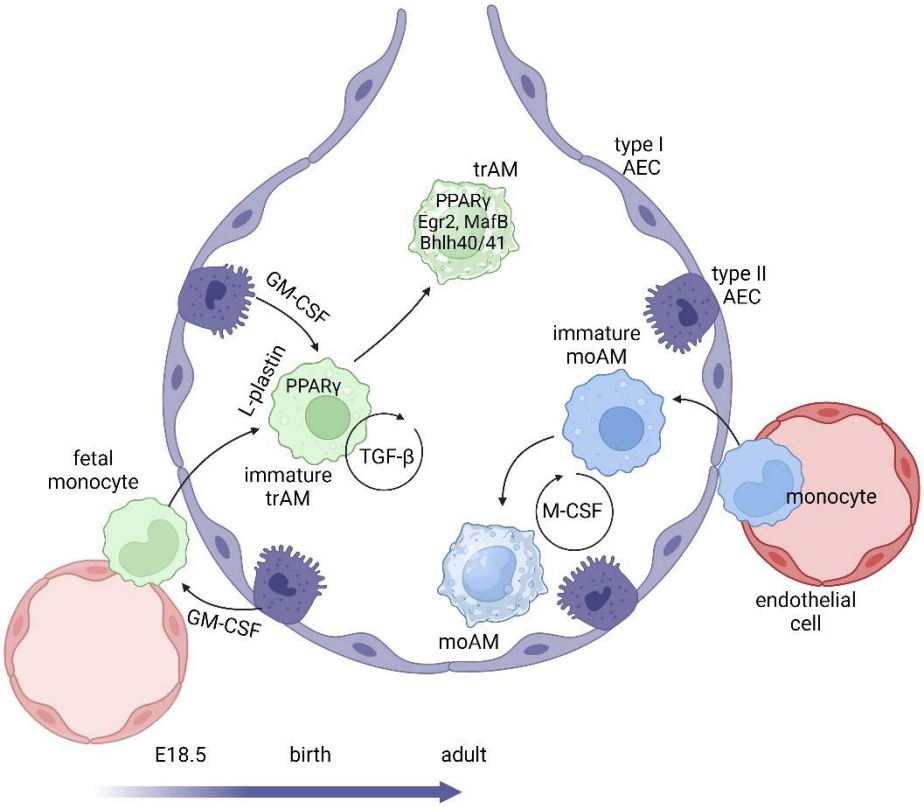

Figure 1: Pre- and postnatal development of alveolar macrophages. During embryonic development, fetal monocytes migrate from the vasculature into the alveolar space around day E18.5. At birth, GM-CSF produced by type II AEC, L-plastin and autocrine TGF-β signalling induce expression of PPARγ committing towards the AM fate. After birth, immature trAM develop into AM and expression of transcription factors like PPARγ, Egr2, MafB and Bhlh40/41 ensures their identity. During adulthood, monocytes from the bone marrow egress from the blood vessel into the alveolus and differentiate into moAM. MoAM are dependent on M-CSF during development and co-exist in the niche together with fetal-derived trAM. Adapted from (2).

Recent approaches delineating the origin of AM in adult mice showed that approximately 20% are monocyte-derived under homeostatic conditions (13). Loss of trAM during ageing, sterile inflammation, lung injury and infections can lead to proliferation of trAM (30, 39) or further emergence of monocyte-derived AM (moAM) to replenish the niche and to restore lung function (12, 13, 40, 41). $CCR2^{+}Ly6c^{+}$ classical monocytes enter the alveolar space and differentiate into moAM that are dependent on M-CSF (42) (**Figure 1**). However, the signals that trigger monocyte influx and differentiation into macrophages remain elusive. MoAM and trAM share the expression of common macrophage markers as CD64, MerTk, CD11c and SiglecF, but mostly differ in their transcriptional and functional phenotype (41). The altered cellular functions of moAM can positively or negatively influence disease settings depending on the context. MoAM secrete higher levels of pro-inflammatory cytokines like IL-6, which confer to a better

clearance of secondary *Streptococcus pneumoniae* infections or protection against allergic asthma (12, 43), but on the other hand accelerate tissue damage and fibrosis (44). These studies show that experienced infections and adaptation to the environment diversifies the AM compartment in the lung, yet a full understanding is still lacking.

I.II.II. Interstitial macrophages

IM reside in the interstitial space between the alveolar epithelium and the endothelium of the blood vessels. IM across the body share a similar transcriptional profile, which is most likely determined by their conserved function (25, 45). Pulmonary IM are maintained by M-CSF signalling and there are at least two to three subpopulations that differ in their spatial localization and function (14, 45, 46). Nerve bundle associated Lyve-1^{low}MHCII^{high} IM express pro-inflammatory mediators like IL-1β and Cxcl12 and regulate immune responses upon inflammatory exposure (14, 46). Blood vessel associated Lyve-1^{high}MHCII^{low} IM are the gatekeepers of the vasculature and have an immunoregulatory signature defined by *Tgfb2*, *Plaur* and *Fcna* (14). Depletion of Lyve-1^{high}MHCII^{low} IM increased vascular leakage and worsened bleomycin fibrosis (14). The origin of IM is still not fully understood. Current literature suggest that IM originate from fetal precursors with self-renewal capacities. Depending on the subpopulation, monocytes partially and gradually replace IM during adulthood (2).

I.III. Influence of environmental exposure on lung immunity

I.III.I. General overview

Diversity of innate immune cells in the lung is driven by the close contact to the environment and by the inhalation of aerosols, particulate matter, pathogens and immunomodulatory substances of pathogens. The environmental pollutants inhaled by humans are mainly gases like carbon monoxide. Particulate matter only accounts for ~5% of environmental pollutants, and the majority is derived from transportation and fuel combustion (1). Recent studies have highlighted that sterile low-grade inflammation induced by inhaled particulate matter reshapes the macrophage compartment (47), impedes recovery after lung injury (48) and even promotes lung adenocarcinoma (49). These negative health effects of inhaled substances are juxtaposed by positive effects upon exposure to different substances. For example, immunomodulatory pathogen-derived substances like endotoxin have been associated with a low incidence of allergies and asthma (50) and protection from secondary bacterial infections (51). These immunomodulatory pathogen-derived substances are macromolecules shed from the surface of bacteria and fungi, mostly polysaccharides from the cell wall that act as pathogen-associated molecular patterns (PAMPs) (52). These PAMPs are recognized by pattern recognition receptors (PRR) expressed on innate immune cells in the lung (53). One

heavily investigated bacterial and fungal derived polysaccharide is β-glucan, which is omnipresent in ambient air and has been linked to airway inflammation, allergy and asthma and the formation of an immune memory in monocytes and macrophages (54–57). Fungal species like *Cladospora* and *Aspergillus* are the major sources for aerial β-glucan concentrations, although other species also contribute (58). Aerial concentrations of β-glucan display seasonal differences with the majority of molecules detected during summer months in urban and agricultural areas, while indoor concentrations are usually low (59, 60). Studies showed that concentrations of fungal fragments are up to 320x higher than actual fungal spores, and therefore contribute to the majority of fungal antigens present in ambient air (61).

I.III.II. B-Glucan: structure, receptor signalling and immune-modulatory impact

B-Glucans are glucose-based polysaccharides that form a layer on top of the cell wall of bacteria, fungi, algae and different cereals such as oats and wheat (62, 63). Structurally, β-glucans form linear polymers with a β-(1,3), -(1,4) or -(1,6) glycosidic backbone and side branches mostly in (1,6) conformation (62). In general, a higher complexity determined by the degree of branching, the tertiary structure and charge of the β-glucan molecule potentiates the receptor activation and their resultant immunomodulatory effects (64). B-Glucans are recognized by a broad range of cell surface receptors, such as Dectin-1, complement receptor 3 (CR3), CD5, CD36, lactosylceramide and Toll-like receptors (TLR) 2, 4 and 6. From these receptors, Dectin-1 and CR3 have been extensively studied in the context of innate immune cells (52). Dectin-1 is expressed on macrophages and to a lesser extent on granulocytes (65), while CR3 can mainly be found on neutrophils, monocytes and NK cells (52). Besides their differential expression, Dectin-1 detects β-glucan in a direct fashion, while CR3 only detects opsonized β-glucan particles prior to phagocytosis (66). As Dectin-1 is the main receptor detecting fungal β-glucans (67), its intracellular signal transduction in the cytoplasm and its transcriptional targets have been well studied. Dectin-1 is a type II C lectin-like membrane PRR encoded by the *Clec7a* gene with an intracellular hemi-immunoreceptor tyrosine-based activation motif (hemITAM) (68, 69). Upon ligand binding, a conformational change in the receptor leads to the clustering of these hemITAM at the cytoplasmic tail, which triggers hemITAM phosphorylation at two tyrosine residues by Src kinases (70). These phosphorylation sites act as docking sites for spleen tyrosine kinase (Syk), which has to be phosphorylated as well to achieve full activation (70, 71). Syk can activate three main downstream targets: Caspase recruitment domain-containing protein 9 (CARD9), phosphoinositide 3 kinase/protein kinase B (PI3K/AKT) and phosphatidylinositol-specific phospholipase Cγ2 (PLCγ2) (70). Signalling via CARD9 leads to the formation of a trimolecular complex together with B cell lymphoma 10 (BCL10) and Mucosa associated lymphoid tissue 1 (MALT1), which subsequently activates NF-κB and the production of IL-6, pro-IL-1β and TNF-α (72). CARD9

can also engage with interferon regulatory factor 5 (IRF5), which stimulates production of type I interferons (73). Signalling via PI3K/AKT mainly leads to reactive oxygen species (ROS) production via the NADPH oxidase and cytokine production (74). PLCγ2 activation leads to Nuclear factor of activated T cells (NFAT) and Extracellular response kinase (ERK) activation, which induce IL-2, IL-10 and ROS production (75, 76). Interestingly, Syk-independent Dectin-1 signalling via Raf-1 stimulates phagocytosis and elevates NF-κB expression (77–79). Additionally, Raf-1 dependent activation of mammalian target of rapamycin (mTOR) and hypoxia inducible factor α (HIF-1α) leads to chromatin modifications and initiates immune memory formation (80, 81) (**Figure 2**). Functionally, it has been shown that the expression of pro-inflammatory cytokines and immune memory formation after adaptation to β-glucan protects against a secondary *Candida albicans* infection (80).

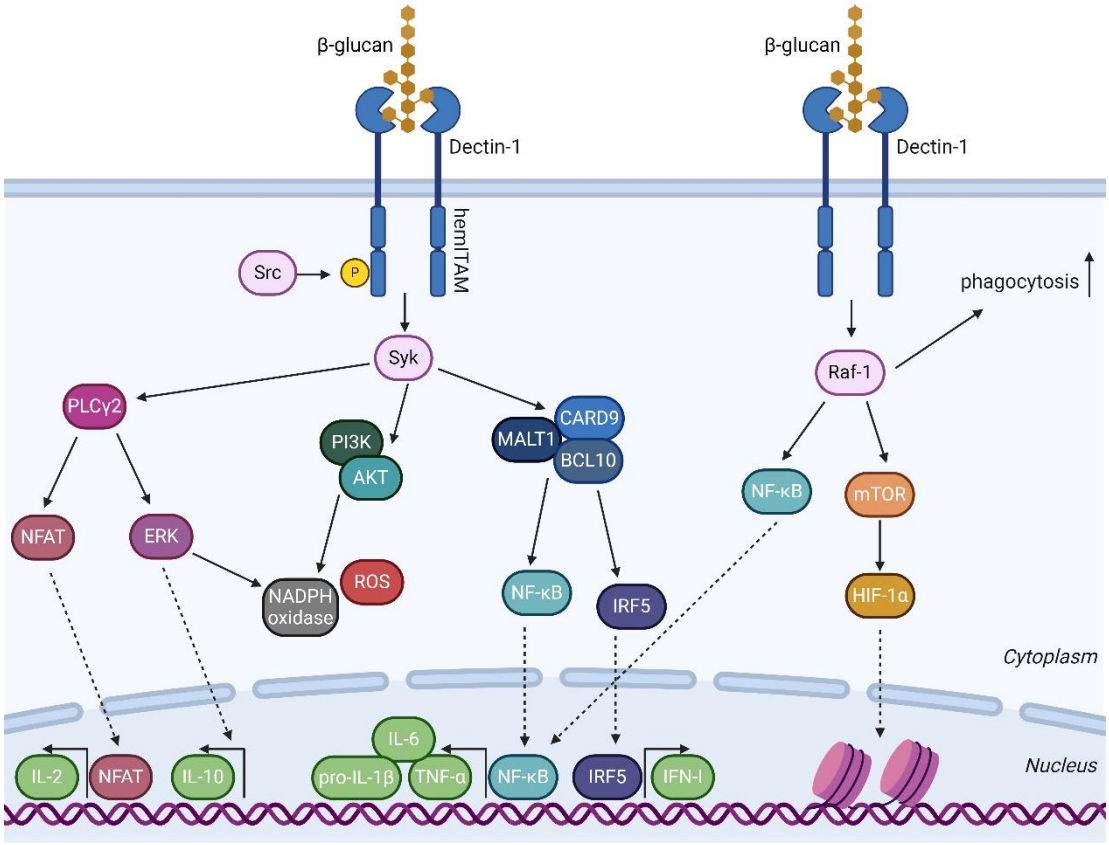

Figure 2: B-Glucan mediated signalling via Dectin-1 and its main downstream signalling pathways. Phosphorylation of Dectin-1 by Src upon ligand binding leads to activation of Syk, which then triggers PLCγ2, PI3K/AKT or CARD9/MALT1/BCL10 downstream cascades. Depending on the pathway, this leads to IL-2, IL-10 and ROS production, NF-κB mediated IL-6, pro-IL-1β and TNF-α or IRF5 mediated IFN-I production. Syk-independent Dectin-1 signalling leads to Raf-1 activation, which triggers phagocytosis, NF-κB activation and mTOR/HIF-1α mediated epigenetic remodelling. Adapted from (70).

I.IV. Apolipoprotein E: Expression, function and relevance for immune responses

Apolipoprotein E (ApoE) is a versatile and polymorphic protein that belongs to the family of apolipoproteins, which are integral components of high-, low- and very low-density lipoproteins (HDL, LDL and VLDL) to maintain their stability (82). The human *Apoe* gene exists as three common major allele variants *Apoe2*, *Apoe3* and *Apoe4* and several other isoforms, while only one isoform exist in mice (83, 82). The majority of ApoE protein is synthesised and secreted by hepatocytes in the liver and then released into the blood and lymph fluid to exert its function (84, 85). In peripheral tissues, macrophages are the main source of ApoE (83). Transcription of *Apoe* is driven by transcription factors belonging to nuclear hormone receptor family, namely liver-X-receptors (Lxr) α and β, that also control other genes involved in cholesterol and fatty acid metabolism (86). The main purpose of ApoE is transport, (re)distribution and metabolism of lipids and lipoproteins, as well as cholesterol efflux (82). Therefore, ApoE is one of the major regulators of blood lipid balance by control of metabolism of endogenous and endogenous lipids, such as cholesterol and triglycerides, in the liver. Endogenous lipids synthesised in the liver are directly bound to ApoE and then released into the blood stream to supply tissues with energy, a process called conventional cholesterol transport (87). In contrast, exogenous lipids from the intestine or macrophages in the periphery are bound to ApoE and transported to the liver via the lymph system and vasculature, known as reverse cholesterol transport (82, 87). After breakdown of triglycerides, cholesterol will be taken up by hepatocytes via the low-density lipoprotein receptor (LDLR) or low-density lipoprotein receptor-related protein 1 (LRP1) (82).

$ApoE^{-/-}$ deficient mice develop hypercholesterolemia and atherosclerosis (88), which can be even aggravated by ablation of ApoE and Lxrα in combination (89). Activation of Lxrβ signalling using synthetic ligands reverses the cholesterol overload in $ApoE^{-/-}$ $Lxr\alpha^{-/-}$ mice mainly by reducing the cholesterol content in macrophages (89). Besides its implication in cardiovascular diseases, dysregulation of ApoE function and lipid homeostasis has also been associated with neurodegenerative diseases like Alzheimer's (reviewed in (90)), which can be explained by its high expression in astrocytes of the central nervous system (91). However, the role of ApoE during inflammation, infection and cancer has not been fully understood. Infection studies found that ApoE deficiency increased the susceptibility to *Klebsiella pneumoniae*, *Listeria monocytogenes* and *Mycobacterium tuberculosis* (92–95). In the setting of cancer, ApoE has been linked to tumour-associated macrophages promoting immunosuppression in the pancreas (96). Further literature describes a dual role of ApoE in other types of cancers, such as melanoma (97), ovarian cancer, lung cancer and glioblastoma (98). Recent studies revealed a distinct lipid associated gene signature marked by high *Apoe* expression in monocytes that extravasate into lung or adipose tissue and subsequently differentiate into

macrophages (12, 99). In summary, these studies highlight the function of ApoE in balancing lipids and cholesterol in a multitude of different disease settings and reveal modulatory properties of ApoE on immune responses.

I.V. Aim of the thesis

As the first line of defence against incoming pollutants and pathogens, pulmonary mononuclear phagocytes, especially alveolar macrophages, are in close and constant contact with the environment. Recent studies highlighted the immunomodulatory effect of pathogen-derived cell wall components like β-glucan, which are omnipresent in ambient air that have been linked to low-grade inflammation and to the formation of an immune memory in monocytes and macrophages. However, it remains elusive how the fine-tuned heterogeneous network of lung mononuclear phagocytes, especially alveolar macrophages, adapts to ambient β-glucan. The aim of this project is to decipher this adaptation process using a mouse model of a single intranasal β-glucan inoculation. We will first establish a reliable tool to resolve the heterogeneity of pulmonary mononuclear phagocytes by flow cytometry and then characterize the quantitative immune cell dynamics post β-glucan inoculation over time. Furthermore, we will assess if glucan stimulation induces changes in canonical alveolar macrophage functions, such as cytokine production and phagocytosis. Transcriptomic analysis will be utilized to reveal how this environmental adaptation is regulated on the gene expression level. Lastly, as β-glucan has been linked to the formation of an innate immune memory, we will investigate if this adaptation in the lung has an effect on a secondary challenge. In summary, a mouse model of a single β-glucan dose will be used to mimic adaptation of pulmonary mononuclear phagocytes to low-grade inflammation inducing environmental cues and innovative techniques will investigate this process from a cellular, functional and transcriptional angle.

II. Material and methods

II.I. Materials

II.I.I. Animal models

Table 1: The following transgenic mouse lines were used in the study.

Mouse Strain	Provider	Identifier
Ai14	The Jackson Laboratory	JAX: 007914
ApoE flox	Prof. J. Heeren	-
C57BL/6J	LIMES GRC	-
CARD9 ko	Prof. J. Ruland	-
CCR2 ko	The Jackson Laboratory	JAX: 004999
CD45.1	The Jackson Laboratory	JAX: 002014
Dectin-1 ko	Prof. D. Brown	JAX: 012337
LysM Cre	Prof. I. Förster	JAX: 004781
Ms4a3 Cre	Prof. F. Ginhoux	-
Ms4a3 CreERT2	Prof. F. Ginhoux	-

II.I.II. Consumables

Table 2: Consumables used in the study and their supplier.

Product	Supplier
1.5 ml microcentrifuge tubes	Sarstedt
15 ml Falcon tubes	Sarstedt
2 ml microcentrifuge tubes	Sarstedt
5 ml microcentrifuge tubes	Greiner Bio-One
50 ml Falcon tubes	Sarstedt
70 µm Easy strainer	Greiner Bio-One
CELLLSTAR® 6, 48 or 96 Well Cell Culture Multiwell Plates	Greiner Bio-One
Disposable syringe Inject® With Luer fitting, 5 or 20 mL	B. Braun
FACS tubes Santo	Sarstedt
Microscope slides	Thermo Fisher Scientific
PCR tubes	VWR
Serological pipettes	Sarstedt
Sterican disposable needles 19G	B. Braun
Sterican disposable needles 22G	B. Braun
TT Cryomolds	Science Services

II.I.III. Chemicals and reagents

Table 3: Chemicals and reagents used in this study and their supplier.

Product	Supplier	Cat. No.
16% Paraformaldehyde	Electron Microscopy Sciences	15710
Albumin Bovine Fraction V, pH 7.0	SERVA	11930
BODIPY	ThermoFisher Scientific	D3922
BS3 crosslinker	ThermoFisher	21580
Collagenase IV	Sigma-Aldrich	C5138-100MG
D-(+)-Sucrose	Sigma-Aldrich	SA84100
DNase I	Sigma-Aldrich	D4263-5VL
Donkey Serum	PAN Biotech	P30-0101
DPBS (10x)	Carl Roth	9130.2
DRAQ5	ThermoFisher Scientific	62254

DRAQ7	BioLegend	424001
EDTA	Invitrogen	15576-028
Endotoxin-free Dulbecco's PBS (1x)	Sigma-Aldrich	TMS-012-A
FCS	Sigma-Aldrich	F7524-500ML
Filipin	Sigma-Aldrich	F4767
Fluoromount G	ThermoFisher	00-4958-02
Fructose	ThermoScientific	A17718
GlutaMAX	Gibco	35050061
Glycerol	ThermoScientific	A16205
HBSS with Ca, Mg	PAN Biotech	P04-32505
Heparin solution	Stemcell Technologies	07980
Hoechst 33342 Trihydrochloride	ThermoFisher	H21492
Insulin-Transferrin-Selenium	ThermoFisher	41400045
GlutaMAX	ThermoFisher	35050061
LPS (*E. coli* O111:B4)	Sigma-Aldrich	LPS25
Matrigel	Corning	354230
MEM non-essential amino acids	Sigma-Aldrich	M7145-100ML
MitoTracker Green	ThermoFisher Scientific	M7514
Na_2CO_3	Carl Roth	6885.2
NH_4Cl	Carl Roth	K298.1
Nuclear stain	Akoya Biosciences	7000003
Penicillin/ Streptomycin	ThermoFisher	15070063
Penicillin/Streptomycin	Gibco	10378016
Precision Count Beads	BioLegend	424902
RPMI1640	PAN Biotech	P04-16500
RTU Animal-Free Block and Diluent	VECTOR	SP-5035-100
Sodium Pyruvate	Gibco	11360070
Staining buffer	Akoya Biosciences	7000008
Storing buffer	Akoya Biosciences	232107
TGF-β	Miltenyi Biotech	130-095-066
Tissue-Tek O.C.T.	Sakura Finetek	4583
Triton X-100	Sigma-Aldrich	T9284
Triton-X-100	ThermoScientific	A16046
Zombie NIR™ Fixable Viability Kit	BioLegend	423106
α-MEM	ThermoFisher	41061029
β-1,3 glucan from *Candida albicans*	provided by Prof. D Wiliams	-
β-Mercaptoethanol	Gibco	21985023

II.I.IV. Commercial assays and kits

Table 4: Commercial assays and kits used in this study and their supplier.

Product	**Supplier**	**Cat. No.**
actb mouse Type4 AF488 Probe PrimeFlow	ThermoFisher Scientific	VB4-10432-PF
apoE mouse Type1 AF647 Probe PrimeFlow	ThermoFisher Scientific	VB1-10244-PF
BD Cytofix/Cytoperm kit	BD Biosciences	554714
CyQUANT NF Cell Quantification Assay Kit	Thermo Fisher Scientific	C7026
GoTaq qPCR master mix	Promega	A6002
Mouse IL-6 ELISA Kit	eBioscience	88-7064-88
MiniElute kit	Qiagen	28004
miRNeasy Micro Kit	Qiagen	217084
Mouse Apolipoprotein E ELISA Kit	Abcam	ab215086
Mouse GM-CSF DuoSet ELISA	R&D Systems	DY415-05
Mouse M-CSF DuoSet ELISA	R&D Systems	DY416-05
pHrodo S. aureus Bioparticles	Sartorius	4619
PrimeFlow RNA Assay Kit	ThermoFisher Scientific	88-18005
QuantiTect Reverse Transcription Kit	Qiagen	205311

II.I.V. Antibodies

Table 5: Antibodies used in this study. Clone, fluorophore and supplier are listed.

Antibody	Fluorophore	Supplier	Cat. No.
Anti-mouse ApoE, Clone: EPR19392	-	Abcam	ab183597
Anti-mouse CD115, Clone: AFS98	PE-CF594	BioLegend	135528
Anti-mouse CD115, Clone: AFS98	PE-Cy7	BioLegend	135523
Anti-mouse CD115, Clone: T38-320	BUV496	BD Biosciences	749974
Anti-mouse CD117, Clone: 2B8	PE-Cy7	BioLegend	105814
Anti-mouse CD11b, Clone: M1/70	BV421	BioLegend	101236
Anti-mouse CD11b, Clone: M1/70	BUV737	BD Biosciences	612800
Anti-mouse CD11b, Clone: M1/70	-	BioLegend	101202
Anti-mouse CD11c, Clone: N418	PerCp-Cy5.5	BioLegend	117328
Anti-mouse CD11c, Clone: N418	BV605	BioLegend	117333
Anti-mouse CD11c, Clone: N418	BV510	BioLegend	117338
Anti-mouse CD11c, Clone: N418	BV510	BioLegend	117302
Anti-mouse CD131, Clone: JORO50	PE	BD Bioscience	559920
Anti-mouse CD135, Clone: A2F10	PE-CF594	BD Biosciences	562537
Anti-mouse CD140α, Clone: APA5	-	eBioscience	14-1401-82
Anti-mouse CD150, Clone: 475301	APC	BioLegend	115910
Anti-mouse CD16/32, Clone: 2.4G2	BUV563	BD Biosciences	741229
Anti-mouse CD16/32, Clone: 93	-	BioLegend	101320
Anti-mouse CD16/32, Clone: 93	APC	BioLegend	101325
Anti-mouse CD19, Clone: 6D5	APC-Cy7	BioLegend	115530
Anti-mouse CD192, Clone: 475301	BUV661	BD Biosciences	750042
Anti-mouse CD206, Clone: C068C2	BV650	BioLegend	141723
Anti-mouse CD24, Clone: M1/69	PE	eBioscience	12-0242-83
Anti-mouse CD24, Clone: M1/69	BUV496	BD Biosciences	564664
Anti-mouse CD24, Clone: M1/69	PE-Cy7	BioLegend	101822
Anti-mouse CD3, Clone: 17A2	APC-Cy7	BioLegend	100222
Anti-mouse CD31, Clone: Mec13.3	FITC	BioLegend	102514
Anti-mouse CD326, Clone: G8.8	-	BioLegend	118202
Anti-mouse CD326, Clone: G8.8	APC-Cy7	BioLegend	118218
Anti-mouse CD335, Clone: 29A1.4	APC-Cy7	BioLegend	137631
Anti-mouse CD34, Clone: SA376A4	BV421	BioLegend	152208
Anti-mouse CD43, Clone: S7	BUV563	BD Biosciences	741238
Anti-mouse CD43, Clone: S7	APC	BD Biosciences	560663
Anti-mouse CD45, Clone: 30-F11	BUV395	BD Biosciences	564279
Anti-mouse CD45, Clone: 30-F11	BUV805	BD Biosciences	748370
Anti-mouse CD45, Clone: 30-F11	-	eBioscience	14-0451-82
Anti-mouse CD45, Clone: 30-F11	FITC	BD Biosciences	553080
Anti-mouse CD45.1, Clone: A20	BUV395	BD Biosciences	565212
Anti-mouse CD45.2, Clone: 104	BUV737	BD Biosciences	564880
Anti-mouse CD45R, Clone: RA3-6B2	APC-Cy7	BioLegend	103224
Anti-mouse CD48, Clone: HM48-1	BV711	BioLegend	103439
Anti-mouse CD64, Clone: X54-5/7.1	PE-Cy7	BioLegend	139314
Anti-mouse CD64, Clone: X54-5/7.1	-	BioLegend	139302
Anti-mouse CD90, Clone: 53-2.1	APC-Cy7	BioLegend	140325
Anti-mouse CX3CR1, Clone: SA011F11	AF700	BioLegend	149035
Anti-mouse F4/80, Clone: BM8	BV785	BioLegend	123141
Anti-mouse GPNMB, Clone: EPR18226-147	-	Abcam	ab234529
Anti-mouse IL-6, Clone: MP5-20F3	APC	BD Biosciences	561367
Anti-mouse Ly6c, Clone: HK1.4	BV605	BioLegend	128036
Anti-mouse Ly6c, Clone: HK1.4	BV711	BioLegend	128037
Anti-mouse Ly6c, Clone: HK1.4	AF488	BioLegend	128021
Anti-mouse Ly6c, Clone: HK1.4	APC	BioLegend	128016
Anti-mouse Ly6c, Clone: HK1.4	FITC	BioLegend	128005
Anti-mouse Ly6g, Clone: 1A8	APC-Cy7	BioLegend	127624
Anti-mouse Ly6g, Clone: 1A8	BV750	BD Biosciences	747072
Anti-mouse Ly6g, Clone: 1A8	FITC	BioLegend	127606

Anti-mouse Ly6g, Clone: 1A8	BUV805	BD Biosciences	741994
Anti-mouse M-CSF, Clone: polyclonal	-	ThermoFisher	PA5-95279
Anti-mouse MERTK, Clone: 108928	BV785	BD Biosciences	747890
Anti-mouse MERTK, Clone: 2B10C42	BV421	BioLegend	151510
Anti-mouse MHC2, Clone: 2G9	BUV496	BD Biosciences	750171
Anti-mouse MHC2, Clone: M5/114.15.2	BV510	BioLegend	107635
Anti-mouse MHC2, Clone: M5/114.15.2	BUV661	BD Biosciences	750280
Anti-mouse MHC2, Clone: M5/114.15.2	-	BioLegend	107602
Anti-mouse Na-K-ATPase, Clone: EP1845Y	-	Abcam	ab76020
Anti-mouse NK-1.1, Clone: PK136	APC-Cy7	BioLegend	108724
Anti-mouse NKP46, Clone: 29A1.4	APC-Fire750	BioLegend	137631
Anti-mouse Sca-1, Clone: D7	PacificBlue	BioLegend	108120
Anti-mouse SiglecF, Clone: E50-2440	PE-CF594	BD Biosciences	562757
Anti-mouse SiglecF, Clone: E50-2440	BUV395	BD Biosciences	740280
Anti-mouse SiglecF, Clone: E50-2440	BV421	BD Biosciences	565934
Anti-mouse SiglecF, Clone: E50-2440	APC-Cy7	BD Biosciences	565527
Anti-mouse TCR β-chain, Clone: H57-597	APC-Cy7	BioLegend	109219
Anti-mouse TER-119, Clone: TER-119	APC-Cy7	BioLegend	116223
Anti-mouse α-SMA, Clone: 1A4	-	BioLegend	904601
Anti-mouse α-SMA, clone: 1A4	FITC	Sigma-Aldrich	F3777
Donkey Anti-Goat IgG Secondary Antibody	Cy3	Sigma-Aldrich	AP180C
Donkey anti-Rabbit IgG Secondary Antibody	AF488	ThermoFisher	A-21206
Donkey anti-Rabbit IgG Secondary Antibody	AF568	ThermoFisher	A10042
Donkey anti-Rat IgG Secondary Antibody	AF488	ThermoFisher	A-21208
Donkey Anti-Rat IgG Secondary Antibody	Cy3	Jackson Research	712-165-153
Donkey Anti-Rabbit IgG Secondary Antibody	Cy3	Abcam	ab150075
Ultra-LEAF™ anti-mouse CSF-1R Antibody	-	BioLegend	135541
Ultra-LEAF™ Rat IgG2a Isotype Ctrl Antibody	-	BioLegend	400573

II.I.VI. Buffers and solutions

Table 6: Buffers and solutions prepared in house used in this study.

Buffer	**Composition**
1x PBS	900 ml ddH_20 100 ml 10x PBS
0.5 M EDTA	186.1 g EDTA 1 l ddH_20 adjust pH to 8.0
Blood and BALF collection buffer	1x PBS with 10 mM EDTA
Complete RPMI1640 cell culture medium	RPMI1640 with 10% FCS 50 U/ml Penicillin/Streptomcyin 2 mM GlutaMAX 1 mM Na-Pyruvate 1% MEM non-essential amino acids 0.1% β-Mercaptoethanol
Complete α-MEM organoid medium	α-MEM with 10% FCS 50 U/ml Penicillin/Streptomcyin 1x Insulin-Transferrin-Selenium 2 µg/ml Heparin
FACS buffer	1x PBS with 0.5% BSA and 2 mM EDTA
Red blood cell lysis buffer	8.32 g NH_4CL 0.84 g $NaHCO_3$ 0.043 g EDTA 1 l ddH_2O

Organ digestion buffer	HBSS with 10% FCS 0.2 mg/ml collagenase IV 0.05 mg/ml DNaseI

II.I.VII. Devices

Table 7: Devices used to collect the data analysed in this study.

Equipment	Source
Brightfield Microscope Eclipse TS100	Nikon
Cell culture incubator	Binder
Centrifuge Concentrator plus	Eppendorf
Centrifuges 5810R, 5424, 5424R	Eppendorf
CODEX work station	Akoya Biosciences
Confocal microscope LSM880	Zeiss
Cryostat CM3050S	Leica
Faxitron CP160	Faxitron
Flow cytometer (Symphony A5)	Becton Dickinson
Flow cytometry sorter (ARIA III)	Becton Dickinson
HybEZ Oven	Advanced Cell Diagnostics
Incubator	Memmert
Microplate reader	TECAN
Microscope AxioObserver	Zeiss
MojoSort magnets	BioLegend
Shaking Incubator Innova44	New Brunswick Scientific

II.II. Methods

II.II.I. Mouse models

All mice used in this study were bred in the GRC animal facility of the LIMES Institute, University of Bonn, Germany or Center for Translational Cancer Research, Klinikum rechts der Isar, Technical University of Munich, Germany. Animals were housed in IVC mice cages with a 12h light/dark cycle and ad libitum access to food and water. Male mice of 8-12 weeks age were used for experiments. If possible, wildtype littermates were used for experiments, otherwise C57BL/6JCrl animals from the LIMES-GRC were added as controls. The government of North Rhine-Westphalia approved all experiments under the licenses 84-02.04.2017.A347 and 81-02.04.2020.A454.

II.II.II. Intranasal and intratracheal application

Mice were anesthetized by intraperitoneal injection of ketamine/xylazine. For the intranasal stimulation, the mice were inoculated drop by drop onto the nostrils with endotoxin-free 1x PBS (EMD Millipore) or 200 µg β-glucan from *Candida albicans*, which was provided by Prof. D. Williams. For intratracheal application, a plastic gavage needle was placed into the trachea through the oral cavity. The application solution was injected with a syringe into the trachea via the gavage needle. Mice were monitored until regaining consciousness.

II.II.III. Transcardial perfusion

Mice were deeply anesthetized by intraperitoneal injection of ketamine/xylazine. The heart was exposed and a Venofix Safety 25G (B.Braun) needle was inserted into the right ventricle to perfuse the lung. A small incision was made at the atrium on top of the heart. The heart was subsequently flushed with 10 ml cold 1x PBS.

II.II.IV. Broncho-alveolar lavage

The broncho-alveolar lavage fluid (BALF) was collected one, three, seven, 14, 21 or 28 days after inoculation. The trachea was exposed and a plastic needle was inserted via a small incision. For cell analysis, the lung was flushed 3x with 1 ml cold 1x PBS supplemented with 10 mM EDTA. The BALF was centrifuged for 5 min at 1350 rpm (365 g) at 4°C prior to discarding the supernatant. For cytokine assessment, the lung was flushed 3x with the same 1 ml of cold 1x PBS with 10 mM EDTA. Afterwards, the samples were centrifuged for 10 min at 14000 rpm at 4°C and the supernatant was frozen in liquid nitrogen until analysis. Supernatants were thawn on ice and centrifuged for 5 min at 10000 rpm at 4°C to remove debris prior to ELISA assessment.

II.II.V. *In vivo* alveolar macrophage transfer

C57BL/6J CD45.2 wildtype donor mice were intranasally stimulated with PBS or β-glucan as described above. At day 5, the BALF was harvested, cells of the same condition were pooled and subsequently resuspended in 1x PBS after centrifugation. $2x10^5$ donor cells in the volume of 35 µl were intratracheally transferred into anesthetized CD45.1 recipient mice. The BALF of the recipients was harvested 48 h post transfer and either analyzed by flow cytometry or used for ex vivo restimulation with LPS (see below).

II.II.VI. *In vivo* CSF-1 receptor blockade

Prior to *in vivo* application, the application volume of the anti-CSF-1R or isotype control antibody was concentrated by factor 4 using a Concentrator Plus vacuum centrifuge (Eppendorf) in V-AQ mode. Mice were anesthetized and subsequently intranasally stimulated with β-glucan mixed with 500 µg anti-CSF-1R antibody (BioLegend) or 500 µg isotype control antibody (BioLegend). 12 h and three days after the initial treatment, intranasal application of 500 µg anti-CSF-1R antibody or the respective isotype control was repeated. Mice were sacrificed at day seven and flow cytometry was performed on the BALF.

II.II.VII. *Legionella pneumophila* infection

Mice were intranasally stimulated with PBS or β-glucan at day 0 followed by intratracheal administration of $5x10^6$ CFU *Legionella pneumophila* per mouse at day seven and sacrifice at

day nine. To determine the bacterial load, part of the BAL fluid or lung tissue lysates were incubated on CYE plates in duplicates for 3-4 days at 37°C in a non-CO_2 incubator.

II.II.VIII. Bone marrow chimeras

Bone marrow chimeras were generated by irradiation of recipient mice with 10 Gy. Twelve to 24 h later, $1.5x10^6$ freshly isolated bone marrow cells from donor animals were intravenously injected into the recipients. Peripheral blood chimerism was assessed 28 days after reconstitution by flow cytometry. Bone marrow chimeras were used in experiments after eight to twelve weeks of reconstitution.

II.II.IX. Preparation of single cell suspensions and flow cytometry

BALF: The BALF was harvested as described above. After centrifugation at 1350 rpm for 5 min at 4°C, cell pellets were resuspended in 100 µl antibody mix and incubated for 30 – 45 min. After washing with FACS buffer (1x PBS with 0.5% BSA and 2 mM EDTA), life/death staining was performed using 100 µl DRAQ7 (pre-diluted 1:1000 in FACS buffer) for 5 min at RT in the dark.

Lung: The more segmented lobe of the lung was miced and enzymatically digested in 3 ml HBSS supplemented with 10% FCS (Sigma-Aldrich), 0.2 mg/ml collagenase IV (Sigma-Aldrich) and 0.05 mg/ml DNase I (Sigma-Aldrich) for 45 min at 37°C. Afterwards, the tissue pieces were homogenized using a 19G syringe and filtered through a 70 µm strainer prior to washing with FACS buffer. After centrifugation for 5 min at 1350 rpm and 4°C, the cells were stained in 200 µl antibody mix for 45 min at 4°C. The cells were washed and red blood cell lysis was performed incubating the cells with 1 ml of red blood cell lysis buffer for 5 min at RT. After centrifugation for 5 min at 1350 rpm and 4°C, life/death staining was performed incubating the cells in 200 µl DRAQ7 (pre-diluted 1:100 in FACS buffer) for 5 min at RT.

Blood: 150 µl blood was collected into 3 ml of 1x PBS supplemented with 10 mM EDTA, centrifuged and stained for 35 min in 150 µl antibody mix at 4°C. Red blood cell lysis was performed twice for 5 min at RT prior to life/death stain with 150 µl pre-diluted DRAQ7.

Bone marrow: Femur and tibia of one mouse leg were flushed with 5 ml 1x PBS with 10 mM EDTA, centrifuged and stained with 350 µl antibody mix for 1 h at 4°C. Red blood cell lysis was performed once prior to life/death staining in 350 µl DRAQ7.

Prior to acquisition at the FACS A5 Symphony (Becton Dickinson), all samples were washed and resuspended in FACS buffer. In case of lung and bone marrow, the samples were once more filtered through a 70 µm strainer. FACS data were analysed using FlowJo v10.8.1 (Becton Dickinson).

II.II.X. Cell sorting by FACS

Cell sorting was performed using an ARIAIII (Becton Dickinson) instrument. Briefly, cells from the BALF were isolated and subsequently stained with 150 µl antibody mix prior to life/death stain with DRAQ7 as described above. Cell sorting was performed using a 100 µm nozzle into cooled 1.5 ml reaction tubes containing FACS buffer or complete RPMI1640 medium.

II.II.XI. RNA detection by flow cytometry

BALFs of three stimulated mice were pooled in 15 ml falcons, centrifuged at 1350 rpm for 5 min at 4°C and resuspended in 300 µl antibody mix for surface staining. Samples were transferred to 1.5 ml microcentrifuge tubes provided by the PrimeFlow RNA Assay Kit (ThermoFisher Scientific) and stained for 35 min at 4° C. Afterwards, life/death staining was performed in 300 µl of Zombie NIR Fixable Viability dye (1:1000 in PBS, BioLegend) for 10 min at RT. In further steps, samples were handled according to manufacturer's instructions.

II.II.XII. *Ex vivo* LPS restimulation and cytokine assessment

BALF of stimulated mice was collected into 15 ml tubes, centrifuged and then resuspended in 1 ml complete RPMI1640 cell culture medium. Cells were manually counted and $0.2x10^5$ cells were seeded into 48 well plates in 500 µl medium. Resting the plates for 2 h at 37°C and 5% CO_2 allowed selection of macrophages by adherence prior to washing away non-adherent cells. Remaining macrophages were subsequently stimulated with 10 ng/ml LPS (Sigma-Aldrich) in a final volume of 500 µl. For cytokine secretion assessment, the cell culture supernatant was harvested and snap frozen after 24 h of LPS stimulation. For further analysis, supernatants were thawn on ice and centrifuged for 5 min at 10000 rpm at 4°C to remove debris. IL-6 protein levels were measured by ELISA (Thermo Fisher) according to manufacturer's protocols.

II.II.XIII. *Ex vivo* phagocytosis assay

pHrodo *S. aureus* bioparticles (Sartorius) were prepared according to manufacturer's instructions. Briefly, the bioparticles were resuspended in ddH_20 and then sonicated for 10 min. Lavage fluid of PBS or β-glucan inoculated mice was harvested at day 7, centrifuged and resuspended in 250 µl complete RPMI1640 cell culture medium. After manual counting, cells were seeded with $0.2 x10^5$ cells per well in a 96 well plate and macrophages were selected by adherence as described above. After 2 h of resting, medium was exchanged to 100 µl medium or 100 µl medium containing 2.5 µg pHrodo *S. aureus* bioparticles. Phagocytosis was monitored every 10 min for 7 h in total using the microscopy-based approach of the Incucyte instrument (Sartorius). Analysis was performed using the Incucyte basic analyzer software in standard mode with two channels (phase and orange).

II.II.XIV. Broncho-alveolar lung organoid (BALO) generation and fibrosis induction

BALOs were generated as previously described (100). Briefly, $CD31^{+}CD45^{+}CD16/32^{+}$ cells were depleted from lung single cell suspensions of adult wildtype mice using antibody-coupled magnetic beads. From the $CD31^{-}CD45^{-}CD16/32^{-}$ fraction, $EpCAM^{high}CD24^{low}Sca\text{-}1^{+}$ BASC and $EpCAM^{-}Sca\text{-}1^{+}$ rMC were flow cytometrically purified, counted and pooled. $5x10^{3}$ BASC and $1.8x10^{4}$ rMC were mixed with growth factor reduced Matrigel (Corning) and seeded on 12 mm cell culture inserts in a 24 well plate. The wells were filled with complete α-MEM organoid medium and cultured for three weeks at 37°C with 5% CO_2. For the BALO – AM co-cultures, $2.5x10^{4}$ AM of day seven PBS or β-glucan inoculated wildtype mice were seeded on top of the Matrigel layer of day 21 BALOs. The BALO – AM cultures were incubated for 24 h and then subsequently treated with medium containing either PBS or 1.05 ng/ml TGF-β (Miltenyi Biotech) for two days to induce fibrosis. Organoids were fixed in 4% PFA for 15 min, permeabilized and blocked over night in 1x PBS with 0.5% Triton-X-100 (ThermoScientific) and 5% donkey serum (PAN Biotech) before primary and secondary antibodies were incubated overnight.

II.II.XV. Filipin, BODIPY-cholesterol and TUNEL staining

$5\text{-}8x10^{4}$ BALF cells were resuspended in complete RPMI1640 cell culture medium and seeded onto 10 mm sterile glass coverslips. After 3 h of adhering at 37°C, cells were washed with 1x PBS and subsequently fixed in 4% PFA for 30 min. After washing, cells were incubated in 100 mM glycine for 10 min and subsequently incubated with 3% BSA containing 50 µg/ml Filipin (Sigma-Aldrich) for 2 h. Cells were washed and stained with antibodies and DRAQ5 (ThermoFisher Scientific).

For BODIPY-cholesterol, BALF cells were seeded in equal numbers into 8 well chamber slides and incubated for 3 h at 37°C. After adhering, cells were treated with complete RPMI1640 cell culture medium supplemented with 0.5 µM BODIPY-cholesterol (Biomol) overnight. Cells were washed with 1x PBS for three times and then fixed for 20 min in 4% PFA. Washing steps were repeated and cells were permeabilized and immunostained.

For TUNEL staining, cells were treated according to manufacturer's instructions and immunofluorescence was performed after TUNEL staining.

II.II.XVI. Immunofluorescence staining and imaging

Trans-cardial perfusion was performed on anesthetized mice using 10 ml ice cold 1x PBS. The lung was infiltrated with 1 ml 50% OCT in 1x PBS via the trachea, removed and fixed for 6 h in 1.3% PFA at 4°C. Lungs were subsequently washed, dehydrated in 10%, 20% and 30%

sucrose for 24 h at 4°C. Lungs were then embedded in OCT and sections of 5 µm were prepared for immunohistochemistry.

Frozen tissue sections on coverslips were dried on drierite beads for 5 min and subsequently fixed on ice cold acetone for 10 min and washed twice with 0.001% Tween-PBS. After permeabilization for 20 min with 0.2% Triton-X-100, sections were washed twice in 1x PBS and photobleached (101). Afterwards, sections were blocked in 3% BSA in 1x PBS for 1 h at RT. Primary antibodies diluted in 0.5% BSA solution were incubated overnight at 4°C. Coverslips were washed three times with 1x PBS and then incubated for 1 h at RT in 0.5% BSA solution containing secondary antibodies and nuclear stain. Coverslips were washed three times in 1x PBS and then mounted on glass slides using mounting medium. If fluorescently labelled primary antibodies were used, these were added after secondary antibody stain and incubated for 2 h at RT. For the BALF, cells seeded onto coverslips, fixed with 4% PFA and permeabilzed without subsequent photobleaching. Images were acquired with a Zeiss LSM 880 Airyscan using a 60x oil immersion objective with a z-spacing of 500 nm and four (405, 488, 561, 640 nm) lasers. Neutrophils and eosinophils were excluded based on their nuclear shape during acquisition.

II.II.XVII. Image analysis

For image analysis of immunostained BALF cells, a customized CellProfiler pipeline was established. In the first detection step, a mask detecting cells based on their nuclear stain was created before adding a mask of all SiglecF$^+$ objects. Both masks were merged and a second detection step was added to distinguish between CD11b$^-$ AM and ApoE$^+$CD11$^+$ AM. Mean intensities of the fluorescent signals were calculated and used for further analysis. For tissue sections, analysis was performed using QuPath following a similar cell identification strategy and signal intensity calculation (102).

For fibrosis quantification in the BALO – AM co-cultures, the area of the organoid was first determined by the nuclear DAPI stain in QuPath. To detect SMA positive areas, a pixel classifier was trained using 5-10 exemplary regions of SMA signal and background spots. The trained model was used to analyse all images to quantify SMA$^+$ area of each organoid.

For the BODIPY-cholesterol image analysis, full z-stacks of single ApoE$^+$CD11b$^+$ AM and CD11b$^-$ AM were uploaded to Fiji and analysed using the JACoP plugin (103). Five randomly selected pictures from each condition were used to set the thresholds and then applied to all images. Afterwards, the percentage of co-localization and overlapping of BODIPY-cholesterol with cell organelle signals was calculated.

II.II.XVIII. CODEX workflow and analysis

Seven days after intranasal PBS or β-glucan exposure, BALF cells from wildtype mice were seeded onto CODEX coverslips and rested for 2 h. Afterwards, cells were fixed with 4% PFA for 20 min and permeabilized for 20 min with 0.2% Triton-X-100. Cells were washed and subsequently stained with a 17-plex CODEX antibody panel overnight at 4°C. The next day, samples were washed with staining buffer, fixed in ice cold methanol and washed before a final fixation step with BS3 crosslinker (Sigma-Aldrich). Coverslips were stored in CODEX storage buffer (Akoya Biosciences) at 4°C until imaging. Manufacturer's instructions were followed to detect the antibodies in multiple cycles using the corresponding fluorescently labelled reporters. Images were acquired with a Zeiss Axio Observer widefield microscope using a 20x air objective (NA 0.85), a z-spacing of 1.5 µm and four (405, 488, 568, 647 nm) channels. Images were processed with the CODEX Processor v1.7 (Akoya Biosciences) including background subtraction, stitching, shading correction, deconvolution and cell segmentation. DAPI and ATPase I membrane staining were used to define cell borders, while cell annotation was performed in CODEX MAV (Akoya Biosciences) following a similar gating strategy as for flow cytometry.

II.II.XIX. Single cell RNA sequencing by Seq-Well and data analysis

Seq-Well arrays and libraries were prepared as previously described (104). Briefly, $1.1x10^5$ barcoded mRNA capture beads were loaded in bead loading buffer after array preparation. The buffer was replaced by RPMI1640 medium supplemented with 10% FCS and incubated for 10 min. The medium was then replaced by $2\text{-}3x10^4$ sorted $CD45^+SSC^{hi}Lin^-DRAQ7^-$ alveolar macrophages and rocked for 10 min. After sealing, the arrays were incubated for 30 min at 37°C followed by incubations with guanidinium-based lysis buffer and hybrisation buffer. The mRNA capture beads were collected and reverse transcription was performed on the bead pellet using a Maxima Reverse Transcriptase reaction (ThermoFisher). After washing, excessive primers were removed by exonuclease ExoI incubation and reverse transcribed cDNA libraries were amplified by PCR. $2\text{-}4x10^4$ beads were pooled and cleaned by AMPure XP beads before assessing the cDNA quality using a High Sensitivity D5000 assay (Agilent) for Tapestation 4200 (Agilent). After annealing and tagmentation, Illumina indices (Illumina) were added to the product by PCR and cleaned by AMPure XP beads before assessing the final library quality again. Sequencing was performed using the High Output v2.1 chemistry (Illumina) on a NextSeq500 system (Illumina) with 21 cycles for custom Drop-Seq Read 1 primer, 8 cycles for the i7 index and 61 cycles for Read 2. Single-cell sequencing data were first demultiplexed using bcl2fastq2 (v2.20) (Illumina) and then pre-processed and mapped to the mouse reference genome mm10 using the Drop-seq pipeline (105). Cells with <500 genes per cell, doublets with >3000 genes per cell and cells with >10% mitochondrial content were

excluded. The Seurat package (v4.1.1) was used for cell clustering analysis (106). After log normalization by factor 10.000, PCA was performed using the top 2000 variable genes for linear dimensionality reduction. The first 10 PCA were used for cell clustering by the Louvain algorithm. The cluster resolution parameter of the FindClusters function was set to 0.25 to obtain 5 major clusters after dimensionality reduction by UMAP. The threshold of the Wilcoxon rank sum test of the FindAllMarkers function was set to >0.25 to identify differentially expressed genes.

Data can be accessed via the NCBI GEO database under number GSE211575 and https://github.com/SchlitzerLab/Trained_immunity_2022.

II.II.XX. Statistics

Statistical analysis and comparison was performed using Prism 10 (GraphPad). Data are shown as mean ± SD. For each experiment, the applied significance test is indicated at the end of the figure legend. In most cases, statistical significance was assessed using an unpaired student's t-test or an ordinary one-way ANOVA with Tukey's multiple comparisons. A *P* value < 0.05 was considered as statistically significant (*P < 0.05, **P < 0.01, ***P < 0.001, ****P < 0.0001). Mice were randomly allocated to the control or treatment groups by the investigator. Mice numbers are indicated as "n" in the figure legends, as well as the number of independent experiments.

III. Results

III.I. Intranasal β-glucan exposure reshapes the pulmonary alveolar macrophage compartment

The lung is one of the largest barrier tissues of our body constantly exposed to a plethora of environmental factors, such as pollutants, allergens and pathogens. Mononuclear phagocytes like DCs, macrophages and monocytes act as the first line of defence against invading airborne particles ensuring efficient pathogen clearance, induction of adaptive immune responses and inflammation resolution. To investigate how environmental stressors influence the composition of the highly heterogeneous mononuclear phagocyte network, we first aimed to develop a multicolour flow cytometry panel and a gating strategy that allows correct identification of all prominent myeloid subsets in the lung. Lungs from naïve C57BL/6J (WT) mice were digested and subsequently stained with a mix of different mononuclear phagocyte specific fluorophore labelled antibodies (**Figure 3A**). After selection of singlets by size and granularity, immune cells were selected by CD45 expression. DRAQ7$^+$ dead cells and cells of lymphocyte origin (Lin$^+$; CD19, B220, Nk1.1, CD90, Nkp46, TCR-β) were excluded. Neutrophils were identified by their expression of Ly6g, while macrophages were gated using CD64 and MerTk. Pulmonary macrophages were subsequently separated into alveolar (AM; Ly6g$^-$ CD64$^+$MerTk$^+$SiglecF$^+$CD11b$^-$) and interstitial macrophages (IM; Ly6g$^-$CD64$^+$MerTk$^+$ SiglecF$^-$ CD11b$^+$). From the CD64$^-$MerTk$^-$ fraction, DCs were identified by their high expression level of MHC-II and CD11c and further subdivided into cDC1 (Ly6g$^-$CD64$^-$MerTk$^-$MHC-II$^+$CD11c$^+$CD11b$^-$) and cDC2/DC3 (Ly6g$^-$CD64$^-$MerTk$^-$MHC-II$^+$CD11c$^+$CD11b$^+$). From the remaining cells, eosinophils (Ly6g$^-$CD64$^-$MerTk$^-$MHC-II$^-$CD11c$^-$CD11b$^+$SiglecF$^+$) and monocytes (Ly6g$^-$CD64$^-$MerTk$^-$MHC-II$^-$CD11c$^-$CD11b$^+$SiglecF$^-$) were split based on SiglecF. Differential expression of CD43 and Ly6c allowed characterization of Ly6c$^+$ monocytes (Ly6g$^-$ CD64$^-$MerTk$^-$MHC-II$^-$CD11c$^-$CD11b$^+$SiglecF$^-$Ly6c$^+$CD43$^-$) and Ly6c$^-$ monocytes (Ly6g$^-$CD64$^-$ MerTk$^-$MHC-II$^-$CD11c$^-$CD11b$^+$SiglecF$^-$Ly6c$^-$CD43$^+$) within the monocyte pool (107).

After establishing a reliable tool to characterize mononuclear phagocytes in the lung, a reductionist mouse model of a single intranasal dose of 200 µg β-glucan was set up to mimic environmental exposure and to investigate how this exposure is integrated on a cellular and molecular level (**Figure 3B**). We stimulated WT mice intranasally with PBS or β-glucan and performed flow cytometry seven days after exposure on the lung tissue using the surface marker panel shown in Figure 3A. Unsupervised clustering of immune cells according to surface marker expression was performed as previously described (108) and confirmed the cell type identification of our manual gating approach. This analysis revelaed a population of cells specifically present in the β-glucan treated animals clustering close to IM and AM (**Figure**

3C). Further investigation confirmed that these cells express classical alveolar macrophage markers like CD64, CD11c, MerTk and SiglecF, but also high levels of CD11b (**Figure 3C, D**) and were therefore termed CD11b$^+$ AM. As AM can be exclusively found in the alveolar space of the lung (6), we performed a bronchoalveolar lavage of the lung, which allows separation of the air-exposed space and the insterstitium. Flow cytometric analysis of the broncho-alveolar lavage fluid (BALF) of day seven PBS or β-glucan experienced WT mice confirmed that CD11b$^+$ AM are present in the BALF and belong to the alveolar compartment (**Figure 3E**). To investigate the cellular dynamics over time, the BALF of β-glucan experienced WT mice was harvested at different time points after exposure and analysed by flow cytometry (**Figure 3B**). Statistically significant numbers of CD11b$^+$ AM were first detected at day three after β-glucan exposure. Absolute numbers of CD11b$^+$ AM peaked at day seven contributing 5.49±2% to the AM pool and gradually declined until day 21 after inoculation (**Figure 3F, G**). In line with these findings, an overall increase in AM numbers in the BALF at day seven after β-glucan was observed (**Figure 3H**). Additionally, the β-glucan mediated emergence of CD11b$^+$ AM was accompanied by a transient influx of neutrophils and eosinophils into the alveolar space up to three days after exposure (**Figure 3I-K**). Taken together, these findings demonstrate that CD11b$^+$ AM are generated as a cellular response to a β-glucan mediated environmental adaptation reshaping the alveolar macrophage pool.

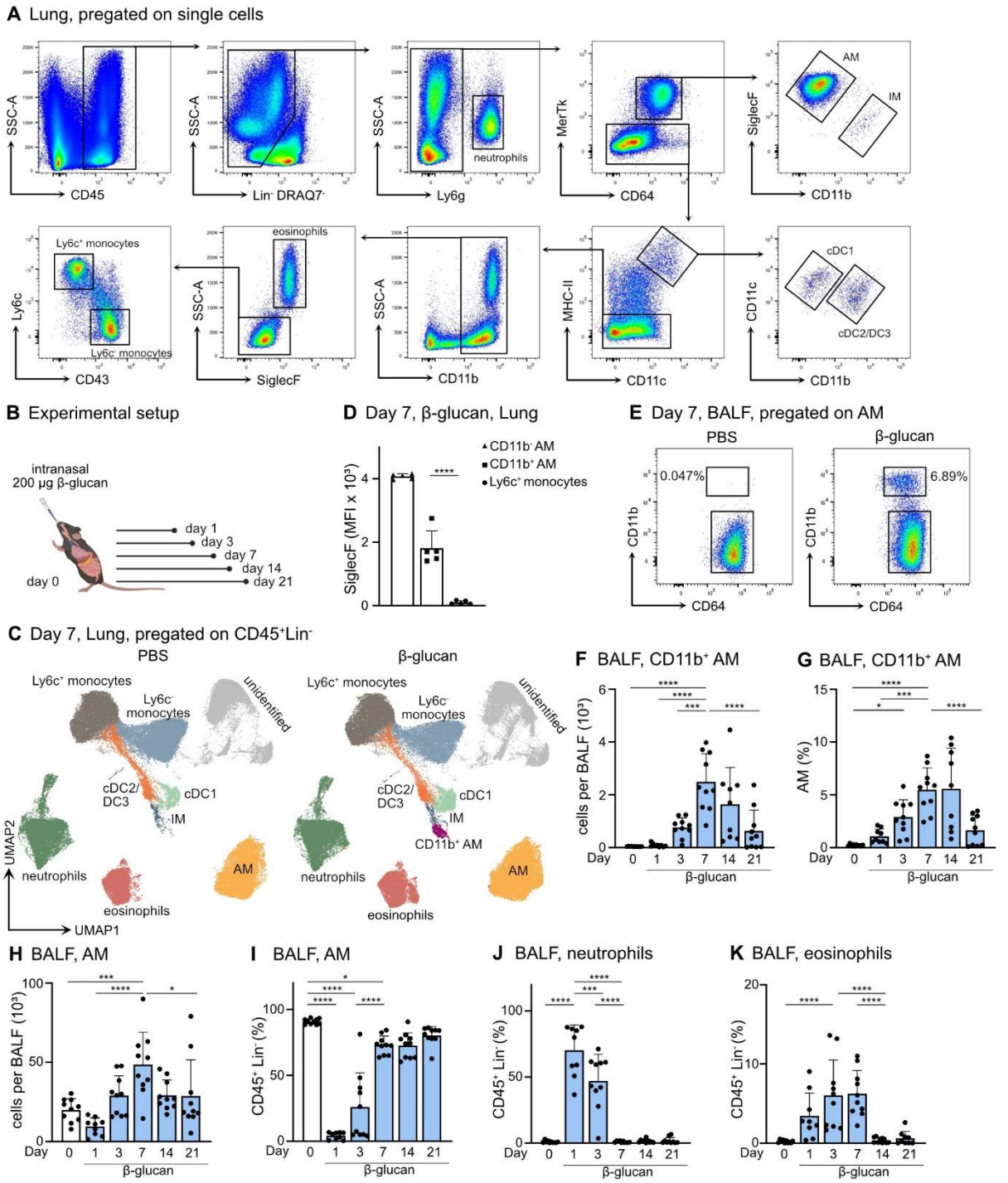

Figure 3: Intranasal β-glucan exposure reshapes the pulmonary mononuclear phagocyte compartment by the recruitment of CD11b⁺ AM to the alveolar space. (A) Representative gating strategy to identify granulocyte, DC, monocyte and macrophage subsets in the murine steady state lung by flow cytometry. Lung tissue from naïve C57BL/6J (WT) mice was enzymatically digested, stained with an antibody cocktail and subsequently 1.5x10^6 events were acquired. **(B)** Experimental setup of intranasal β-glucan inoculation. Lung tissue or BALF were harvested at indicated time points after β-glucan. **(C)** UMAP representation of 7.5x10^4 CD45$^+$ DRAQ7$^-$ Lin$^-$(Ly6g, B220, CD19, CD3ε, Nk1.1, Ter-119) immune cells of the WT lung seven days after intranasal β-glucan by flow cytometry using the surface marker panel shown in (A) (n=3 mice pooled per condition). **(D)** Mean fluorescence intensity (MFI) of SiglecF expression on indicated cell subsets in the lung seven days post stimulation with β-glucan (n=5 mice, two independent experiments). *Figure legend continues on next page.*

Figure 1: (E) Representative flow cytometry gating strategy pre-gated on AM to define CD11b$^+$ AM in the BALF seven days after intranasal PBS or β-glucan exposure. **(F, G)** Flow cytometric quantification of CD11b$^+$ AM numbers (F) and frequency among AM (G) in the BALF in a time course from 1 to 21 days post β-glucan stimulation of WT mice (n=9-10 mice, two independent experiments). **(H)** Quantification of absolute AM numbers in the BALF in a time course from 1 to 21 days post β-glucan stimulation of WT mice (n=9-10 mice, two independent experiments). **(I-K)** Flow cytometric quantification of AM (I), neutrophil (J) and eosinophil (K) frequencies among CD45$^+$Lin$^-$ cells in the BALF in a time course from 1 to 21 days post β-glucan stimulation of WT mice (n=9-10 mice, two independent experiments). Data are depicted as mean ±SD, (D, F-K) ordinary one-way ANOVA with Tukey's multiple comparisons.

III.II. CD11b$^+$ AM are enriched for genes associated with an inflammatory monocyte-derived macrophage phenotype

To characterize the phenotype and gene expression profile of macrophages upon environmental adaptation in more depth, CD45$^+$Lin$^-$SSC^{hi} cells from C57BL/6J mice were sorted from the BALF seven days after PBS or β-glucan exposure and further analysed by single-cell RNA sequencing (**Figure 4A-E**). After data processing and quality control (see methods, chapter II.II.XIX.), 10202 cells were used for downstream analysis. Using dimensionality reduction and unsupervised clustering, five distinct clusters were identified (**Figure 4A**). Expression of the marker genes *SiglecF* and *Itgax* across all five clusters confirmed their AM identity (**Figure 4B, C**) (35). To annotate the five different cluster, the top ten highly expressed genes per cluster were investigated and compared to published data sets. The gene expression pattern of cluster 0 and cluster 1 revealed genes associated with a resident AM signature, such as *Ear2*, *Wfdc21* and *Hmox1* (35, 109). Genes associated with proliferation like *Top2a*, *Mki67* and *Birc5* were abundantly expressed in cluster 2, therefore here referred to as proliferative AM (110). Cluster 3, here labelled as ApoE$^+$ AM, expressed *Apoe*, *Gpnmb*, *Spp1*, *Cd63* and *Trem2*, which have been previously linked to monocyte-derived macrophages with an inflammatory and lipid associated phenotype (12, 99). Based on their expression of interferon-stimulated genes (ISG) like *Ifit2*, *Ifit3*, *Ifi204*, and *Isg15*, cluster 4 was identified as ISG$^+$ AM (**Figure 4D**). To assess if one of the clusters was exclusively linked to the environmental adaptation, the cells were split by their stimulation condition (**Figure 4E-F**). We observed that ApoE$^+$ AM were only present in the BALF of mice that have been exposed to β-glucan seven days prior. Furthermore, the relative contribution of each of the stimuli to the cell clusters was calculated showing that the emergence of ApoE$^+$ AM is accompanied by a reduction in proliferative AM, while the resident and ISG$^+$ AM do not change (**Figure 4G**). In comparison to the previous results (**Figure 3C-F**), we hypothesized that the CD11b$^+$ AM previously identified by flow cytometry correspond to the ApoE$^+$ AM from the single-cell data set. Using fluorescently labelled probes, we detected *Apoe* RNA expression in the BALF of WT mice seven days after environmental adaptation by flow cytometry. This analysis

demonstrated that *Apoe* and CD11b were indeed co-expressed in the β-glucan elicited population, therefore terming these cells ApoE^{+}CD11b^{+} AM (**Figure 4H**). Finally, we performed co-detection by indexing (CODEX) multiparameter imaging to visualize this co-expression on a protein level in AM selected by adherence from the BALF of PBS or β-glucan experienced WT mice (111). In concordance with the previous results, ApoE and CD11b protein expression was not detectable in resident AM in the PBS condition, but in the β-glucan elicited AM population (**Figure 4I**). In conclusion, ApoE^{+}CD11b^{+} AM with a pro-inflammatory and lipid associated gene signature are recruited to the alveolar space and retained for at least 21 days upon β-glucan mediated environmental adaptation.

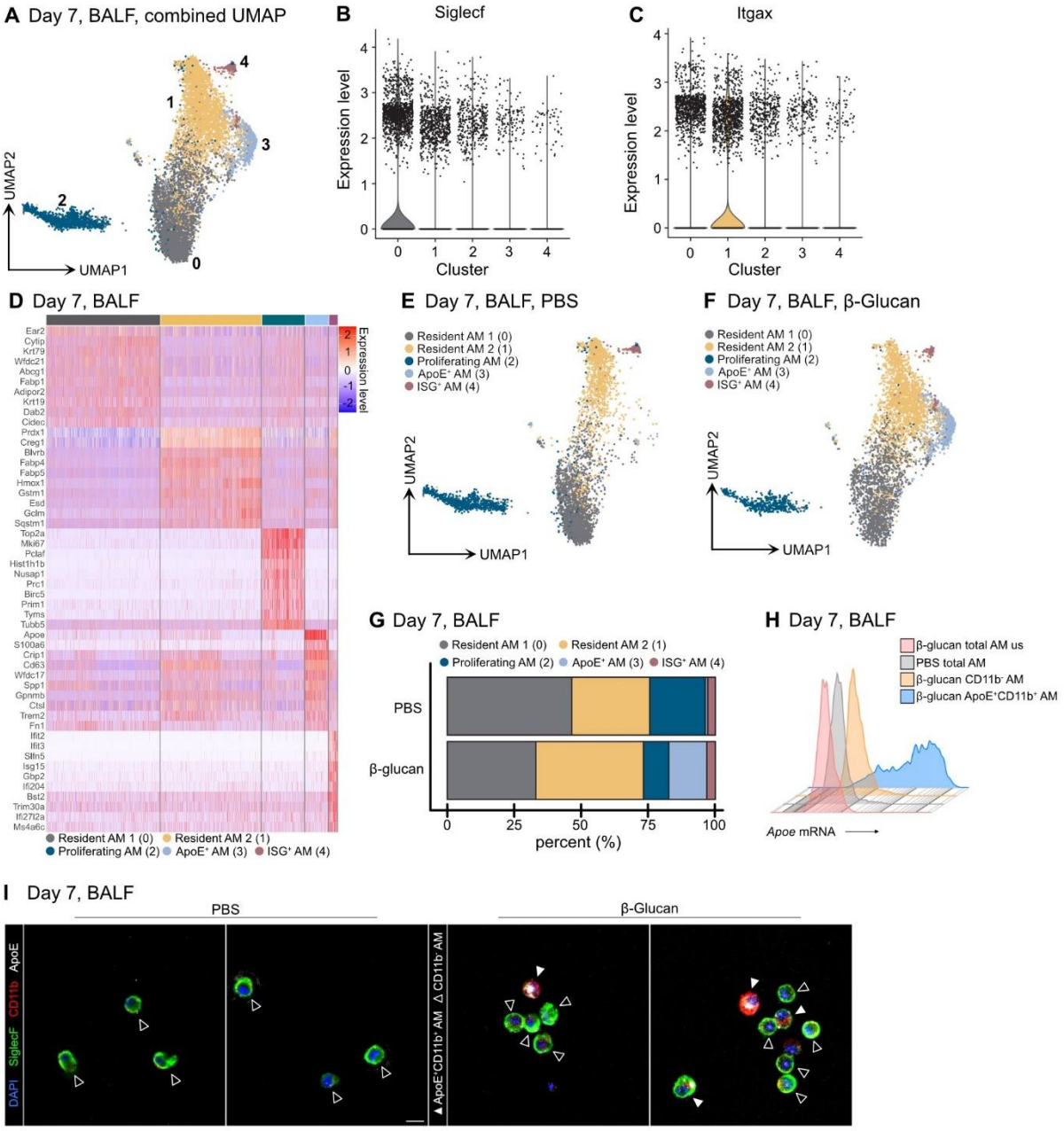

Figure 4: CD11b⁺ AM express high levels of Apolipoprotein E and are enriched for genes associated with an inflammatory monocyte-derived macrophage phenotype. (A-G) Single-cell RNA sequencing of the BALF of male C57BL/6 (WT) mice after intranasal stimulation with PBS or β-glucan. Seven days after exposure, the BALF of three animals was pooled and sorted for SSC^{hi}, Lin^{-} (B220, CD19, CD3ε, Nk1.1,Ter-119), DRAQ7^{-} singlets (n=3 mice per condition, 10202 cells). (A) Dimensionality reduction by UMAP and unsupervised clustering using the Louvain algorithm identified five distinct clusters. (B-C) Violin plot of *Siglecf* (B) and *Itgax* (C) RNA expression per cluster. (D) Heatmap of top ten highly expressed genes for each of the five clusters. (E, F) UMAP from (A) separated by PBS (C, n=4845 cells) or β-glucan (D, n=5357 cells) condition. (G) Percentage of contribution of the five annotated clusters to overall cells split by conditions. **(H)** Detection of *Apoe* mRNA expression in AM subsets of the BALF seven days after intranasal PBS or β-glucan stimulation of WT mice by flow cytometry (n=3 mice pooled per group, one out of two independent experiments shown). **(I)** AM from PBS or β-glucan treated WT mice were selected by adherence from the BALF seven days after intranasal inoculation and subsequently stained with a 17-plex CODEX antibody panel. AM subsets were identified using the overlay images of the stained surface markers. Filled arrows indicate ApoE^{+}CD11b^{+} AM, while open arrows indicate CD11b^{-} AM. Scale bar represents 10 µm.

III.III. Monocyte-derived ApoE^{+}CD11b^{+} AM are long-lived and depend on CCR2

Previous studies were published showing a recruitment of monocyte-derived macrophages to the alveolar space upon acute or chronic inflammation (12, 30, 42). Our single-cell RNA sequencing analysis demonstrated that ApoE^{+}CD11b^{+} AM were enriched for genes of monocyte-derived macrophages with an inflammatory and lipid associated phenotype (**Figure 4D**). To investigate if the β-glucan elicited ApoE^{+}CD11b^{+} AM were monocyte-derived, we first analysed the influx of Ly6c^{+} monocytes into the alveolar space by flow cytometry. This revealed that Ly6c^{+} monocytes are significantly more abundant in the alveolar space three days after β-glucan exposure with slowly decreasing numbers until day 21 (**Figure 5A, B**). Additionally, we utilized the Ms4a3^{Cre}R26^{tdTomato} fate mapper mouse model, where the progeny of granulocyte-monocyte progenitors (GMP) in the bone marrow can be traced by tdTomato labelling (13). Analyzing the BALF of PBS or β-glucan experienced Ms4a3^{Cre}R26^{tdTomato} mice by flow cytometry, we observed that 86%±7.8% of ApoE^{+}CD11b^{+} AM were labelled by tdTomato supporting their monocyte origin (**Figure 5C**). In concordance with previous publications, monocytes were exclusively labelled by tdTomato, while only part of the resident CD11b^{-} AM pool was labelled (**Figure 5C, D**) (13). To understand if there is a systemic recruitment of Ly6c^{+} monocytes to the alveolar space, we assessed the blood and bone marrow after β-glucan mediated environmental adaptation. Ly6c^{+} monocytes were significantly decreased in the blood in line with a recruitment to the lung (**Figure 5E**), while Ly6c^{+} monocyte were increased in the bone marrow (**Figure 5F**) in the β-glucan condition. No effect on common monocyte progenitors (cMOP) was observed in the bone marrow (**Figure 5G**). As the egress of monocytes from the bone marrow to the periphery is dependent on C-C chemokine receptor type 2 (CCR2) (112), we stimulated CCR2$^{-/-}$ mice with PBS or β-glucan and analysed the BALF by flow cytometry. Together with our previous results, we confirmed that ApoE^{+}CD11b^{+} AM stem from monocytes as CCR2$^{-/-}$ mice fail to generate these cells upon environmental adaptation (**Figure 5H**). Our kinetic analysis of ApoE^{+}CD11b^{+} AM at different time points after environmental adaptation showed gradually decreasing numbers from day seven on (**Figure 3F**). Previous publications showed a longevity of monocyte-derived AM up to eight weeks in the alveolar space (12). To investigate if β-glucan elicited ApoE^{+}CD11b^{+} AM undergo cell death after 21 days or are integrated into the pool of resident AM, we utilized an inducible Ms4a3^{CreERT}R26^{tdTomato} mouse line (13). Five and two days before intranasal PBS or β-glucan treatment, Cre recombination was induced by two intraperitoneal injections of tamoxifen followed by flow cytometric analysis at day 28 (**Figure 5I**). As expected, a small fraction of ApoE^{+}CD11b^{+} AM were present in the BALF 28 days after inoculation. Overlay of tdTomato^{+} AM with the ApoE^{+}CD11b^{+} AM and CD11b^{-} AM subsets revealed that the majority of tdTomato^{+} AM fell into the CD11b^{-} AM gate (**Figure 5J**). Furthermore, quantification of tdTomato labelling

directly in the $CD11b^-$ AM population demonstrated no labelling in the PBS inoculated group, while β-glucan treated mice show up to 23.7% of labelling (**Figure 5K**). In summary, these data verify that β-glucan elicited $ApoE^+CD11b^+$ AM stem from monocytes and persist in the alveolar space for at least four weeks while downregulating CD11b and potentially being integrated into the resident AM pool.

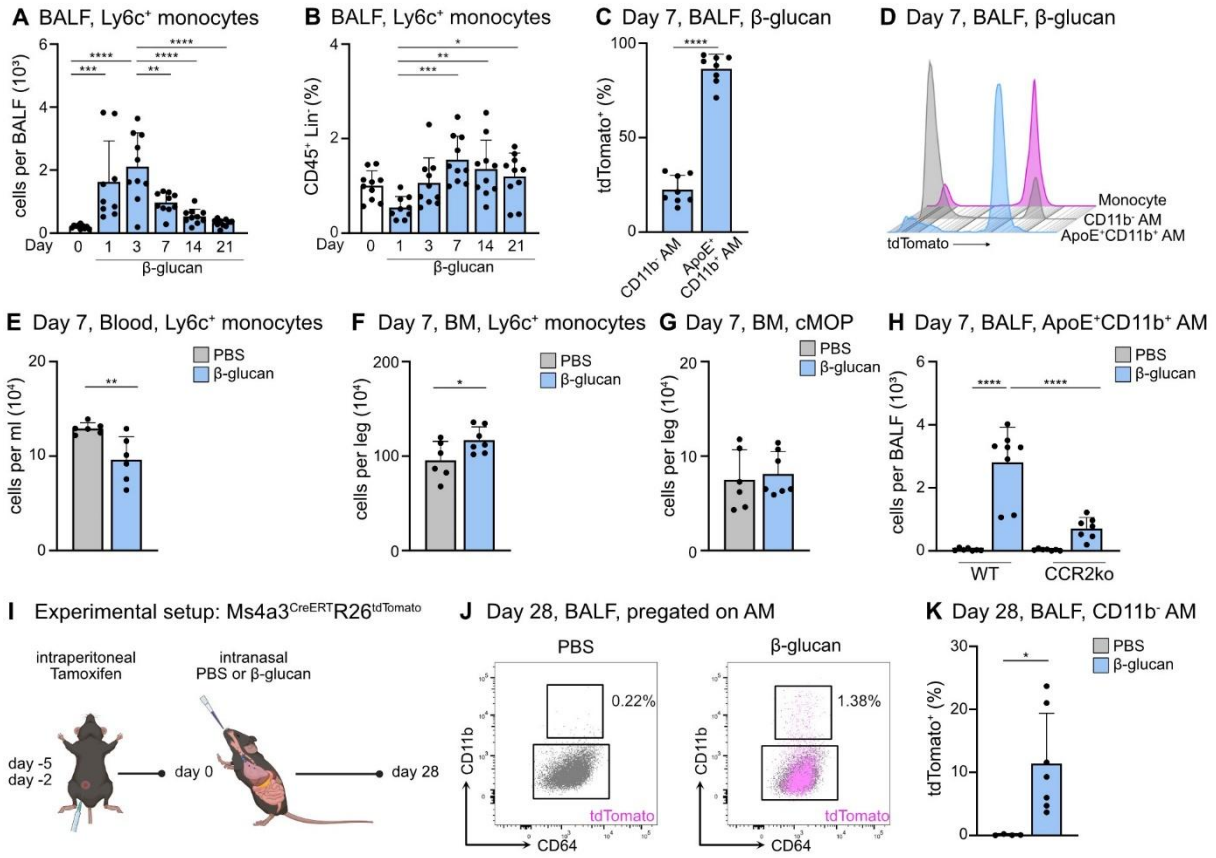

Figure 5: Intranasal β-glucan exposure elicits monocyte-derived ApoE^{+}CD11b^{+} AM in a CCR2-dependent manner, which persist in the alveolar space for at least 4 weeks while downregulating CD11b. (A, B) Flow cytometric quantification of Ly6c^{+} monocytes (CD45^{+}Ly6g^{-}SiglecF^{-} CD64^{int}CD11b^{+}Ly6c^{+}) in absolute numbers (A) and as percent among CD45^{+}Lin^{-} cells (B) in the BALF 1 to 21 days post β-glucan stimulation of WT mice (n=9-10 mice, two independent experiments). **(C, D)** Flow cytometric analysis of the BALF from Ms4a3^{Cre}R26^{tdTomato} mice seven days after intranasal PBS or β-glucan exposure (n=8 mice, two independent experiments). (C) Percentage of tdTomato labelling in ApoE^{+}CD11b^{+} AM and CD11b^{-} AM and respective histogram (D) comparing the proportion of tdTomato labelling in ApoE^{+}CD11b^{+} AM and CD11b^{-} AM to monocytes. **(E-G)** Absolute counts of Ly6c^{+} monocytes in the blood (E), Ly6c^{+} monocytes (F) and cMOP (G) in the bone marrow of WT mice seven days after PBS or β-glucan exposure by flow cytometry (n=6 mice, two independent experiments). **(H)** Flow cytometric quantification of absolute ApoE^{+}CD11b^{+} AM numbers in the BALF seven days after β-glucan exposure in WT or CCR2$^{-/-}$ mice (n=7-8 mice, two independent experiments). **(I)** Experimental setup for tracking ApoE^{+}CD11b^{+} AM over time using the inducible Ms4a3^{CreERT}R26^{tdTomato} mouse model. 1.75 mg tamoxifen were intraperitoneally injected two and five days before intranasal PBS or β-glucan inoculation followed by flow cytometric analysis at day 28. **(J)** Overlay of tdTomato^{+} AM (in pink) with ApoE^{+}CD11b^{+} AM and CD11b^{-} AM subsets 28 days after tamoxifen injection and intranasal stimulation displayed as representative flow cytometry plots. **(K)** Percentage of tdTomato labelling in CD11b^{-} AM 28 days after tamoxifen injection and intranasal stimulation (n=4-7 mice, two independent experiments). Data are depicted as mean ±SD, (A, B, H) ordinary one-way ANOVA with Tukey's multiple comparisons, (E-G, K) unpaired student's *t*-test.

III.IV. ApoE^{+}CD11b^{+} AM release elevated levels of Interleukin-6

In previous publications, monocyte-derived macrophages elicited by respiratory viral infections have been shown to secrete high levels of pro-inflammatory cytokines, such as IL-6, that confer to an enhanced protection from secondary bacterial infections (12). To investigate how the mononuclear phagocytes in the alveolar space functionally adapt to the β-glucan mediated low-grade inflammation, we selected AM from the BALF seven days after inoculation by adherence and restimulated the cells *in vitro* with LPS for 24 h (**Figure 6A**). Quantification of cytokine levels by ELISA showed an enhanced release of IL-6 by AM from mice pretreated with β-glucan (**Figure 6B**). To further link this enhanced IL-6 secretion to an AM subset, we flow cytometrically purified equal numbers of ApoE^{+}CD11b^{+} AM or CD11b^{-} AM from the BALF of PBS or β-glucan experienced mice and restimulated the cells *in vitro* with LPS as described previously (**Figure 6A**). Compared to CD11b^{-} AM, ApoE^{+}CD11b^{+} AM released high levels of IL-6 into the cell culture supernatant, identifying ApoE^{+}CD11b^{+} AM as the major IL-6 source (**Figure 6C**). In line with these findings, AM from CCR2$^{-/-}$ mice displayed a significantly decreased ability to secrete IL-6 upon environmental adaptation prior to *in vitro* LPS restimulation (**Figure 6D**). To further confirm that these functional alterations are a cell intrinsic feature of the macrophages and also stable in a non-inflammatory tissue context, transfer experiments were performed. AM of PBS or β-glucan experienced WT CD45.2 mice were harvested five days after stimulation and intratracheally transferred into naïve WT CD45.1 recipients. Two days post transfer, the BALF of the recipient mice was harvested for analysis (**Figure 6E**). *In vitro* restimulation of the BALF from recipients two days post transfer showed a significantly increased release of IL-6 from mice that have been transferred with AM isolated from β-glucan experienced mice (**Figure 6F**). Additionally, we performed flow cytometry on the BALF of recipient mice two days post transfer to confirm the presence of CD45.2^{+} donor AM on a cellular level (**Figure 6G**). As expected, the majority of ApoE^{+}CD11b^{+} AM stem from CD45.2^{+} donor mice. However, a small proportion of ApoE^{+}CD11b^{+} AM was derived from CD45.1^{+} recipient mice, which can be explained by residual β-glucan present in the transferred cell solution. Taken together, these data demonstrate that monocyte-derived ApoE^{+}CD11b^{+} AM are the primary source of IL-6 upon restimulation with LPS and that this environmental adaptation induced functional rewiring is a cell intrinsic feature restricted to the macrophage compartment.

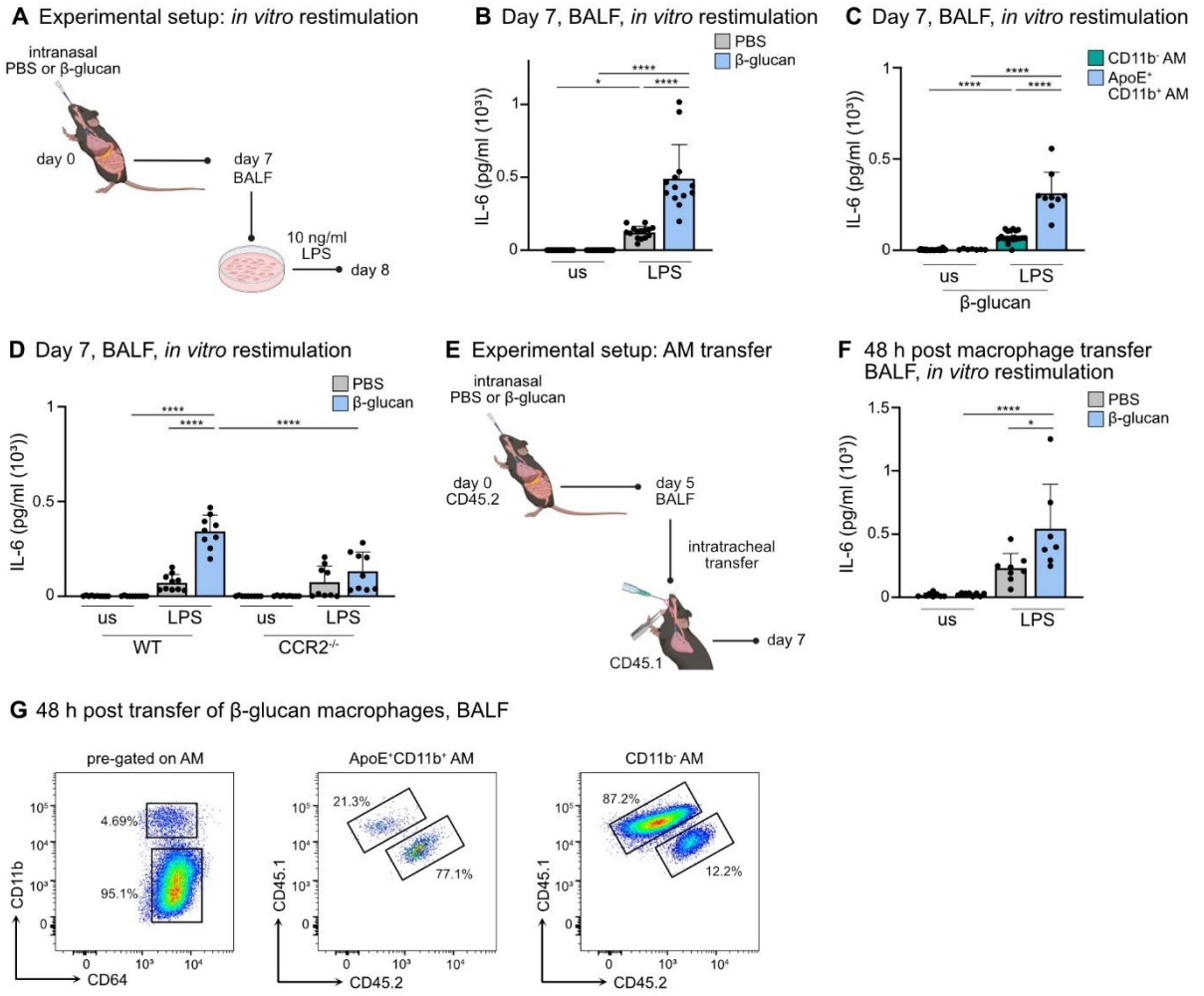

Figure 6: Environmental adaptation induced monocyte-derived ApoE^{+}CD11b^{+} AM release elevated levels of Interleukin-6 as a cell intrinsic feature. (A) Experimental setup of *in vitro* restimulation of PBS or β-glucan experienced AM with LPS. AM are selected by adherence or FACS from the BALF seven days post stimulation and subsequently treated with 10 ng/ml LPS for 24 h. **(B)** Quantification of IL-6 protein levels by ELISA in the cell culture supernatant 24 h after LPS restimulation of WT mice (n=13-15 mice, three individual experiments). **(C)** CD11b^{+}Ms4a3^{+} AM and CD11b^{-}Ms4a3^{-} AM were FACS purified from the pooled BALF of PBS or β-glucan stimulated Ms4a3^{Cre}R26^{tdTomato} mice and seeded with 0.2x10^{5} cells per well prior to LPS restimulation (n= 9 mice for PBS, n= 31 mice for β-glucan, one dot represents the pooled supernatant of two technical replicate wells, here minimum 9 data points per group, two individual experiments). **(D)** Quantification of IL-6 protein levels by ELISA in the cell culture supernatant 24 h after restimulation with LPS of WT and CCR2$^{-/-}$ mice (n=9-10 mice, two individual experiments). **(E)** Experimental setup of AM transfer. PBS or β-glucan experienced CD45.2^{+} WT macrophages were harvested five days after stimulation and intratracheally transferred into CD45.1^{+} mice. Readout per flow cytometry or *in vitro* restimulation at day 7 (48 h after transfer). **(F)** Quantification of IL-6 protein levels by ELISA in the cell culture supernatant 24 h after restimulation with LPS 48 h post AM transfer (n=7-8 mice, two independent experiments). **(G)** Representative flow cytometry plot of the BALF of CD45.1^{+} recipient mice 48 h post transfer of β-glucan experienced CD45.2^{+} donor macrophages. Data are depicted as mean ±SD, (A-D, F) ordinary one-way ANOVA with Tukey's multiple comparisons.

III.V. B-glucan exposure improves bacterial clearance and ameliorates lung fibrosis *in vitro*

Phagocytosis is one of the key features of AM in the lung, as they are involved in clearing excessive mucus and clearance of pathogens. A previous study has shown that influenza A virus induced monocyte-derived macrophages conferred increased bacterial clearance upon a secondary *S. pneumoniae* challenge (12). To assess how the β-glucan mediated environmental adaptation influences phagocytosis, AM from the BALF of PBS or β-glucan adapted WT mice were selected by adherence seven days after inoculation and treated with pHrodo *S. aureus* particles for seven hours *in vitro* (**Figure 7A**). Upon uptake of the particles into the phagosome, the pH-sensitive fluorophore of the particles allows robust detection of phagocytosis$^+$ cells by microscopy. Quantification of phagocytosis$^+$ AM revealed a significant higher phagocytic activity for β-glucan experienced AM compared to the PBS adapted cells (**Figure 7B**) as early as two hours post adding *S. aureus* (**Figure 7C**). Further analysis of the fluorescent intensity showed higher levels of the phagocytosis signal in the β-glucan experienced AM (**Figure 7D, E**) indicating that environmental adaptation enhances the number of particles taken up per cell. To test if this observed increase in phagocytic capacity has a functional effect on bacterial clearance during an acute infection, we infected day seven PBS or β-glucan experienced WT mice with *Legionella pneumophila* and analysed the BALF after two days (**Figure 7F**). Mice previously exposed to β-glucan prior to *Legionella* infection displayed significantly reduced the bacterial burden within the lavage fluid, as well as increased numbers of ApoE$^+$CD11b$^+$ AM (**Figure 7G, H**). Next, we investigated if the β-glucan mediated environmental adaptation has an effect on chronic inflammatory conditions like lung fibrosis. We utilized an *in vitro* broncho-alveolar lung organoid (BALO) model and generated organoids as previously described (100). Flow cytometrically purified lung-resident mesenchymal and bronchioalveolar stem cells were cultivated for 21 days growing into BALOs mimicking the cellular and structural patterning of the bronchioalveolar compartment. Day seven PBS or β-glucan adapted AM from the BALF of inoculated WT mice were added to the lung organoids at day 21, co-cultured for 24 h and then treated with TGF-β for 48 h to promote fibrosis (**Figure 7I**). BALOs treated with TGF-β without AM developed fibrosis, which has been confirmed by high abundance of smooth muscle actin (SMA) in immunohistochemical stainings. BALOs co-cultured with PBS adapted AM and TGF-β treated showed comparable levels of SMA production as BALOs treated only with TGF-β. Interestingly, BALOs co-cultured with β-glucan experienced AM exhibited lower smooth muscle actin (SMA) levels compared to BALOs co-cultured with PBS adapted AM upon TGF-β treatment (**Figure 7J, K**). In summary, these data demonstrate that exposure to β-glucan positively modulates the outcome of an acute

secondary infection by enhanced bacterial clearance and limits disease progression in a lung organoid-based fibrosis model.

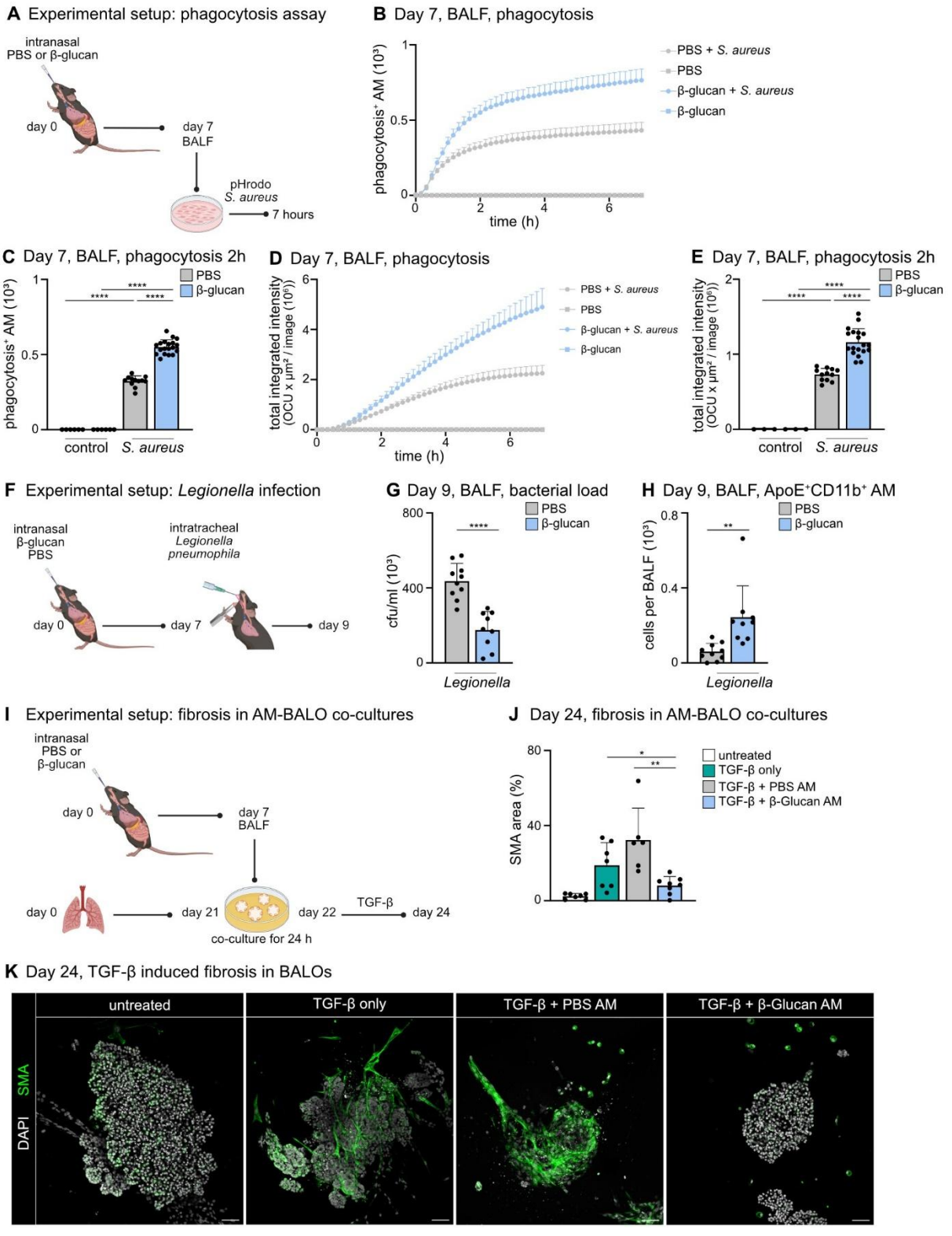

Figure 7: Environmental adaptation induced by β-glucan improves the bacterial clearance *in vitro* and *in vivo* and ameliorates fibrosis in a BAL organoid model. *Figure legend continues on next page.*

Figure 7: (A) Experimental setup of phagocytosis assay. Seven days after intranasal PBS or β-glucan exposure, AM from WT mice were selected by adherence and subsequently incubated with 2.5 µg pHrodo *Staphylococcus aureus* bioparticles. **(B-E)** Representative curve of absolute phagocytosis$^+$ AM numbers (B) and the total integrated intensity (D, OCU x µm²/image) of the phagocytosis signal over the time course of 7 h (here shown as mean ±SD of all technical replicates) and quantification of both parameters 2 h after adding the bioparticles (C, E) (n=3 mice pooled per condition, technical replicates: 6 control wells, 12-19 treated wells per group, one out of two independent experiments shown). **(F)** Experimental setup of *Legionella* infection. Intranasal PBS or β-glucan stimulation of WT mice at day zero was followed by intratracheal inoculation with 5x10^6 CFU *Legionella pneumophila* at day seven and sacrifice at day 9. **(G, H)** Quantification of bacterial load in BALF (G) and absolute numbers of ApoE$^+$CD11b$^+$ AM (H) by flow cytometry nine days post *Legionella* infection (n=9-10 mice, two independent experiments). **(I)** Experimental setup of fibrosis in AM – BALO co-cultures. Day 21 BALOs were co-cultured with 2.5x10^4 PBS or β-glucan experienced AM from WT mice for 24 h. Afterwards, fibrosis was induced by stimulation of AM – BALO co-cultures with 1.05 ng/ml TGF-β for 48 h prior to fixation and antibody staining. **(J, K)** Quantification of SMA area (J) and representative confocal images (K) of AM – BALO co-cultures (n=6-8 organoids per condition from two replicate wells, one out of two independent experiments shown). Scale bars in (K) represent 50 µm. Data are depicted as mean ±SD, (C, E) ordinary one-way ANOVA with Tukey's multiple comparisons, (G, H) unpaired student's *t*-test, (J) Two-tailed Mann-Whitney test.

III.VI. Recruitment of ApoE$^+$CD11b$^+$ AM is dependent on the Dectin-1 – CARD9 signalling axis

Dectin-1 is the most predominantly expressed receptor for β-glucan on mononuclear phagocytes, although also a variety of other receptors like CD5 and CR3 recognize β-glucan (65, 70). It remains elusive how the recruitment and differentiation of β-glucan elicited ApoE$^+$CD11b$^+$ AM is controlled on a molecular level. We first profiled homeostatic Dectin-1 expression on BALF resident myeloid cells from WT mice by flow cytometry. Dectin-1 expression was mainly restricted to resident CD11b$^-$ AM and a small fraction of monocytes (**Figure 8A**). To assess if Dectin-1 is directly needed for ApoE$^+$CD11b$^+$ AM generation, we stimulated WT or Dectin-1$^{-/-}$ mice intranasally and analysed the BALF seven days after exposure. This data demonstrated that ApoE$^+$CD11b$^+$ AM, but not Ly6c$^+$ monocyte numbers are significantly decreased in absence of Dectin-1, indicating that Dectin-1 is crucial for the generation of ApoE$^+$CD11b$^+$ AM but not for the initial monocyte infiltration (**Figure 8B, C**). To further investigate if immune cell-intrinsic expression of Dectin-1 is determining the ApoE$^+$CD11b$^+$ AM generation, WT or Dectin-1$^{-/-}$ bone marrow was injected into irradiated CD45.1 recipient mice to generate chimeras. Analysis of the Dectin-1$^{-/-}$ chimeras seven days after β-glucan confirmed the significant reduction of ApoE$^+$CD11b$^+$ AM in the BALF (**Figure 8D**) and a high contribution of donor Ly6c$^+$ monocytes in the blood (**Figure 8E**). Activation of Dectin-1 upon ligand binding can lead to the induction of CARD9, which together with other proteins can subsequently induce NF-κB to trigger the production of cytokines like TNF-α and IL-6 (70, 72). To test if the β-glucan induced ApoE$^+$CD11b$^+$ AM infiltration is dependent on

CARD9, CD45.2 WT or CARD9$^{-/-}$ bone marrow was transferred into irradiated CD45.1 recipient mice to generate chimeras. Analysis of CARD9$^{-/-}$ chimeras seven days after β-glucan revealed significant decreased ApoE^{+}CD11b^{+} AM numbers in the BALF (**Figure 8F**) and a high contribution of donor Ly6c^{+} monocytes in the blood (**Figure 8G**). Furthermore, we investigated if abrogation of Dectin-1 or CARD9 signalling also leads to the loss of IL-6 secretion upon environmental adaptation. AM of Dectin-1$^{-/-}$ or CARD9$^{-/-}$ mice were selected by adherence and restimulated *in vitro* with LPS. Similar to our results from CCR2$^{-/-}$ mice, secretion of IL-6 upon restimulation with LPS was abolished in absence of Dectin-1 and CARD9 (**Figure 8H, I**). Together, these data indicate that the generation of ApoE^{+}CD11b^{+} AM is dependent on the Dectin-1 – CARD9 signalling axis and that abrogation of this pathway results in the loss of of ApoE^{+}CD11b^{+} AM and hence IL-6 secretion upon environmental adaptation.

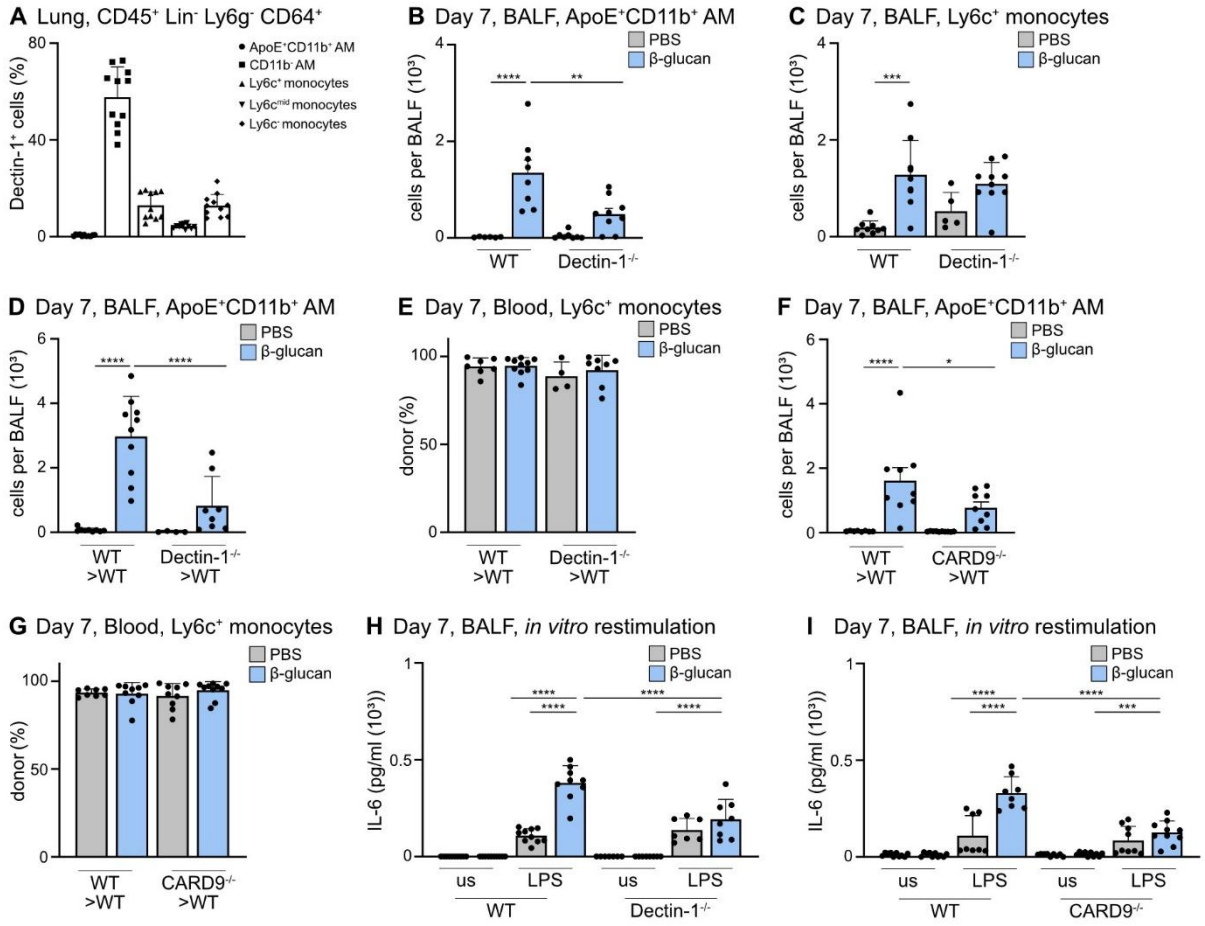

Figure 8: Environmental adaptation induced recruitment of ApoE^{+}CD11b^{+} AM is dependent on the Dectin-1 – CARD9 signalling axis. (A) Percentage of monocyte and macrophage subsets contributing to Dectin-1^{+} myeloid cells pre-gated on CD45^{+}Lin^{-}Ly6g^{-}CD64^{+} cells in the WT mouse lung by flow cytometry (n=11 mice, two independent experiments). **(B, C)** Absolute numbers of ApoE^{+}CD11b^{+} AM (B) and Ly6c^{+} monocytes (C) in the BALF seven days after PBS or β-glucan exposure in WT or Dectin1$^{-/-}$ mice by flow cytometry (n=5-9, two independent experiments). **(D, E)** Absolute ApoE^{+}CD11b^{+} AM numbers (D) in the BALF of WT or Dectin-1$^{-/-}$ bone marrow chimeras and the percentage of donor Ly6c^{+} monocytes (E) assessing the peripheral blood chimerism seven days after PBS or β-glucan stimulation by flow cytometry (n=4-10, two independent experiments). **(F, G)** Absolute ApoE^{+}CD11b^{+} AM numbers (F) in the BALF of WT or CARD9$^{-/-}$ bone marrow chimeras and the percentage of donor Ly6c^{+} monocytes (G) assessing the peripheral blood chimerism seven days after PBS or β-glucan stimulation by flow cytometry (n=8-9 mice, two independent experiments). **(H, I)** Quantification of IL-6 protein levels in the cell culture supernatant of WT and Dectin-1$^{-/-}$ (H, n=7-10 mice, two independent experiments) or WT and CARD9$^{-/-}$ mice (n=9-10 mice, two independent experiments) 24 h after LPS restimulation by ELISA. Data are depicted as mean ±SD, (B-D, F, H, I) ordinary one-way ANOVA with Tukey's multiple comparisons.

III.VII. Paracrine myeloid derived ApoE controls the survival of ApoE^{+}CD11b^{+} AM upon environmental adaptation

ApoE is a prominent lipid carrier in lipoproteins and has been linked to cholesterol efflux and lipid metabolism (82). Differentiation of monocytes into macrophages *in vitro* is linked to secretion of ApoE (113) and also obesity or viral infection induced monocyte-derived

macrophages show high *Apoe* expression (12, 99). However, the role of ApoE in monocyte-derived macrophages upon low-grade inflammation has not been elucidated. Quantification of protein levels in the BALF supernatant of β-glucan stimulated WT mice revealed an early release of ApoE into the alveolar space already at day one after inoculation, coinciding with the influx of $Ly6c^+$ monocytes (**Figure 9A, 5A**). To investigate the functional role of ApoE in our β-glucan elicited moAM, we generated $ApoE^{flox}LysM^{Cre}$ mice to abrogate *Apoe* expression in monocytes and macrophages and subsequently treated them with PBS and β-glucan prior to flow cytometric analysis. $ApoE^+CD11b^+$ AM and $Ly6c^+$ monocyte numbers in the BALF of $ApoE^{flox}LysM^{Cre}$ mice were significantly reduced seven days after treatment compared to the Cre-negative littermates (**Figure 9B, C**). According to our previous observations, $Ly6c^+$ monocytes were decreased in the blood and increased in the bone marrow of control mice, whereas this effect was lost in $ApoE^{flox}LysM^{Cre}$ mice (**Figure 9D, E**). No changes in cMOP numbers were observed in control or $ApoE^{flox}LysM^{Cre}$ mice seven days after β-glucan (**Figure 9F**). Next, it was investigated if paracrine or autocrine ApoE signalling controls the generation of $ApoE^+CD11b^+$ AM upon environmental adaptation, as both have been described previously (114). We generated chimeras that were reconstituted with WT CD45.1 mixed with $ApoE^{flox}LysM^{Cre}$ CD45.2 bone marrow in a 1:1 ratio or the respective WT CD45.1 mixed with WT CD45.2 bone marrow control chimeras. After reconstitution and intranasal stimulation with PBS or β-glucan, BALF and blood were analysed seven days after inoculation by flow cytometry. Both groups of WT/WT and WT/$ApoE^{flox}LysM^{Cre}$ chimeras efficiently generated $ApoE^+CD11b^+$ AM in the alveolar space (**Figure 9G**). Furthermore, both WT $CD45.1^+$ and $ApoE^{flox}LysM^{Cre}$ $CD45.2^+$ cells contributed to the pool of $ApoE^+CD11b^+$ AM in the BALF of WT/$ApoE^{flox}LysM^{Cre}$ chimeras (**Figure 9H**). To control for a reconstitution bias, we investigated the chimerism of $Ly6c^+$ monocytes in the blood and BALF and found a high chimerism efficiency (≥ 90%) and an equal contribution of donors (**Figure 9I**). These results suggest that paracrine production of ApoE by neighbouring myeloid cells is sufficient to rescue the loss of ApoE-deficient $CD11b^+$ AM in WT/$ApoE^{flox}LysM^{Cre}$ chimeras. To elucidate if ApoE controls the initial recruitment or the survival of $ApoE^+CD11b^+$ AM in the alveolar space upon environmental adaptation, $ApoE^{flox}LysM^{Cre}$ mice and their respective control littermates were stimulated with PBS or β-glucan and analysed three days later. Flow cytometric quantification showed no difference in $ApoE^+CD11b^+$ AM and $Ly6c^+$ monocyte numbers between control and $ApoE^{flox}LysM^{Cre}$ mice (**Figure 9J, K**). Together, these data demonstrate that paracrine myeloid-derived ApoE controls the maintenance and survival of $ApoE^+CD11b^+$ AM in the alveolar space and not the initial recruitment and differentiation upon β-glucan mediated environmental adaptation.

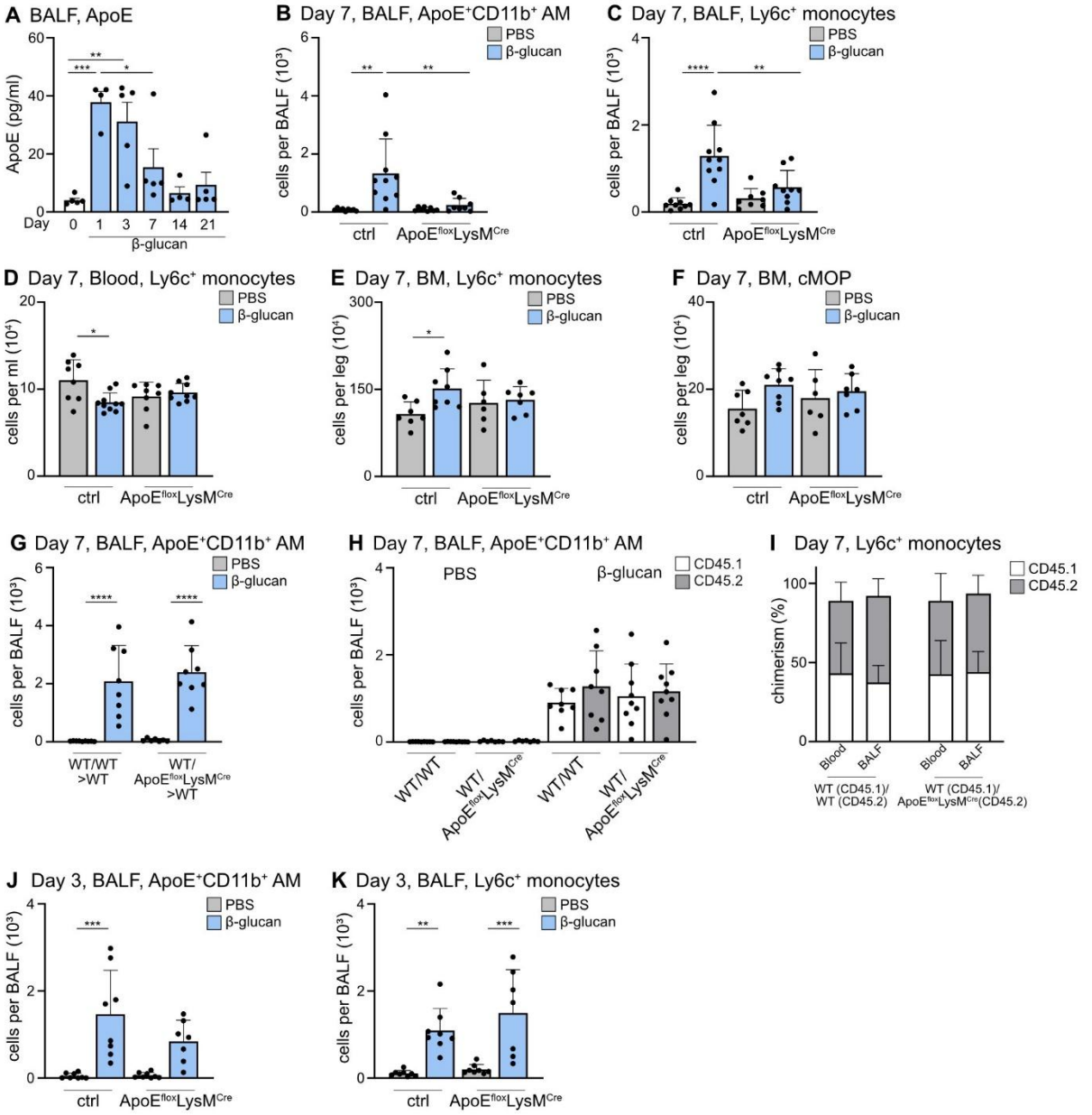

Figure 9: Paracrine myeloid derived ApoE controls the survival of ApoE$^+$CD11b$^+$ AM upon β-glucan mediated environmental adaptation. (A) Quantification of ApoE protein levels from the BALF supernatant in a time course from 1 to 21 days post β-glucan stimulation of WT mice (n=4-5 mice, one independent experiment). **(B, C)** Absolute numbers of ApoE$^+$CD11b$^+$ AM (B) and Ly6c$^+$ monocytes (C) in the BALF seven days after intranasal β-glucan exposure of control or ApoE^{flox}LysM^{Cre} mice by flow cytometry (n=8-10 mice, three independent experiments). **(D-F)** Absolute Ly6c$^+$ monocyte numbers in the blood (D) or bone marrow (E) and absolute cMOP numbers in the bone marrow (F) of control or ApoE^{flox}LysM^{Cre} mice seven days intranasal β-glucan stimulation by flow cytometry (n=6-8 mice, two independent experiments). **(G-I)** Lethally irradiated CD45.1$^+$/CD45.2$^+$ mice were reconstituted with 1.5x10^6 WT CD45.1$^+$ mixed with WT CD45.2$^+$ (WT/WT) or WT CD45.1$^+$ mixed with ApoE^{flox}LysM^{Cre} CD45.2$^+$ (WT/ApoE^{flox}LysM^{Cre}) bone marrow cells to generate chimeras and subsequently intranasally stimulated with PBS or β-glucan (n=8-9 mice, two independent experiments). Flow cytometric quantification of ApoE$^+$CD11b$^+$ AM numbers (G) and contribution of donor cells (CD45.1$^+$ or CD45.2$^+$) to the ApoE$^+$CD11b$^+$ AM pool (H) seven days after exposure. (I) Ly6c$^+$ monocyte chimerism in the blood and bone marrow shown as percentage of CD45.1$^+$ or CD45.2$^+$ donor cell contribution. *Figure legend continues on next page.*

Figure 9: (J, K) Absolute numbers of ApoE^{+}CD11b^{+} AM (J) and Ly6c^{+} monocytes (K) in the BALF three days after intranasal β-glucan exposure of control or ApoE^{flox}LysM^{Cre} mice by flow cytometry (n=7-8 mice, two independent experiments). Data are depicted as mean ±SD, (A-K) ordinary one-way ANOVA with Tukey's multiple comparisons.

III.VIII. Apolipoprotein E controls the survival of ApoE^{+}CD11b^{+} AM by regulation of cholesterol storage and M-CSF secretion

As ApoE is crucial for cholesterol efflux, we hypothesized that the impaired survival of ApoE-deficient CD11b^{+} AM upon β-glucan exposure might be linked to lipid accumulation and dysregulation of lipid metabolism in the cells. First, we selected AM from the BALF of day three PBS or β-glucan experienced control or ApoE^{flox}LysM^{Cre} mice by adherence, fixed the cells and stained the cholesterol content using Filipin. ApoE-deficient CD11b^{+} AM showed significantly higher signal intensities of intracellular cholesterol compared to ApoE-proficient CD11b^{+} AM of glucan experienced mice, while cells from PBS treated mice showed no difference (**Figure 10A, B**). A previous publication by Blanchard *et al.* showed a cholesterol accumulation in the endoplasmic reticulum (ER) leading to impaired protein synthesis upon ApoE deficiency in oligodendrocytes (115). To test if this is also the case for ApoE-deficient CD11b^{+} AM, AM from the BALF of day three PBS or β-glucan experienced control or ApoE^{flox}LysM^{Cre} mice were selected by adherence and incubated with BODIPY-cholesterol overnight. As the cells were not fixed, fluorescent BODIPY-cholesterol was actively taken up by AM, which allowed intracellular tracking. Immunofluorescence allowed co-staining of BODIPY-cholesterol with the cell organelle-specific markers calreticulin (ER), EEA1 (endosomes) and LAMP1 (lysosomes) (**Figure 10C**). BODIPY-cholesterol signals co-localized with calreticulin signals in ApoE-deficient CD11b^{+} AM indicating a cholesterol accumulation in the ER of those cells (**Figure 10D**). Overloading of the ER with cholesterol could affect protein synthesis and folding of cytokines involved in macrophage differentiation and survival. We therefore hypothesized that the ApoE-mediated cholesterol accumulation could impair the production of M-CSF, a growth factor that has been linked to differentiation and survival of monocytes into macrophages in the lung (42). WT mice were stimulated with PBS or β-glucan and the BALF supernatant was harvested for quantification of M-CSF protein levels at different time points after exposure showing an early release at day one coinciding with monocyte infiltration into the alveolar space (**Figure 10E, 5A**). Further immunohistochemical analyses of lung samples of WT mice one day post β-glucan inoculation by immunofluorescence showed co-localization of M-CSF protein with ApoE^{+}CD11b^{+} AM within the alveolar space (**Figure 10F, G**). We also compared extracellular and intracellular M-CSF levels from control or ApoE^{flox}LysM^{Cre} mice upon environmental adaptation. Secretion of M-CSF into the alveolar space was measured in the BALF supernatant by ELISA one day after β-glucan and showed significantly decreased levels

in ApoE^{flox}LysM^{Cre} mice compared to controls (**Figure 10H**). Additionally, reduced M-CSF signal intensities were detected in ApoE-deficient CD11b^{+} AM one day after β-glucan by immunofluorescence (**Figure 10I**). Finally, we hypothesized that cholesterol accumulation in the ER and subsequently reduced production of M-CSF is triggering the loss of ApoE-deficient CD11b^{+} AM from day three to seven upon β-glucan inoculation. AM from the BALF of day three PBS or β-glucan experienced control or ApoE^{flox}LysM^{Cre} mice were selected by adherence and stained for TUNEL followed by conventional immunofluorescence. Analysis confirmed higher TUNEL signal intensities in ApoE-deficient CD11b^{+} AM three days after β-glucan (**Figure 10J**) confirming cell death. To further validate the necessity of M-CSF for the differentiation and maintenance of ApoE^{+}CD11b^{+} AM in the alveolar space, M-CSF signalling was blocked *in vivo* treating WT mice with β-glucan in combination with an anti-CSF-1R antibody or the respective isotype control followed by flow cytometric analysis seven days after initial β-glucan inoculation (**Figure 10K**). Blocking of M-CSF signalling resulted in significantly reduced numbers of ApoE^{+}CD11b^{+} AM in the alveolar space compared to the mice treated with the isotype control (**Figure 10L**), but did not affect CD11b^{-} AM or Ly6c^{+} monocyte numbers (**Figure 10M, N**). In summary, these data show that ApoE is regulating monocyte to macrophage differentiation and survival by controlling intracellular cholesterol levels and signalling via the M-CSF – CSF-1R axis upon environmental adaptation.

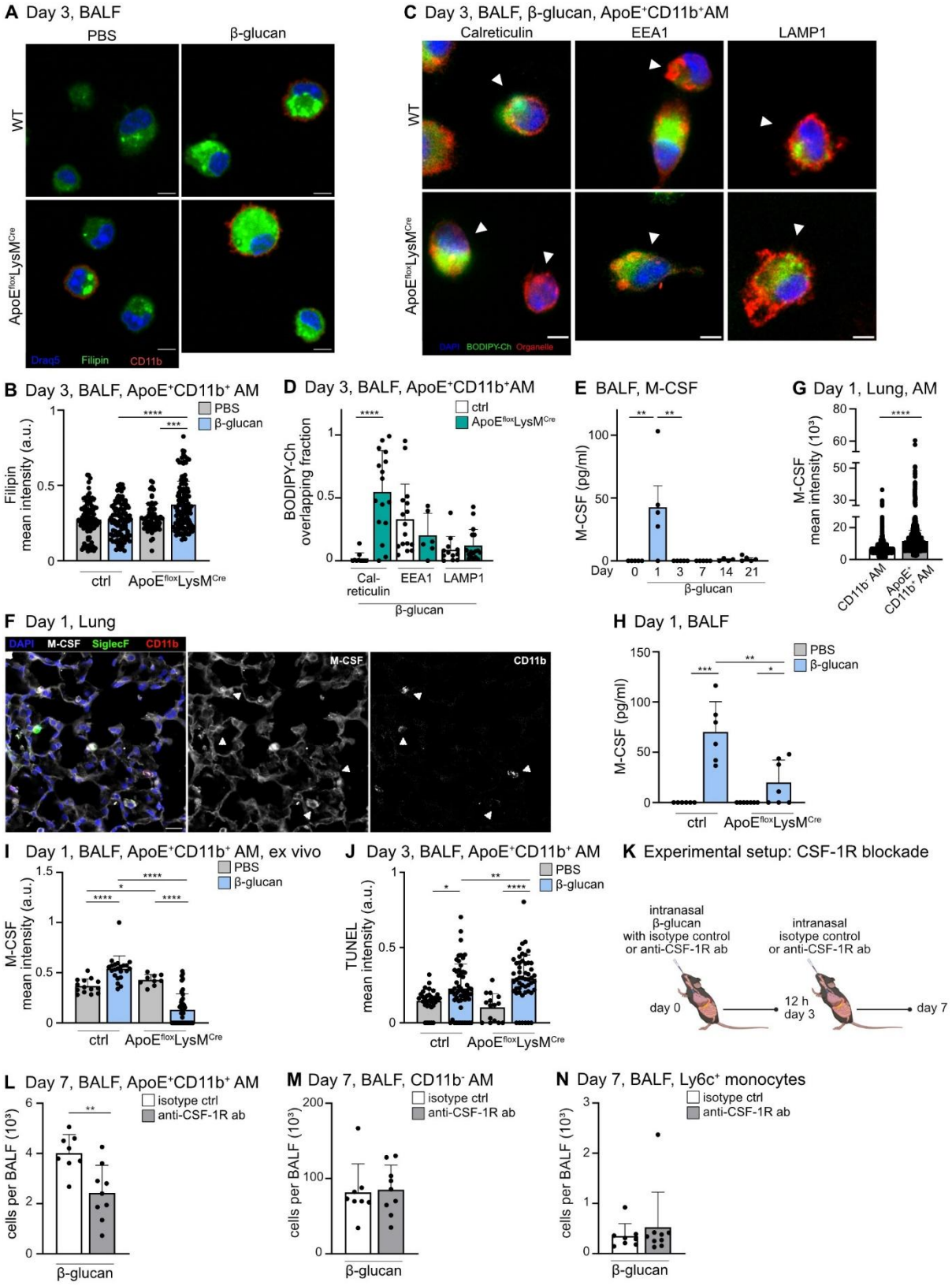

Figure 10: Myeloid-derived Apolipoprotein E controls survival of ApoE⁺CD11b⁺ AM by regulation of cholesterol storage and M-CSF secretion. *Figure legend continues on next page.*

Figure 10: (A, B) AM from PBS or β-glucan experienced control or ApoE^{flox}LysM^{Cre} mice were selected by adherence from the BALF three days after stimulation and subsequently fixed. Filipin staining was performed followed by immunofluorescence staining. Representative images of Filipin stainings are shown in (A), scale bars represent 5 µm. (B) Quantification of mean Filipin signal intensities in ApoE^{+}CD11b^{+} AM in the different conditions (n=3 mice per condition, two independent experiments). **(C, D)** Control or ApoE^{flox}LysM^{Cre} mice were stimulated with PBS or β-glucan and three days later AM from the BALF were selected by adherence and incubated overnight with 0.5 µM BODIPY-Cholesterol. Immunofluorescence staining was performed the next day after fixing the cells for 15 min. (C) Representative confocal images of ApoE^{+}CD11b^{+} AM treated with BODIPY-cholesterol and co-stained for the endoplasmic reticulum (Calreticulin), endosomes (EEA1) or lysosomes (LAMP1). Scale bar represents 5 µm. (D) Quantification of overlapping signals of BODIPY-cholesterol and the three organelle markers (n= 2 mice per condition, two independent experiments). **(E)** M-CSF protein levels in the BALF supernatant of WT mice in a time course from 1 to 21 days post β-glucan stimulation (n=5 mice, one independent experiment). **(F, G)** Lungs of WT mice were harvested 24 h post β-glucan stimulation, fixed and frozen in OCT. 5 µm sections were stained for SiglecF, CD11b and M-CSF. (F) Representative confocal images, arrows indicate ApoE^{+}CD11b^{+} AM. (G) Seven regions of the same size from the samples were analysed and M-CSF mean signal intensities of CD11b^{-} AM and ApoE^{+}CD11b^{+} AM were determined. Each dot represents one cell. **(H)** M-CSF protein levels in the BALF supernatant of control or ApoE^{flox}LysM^{Cre} mice one day after PBS or β-glucan assessed by ELISA (n=6 mice, two independent experiments). **(I)** AM from PBS or β-glucan experienced control or ApoE^{flox}LysM^{Cre} mice were selected by adherence from the BALF one day after stimulation, fixed and immunostained for SiglecF, CD11b and M-CSF. Quantification of mean M-CSF signal intensities in ApoE^{+}CD11b^{+} AM (n=3 mice per condition, two independent experiments). **(J)** TUNEL staining in AM from PBS or β-glucan experienced control or ApoE^{flox}LysM^{Cre} mice selected by adherence three days after inoculation. Cells were fixed followed by TUNEL staining and conventional immunofluorescence. Plot shows mean TUNEL signal intensities of ApoE^{+}CD11b^{+} AM (n=3 mice, two independent experiments). **(K)** Experimental setup for CSF-1R blockade upon environmental adaptation. WT mice were stimulated with β-glucan together with 500 µg anti-CSF-1R antibody or the respective isotype control. Intranasal application of the anti-CSF-1R antibody or the respective isotype control was repeated 12h and three days after initial treatment. **(L-N)** Quantification of ApoE^{+}CD11b^{+} AM (L), CD11b^{-} AM (M) and Ly6c^{+} monocyte (N) numbers in the BALF of WT mice seven days after treatment with β-glucan together with anti-CSF-1R antibody or the respective isotype control. Data are depicted as mean ±SD, (B, D, E) Two-tailed Mann-Whitney test, (G-J) ordinary one-way ANOVA with Tukey's multiple comparisons, (L-N) unpaired student's *t*-test.

III.IX. Repetitive exposure to β-glucan enhances the emergence of ApoE^{+}CD11b^{+} AM

In the chapters above, we described the effect of a single dose of β-glucan on the mononuclear phagocyte compartment of the lung as a model to mimic environmental adaptation to external stressors. As β-glucan is omnipresent in ambient air and abundantly inhaled over time, we established an experimental setup for a repetitive exposure to β-glucan. Mice were stimulated at day 0, 3 and 6 with PBS or β-glucan and sacrificed at day 14 (**Figure 11A**). Quantification of pulmonary macrophage subsets by flow cytometry showed exclusive emergence of ApoE^{+}CD11b^{+} AM in mice repetitively stimulated with β-glucan and also increased numbers of tissue-resident CD11b^{-} AM (**Figure 11B, C**). Unsupervised clustering of pulmonary immune cells based on their surface marker expression demonstrated that, besides the emergence of

ApoE^{+}CD11b^{+} AM, only minor changes in cell composition occurred in granulocytes, DC and monocyte populations upon repetitive β-glucan inoculation (**Figure 11D**). Comparison of these results with the results obtained after a single dose of β-glucan (**Figure 3C, F**) showed no extensive differences. However, focusing on the composition of the alveolar macrophage compartment, repetitive β-glucan exposure boosted the abundance of ApoE^{+}CD11b^{+} AM up to 22% compared to a single dose (**Figure 11E**). In conclusion, repetitive exposure to β-glucan increases the abundance of ApoE^{+}CD11b^{+} AM in the AM compartment without impacting other mononuclear phagocytes in the murine lung.

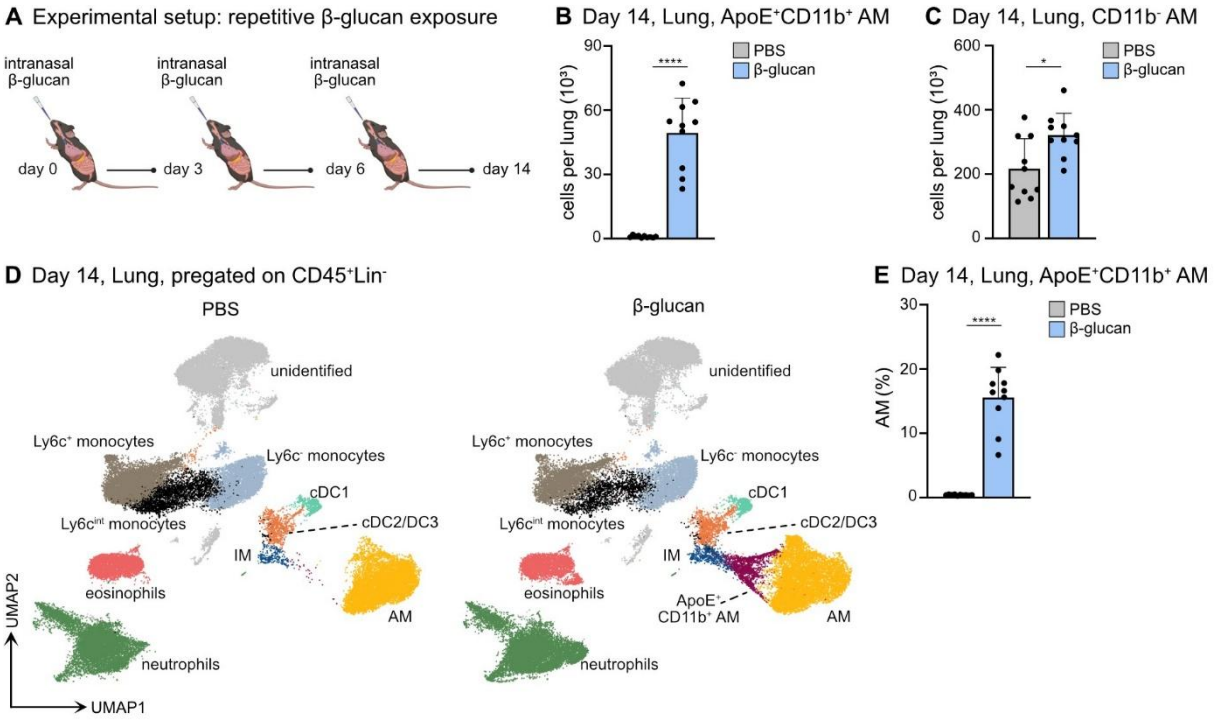

Figure 11: Repetitive exposure to β-glucan enhances the emergence of ApoE^{+}CD11b^{+} AM compared to a single dose. (A) Experimental setup for repetitive β-glucan exposure. WT or Ms4a3^{Cre}R26^{tdTomato} mice were inoculated with PBS or β-glucan on day 0, 3 and 6 and analysed on day 14 by flow cytometry. **(B, C)** Absolute numbers of ApoE^{+}CD11b^{+} AM (B) and CD11b^{-} AM (C) in the lung of mice repetitively stimulated with β-glucan assessed by flow cytometry at day 14 (n=10 mice, two independent experiments). **(D)** UMAP representation of 5x10^{4} CD45^{+} DRAQ7^{-} Lin^{-} (Ly6g, B220, CD19, CD3ε, Nk1.1, Ter-119) immune cells of the Ms4a3^{Cre}R26^{tdTomato} lung after repetitive intranasal β-glucan stimulation from flow cytometry data using the surface marker panel shown in Figure 3A (n= 5-6 mice pooled per condition). **(E)** Percentage of ApoE^{+}CD11b^{+} AM among AM in the lung of mice repetitively stimulated with β-glucan assessed by flow cytometry at day 14 (n=10 mice, two independent experiments). Data are depicted as mean ±SD, (B, C, E) unpaired student's t-test.

IV. Discussion

Interaction with our modern-day environment brings ourselves close to a multitude of environmental particles, including aerosols, particulate matter, pathogens and immunomodulatory substances derived from pathogens. While exposure to particulate matters has been mainly negatively correlated to lung injury and adenocarcinoma outcomes (48, 49), inhalation of low dose β-glucan has been linked to airway inflammation, allergy and asthma (54–56). However, it remained elusive how ambient β-glucan affects mononuclear phagocytes, which form the first line of defence and abundantly express receptors recognizing β-glucan, on an immunological and molecular level. Thus, we developed a murine model of a low dose inoculation to mimic environmental exposure to the omnipresent fungal polysaccharide β-glucan. Flow cytometric analysis of the mononuclear phagocyte compartment of the lung post β-glucan revealed a CCR2-dependent recruitment of Ly6c$^+$ monocytes from the blood into the alveolar space that further differentiate into CD11b$^+$ AM. At the transcriptional level, these recruited CD11b$^+$ AM express high amounts of genes associated with a monocyte-derived lipid associated macrophage, such as *Apoe*, *Spp1*, *Trem2* and *Gpnmb*.

Molecularly, the process of recruitment and differentiation process is dependent on the Dectin-1 – CARD9 signalling axis, while ApoE acts as a crucial determinant of monocyte-derived macrophage maintenance in the environment of the alveolar lumen. Ablation of ApoE in CD11b$^+$ AM leads to accumulation of cholesterol in the endoplasmic reticulum, which impedes secretion of M-CSF and survival of the cells upon environmental adaptation to β-glucan. Functionally, β-glucan mediated environmental adaptation leads to increased release of pro-inflammatory IL-6 specifically from ApoE$^+$CD11b$^+$ AM upon *ex vivo* restimulation with LPS, to enhanced bacterial clearance in a secondary bacterial infection and to reduced fibrosis in an *in vitro* lung organoid model (**Figure 12**). Furthermore, we show that repetitive exposure to β-glucan increases the inflammatory amplitude, but its effect is still only restricted to the elevated emergence of ApoE$^+$CD11b$^+$ AM. In summary, we show how β-glucan mediated environmental adaptation modulates lung resilience and disease susceptibility by reshaping the alveolar macrophage pool and how the differentiation process of monocytes into alveolar macrophages is linked to cellular cholesterol metabolism.

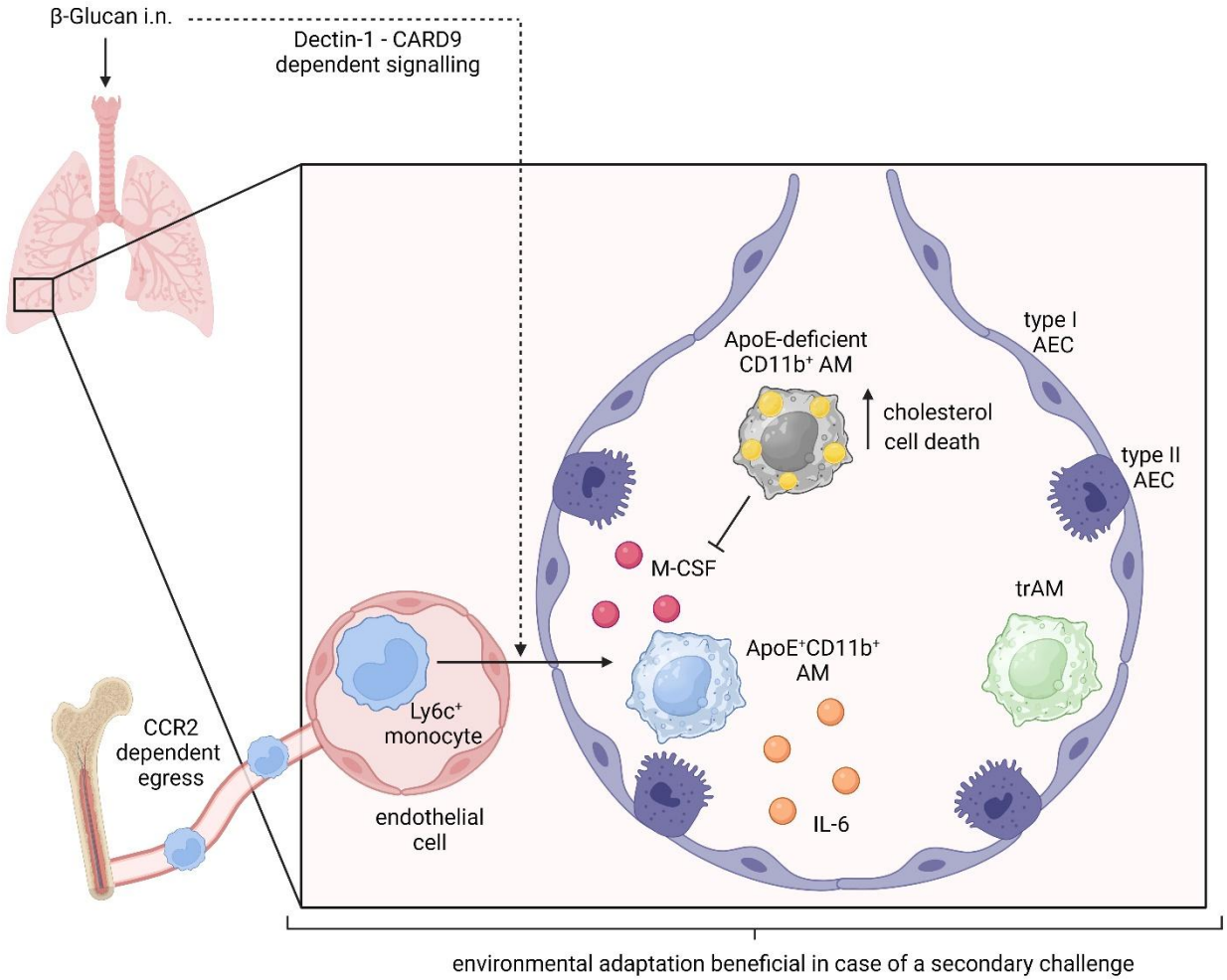

Figure 12: B-Glucan induced environmental adaptation reshapes the pulmonary alveolar macrophage pool, which positively affects lung resilience and disease susceptibility and links cellular cholesterol metabolism to monocyte to macrophage differentiation. Intranasal exposure to β-glucan triggers Ly6c⁺ monocyte influx into the alveolar space via the Dectin-1 – CARD9 signalling axis and induces differentiation into ApoE⁺CD11b⁺ AM, which release elevated levels of IL-6. Regulation of intracellular cholesterol levels and M-CSF production are controlled ApoE, which affect survival of ApoE⁺CD11b⁺ AM upon ablation of ApoE.

IV.I. B-glucan, an environmentally derived immune modulator, elicits monocyte-derived ApoE⁺CD11b⁺ AM via the Dectin-1 – CARD9 signalling axis

Using a murine model to mimic environmental exposure with a low dose β-glucan inoculation, we characterized the mononuclear phagocyte compartment at several time points post exposure by flow cytometry based on previous published gating strategies (116). Transient influx of eosinophils and neutrophils into the alveolar space up to seven days after treatment indicates a low-grade inflammation upon environmental exposure, as previously described confirming our model (51, 54). Although the initial inflammation is minimal, β-glucan exposure is accompanied by the emergence of a population of alveolar macrophages that express high

levels of CD11b together with classical alveolar macrophage markers like CD64, MerTk and intermediate levels of SiglecF. Transcriptomic analysis shows that the majority of macrophages belongs to *bona fide* tissure resident or proliferative AM in line with previous publications (35, 109, 110). Differential genes expressed by the cluster of AM specific to the β-glucan condition consist of *Apoe*, *Gpnmb*, *Spp1*, *Cd63* and *Trem2*, which have been previously described as genes associated to monocyte-derived macrophages with an inflammatory and lipid associated phenotype (12, 99). As this signature occurs in monocyte-derived macrophages in other inflammatory settings, it can be speculated that these genes potentially guide the differentiation process from monocytes to macrophages and support the adaptation to a lipid rich environment like the lung or the adipose tissue. The observation that ApoE and CD11b are co-expressed on the RNA and protein level indicates that the lipid associated phenotype is linked to a higher inflammatory potential (117).

The emergence of ApoE$^+$CD11b$^+$ AM coincides with an influx of Ly6c$^+$ monocytes into the alveolar space and together with the expression of genes previously found in monocyte-derived macrophages, support the monocyte origin of ApoE$^+$CD11b$^+$ AM. Fate mapping by *Ms4a3* expression in GMP of the bone marrow confirms that ApoE$^+$CD11b$^+$ AM are almost exclusively monocyte-derived, while similar to published data approximately 20% of CD11b$^-$ AM are labelled (13). We demonstrate that CCR2 signalling is crucial for the emergence of monocyte-derived AM, which is in line with evidence from influenza A virus infections (12). Ly6c$^+$ monocytes lacking CCR2 accumulate in the bone marrow, as they are not able to respond to MCP-1 and migrate to the periphery (112). However, CCR2 is dispensable for migration of Ly6c$^+$ monocytes from the blood stream to the exposed tissue (112). Systemic application of β-glucan has previously been shown to modulate myelopoiesis via GMP in the bone marrow (118). In our model, a topical low dose administration of β-glucan does not alter GMP (data not shown) and cMOP populations, but increases Ly6c$^+$ monocytes in the bone marrow indicating that only the latest stage of monocyte development is affected. In contrast, Ly6c$^+$ monocytes in the blood are decreased indicating that increased Ly6c$^+$ monocyte production in the bone marrow compensates for recruitment of Ly6c$^+$ monocytes from the blood circulation to the alveolar space.

B-glucan is an essential component of cell walls across many fungal species and ubiquitously found in the atmosphere. Monocytes and monocyte descentants have been identified as potent antifungal mediators in mice and man, and have been shown to incite CD4$^+$ T cell responses (119–121). Influx of Ly6c$^+$ monocytes into the alveolar space and subsequent differentiation into ApoE$^+$CD11b$^+$ AM upon β-glucan exposure could therefore be a crucial part of the host defense by modulating adaptive responses against fungal species. However, signals that trigger monocyte influx and differentiation into macrophages remain poorly understood on a

molecular level. Based on current evidence in the literature, receptor-dependent or phagocytosis-mediated intracellular signalling and death of trAM could be drivers for monocyte recruitment. Binding of β-glucan by surface receptors triggers production of a variety of different pro-inflammatory cytokines, while the fungal polysaccharide is also phagocytosed by alveolar macrophages (53). Once their phagocytic capacity is surpassed, tissue-resident macrophages can initiate inflammation and secrete mediators like type I IFNs, TNF-α and IL-1β, attracting monocytes and neutrophils (29, 30). Pulmonary bacterial or viral infections like influenza A virus or *Legionella pneumophila* often cause early loss of trAM, which is additionally accompanied by emergence of moAM in the acute phase, while later stages of the infections are characterized by proliferation of the remaining trAM to restore organ function (41, 122). Exposure to β-glucan triggers a reduction in trAM numbers one day after exposure as quantified by flow cytometry, confirming a mild initial loss. However, trAM numbers are rapidly expanding from day three to day seven beyond the emergence of $ApoE^{+}CD11b^{+}$ AM, indicating local trAM proliferation. Interestingly, the percentage of proliferating AM is reduced in our single-cell RNA sequencing data at day seven post β-glucan, which could explain the decline of trAM back to baseline levels from day seven to day 14 assessed by flow cytometry. In summary, monocytes and moAM could act as antifungal effectors and compensate for the loss of trAM upon β-glucan exposure, as trAM proliferation is slower than monocyte recruitment.

Regarding the life span of moAM, recent publications show that moAM and trAM co-exist in the lung for more than eight weeks after influenza A virus infection (12, 41). Tracking of β-glucan elicited $ApoE^{+}CD11b^{+}$ AM over time based on CD11b expression shows a peak at day seven and subsequently decreasing numbers. To investigate the life span of $ApoE^{+}CD11b^{+}$ AM, monocytes were fluorescently labelled prior to β-glucan exposure using an inducible *Ms4a3* reporter model. Analysis after 28 days showed that tdTomato labelling was present in $ApoE^{+}CD11b^{+}$ AM and $CD11b^{-}$ AM of β-glucan exposed mice, while control mice showed no labelling. Together with data from the constitutive labelling approach, these results indicate that $ApoE^{+}CD11b^{+}$ AM persist in the alveolar space beyond 28 days, where they gradually downregulate CD11b. This raises the hypothesis that moAM are phenotypically and functionally adapting to the tissue microenvironment of the lung by integration into the pool of trAM over time. However, the factors that drive the adaptation of moAM to the established niche and the functional consequences remain elusive.

Molecularly, we show that the environmental adaptation to β-glucan is dependent on the Dectin-1 – CARD9 signalling axis. Activation of Dectin-1, which is the predominant receptor for β-glucan, triggers a variety of pro-inflammatory or tolerance responses depeding on the ligand engaged (70). In line with previous findings, we confirm that Dectin-1 is expressed on alveolar macrophages and monocytes in the lung (65), which allows rapid sensing of fungal species as

part of protective immune responses for host defence. Global ablation of Dectin-1 significantly decreases the emergence of ApoE^{+}CD11b^{+} AM upon environmental adaptation, but not Ly6c^{+} monocytes, indicating that Dectin-1 is crucial for monocyte to macrophage differentiation and not required for the influx of Ly6c^{+} monocytes into the alveolar space in the first place. Furthermore, we show that differentiation of ApoE^{+}CD11b^{+} AM is dependent on CARD9, a signalling adaptor downstream of Dectin-1. The decreased emergence of ApoE^{+}CD11b^{+} AM also occurs in Dectin-1$^{-/-}$ and CARD9$^{-/-}$ bone marrow chimeras, where ablation is only restricted to circulating immune cells like monocytes, showing that intrinsic expression of both molecules in monocytes is crucial to react to β-glucan and to initiate differentiation.

IV.II. Adaptation to β-glucan modulates cytokine production, bacterial clearance and fibrosis outcome

Previous studies have identified increased IL-6 release as a functional consequence in circulating monocytes adapted to β-glucan (80, 123), but lack understanding on the level of the tissue exposed. Adaptation of AM to β-glucan in the lung induces release of high levels of pro-inflammatory IL-6 upon restimulation with LPS. Further experiments confirmed that ApoE^{+}CD11b^{+} AM are the major source of IL-6 compared to tissue-resident CD11b^{-} AM, which is concordance with a higher inflammatory potential observed on CD11b expressing macrophages (117). Molecularly, induction of IL-6 transcription by NF-κB is one of the main targets of the Dectin-1 – CARD9 signalling circuit (72). Abrogation of Dectin-1 or CARD9 signalling upon environmental adaptation does not only reduce ApoE^{+}CD11b^{+} AM numbers, but also IL-6 production in the alveolar space. Transfer of β-glucan adapted AM to naïve tissue context reveals that IL-6 production is a cell intrinsic feature acquired upon environmental adaptation suggesting transcriptional alterations on the moAM level as previously published for monocytes (123, 124). Interestingly, there was no difference in TNF-α release from control or β-glucan adapted AM upon LPS restimulation (data not shown), although NF-κB is also inducing transcription of TNF-α (72). Previous publications have demonstrated a co-release of IL-6 and TNF-α in monocytes upon LPS re-challenge (12, 80, 123), although others report no increased TNF-α release from moAM (12). Prompt release of IL-6 from myeloid cells in presence of sterile or non-sterile pathogens stimulates antibody production and plasma cell differentiation in B cells and shifts T helper cell differentiation from tolerance to inflammation as part of the adaptative host defence (125). IL-6 release by ApoE^{+}CD11b^{+} AM could therefore be a key player in the initiation of adaptive defence responses against fungal species.

Besides initiation and termination of inflammation by cytokine secretion, AM perform phagocytosis and efferocytosis to clear foreign microorganisms and apoptotic cells. We show

that β-glucan adaptation enhances phagocytosis in AM *in vitro* compared to PBS controls. Furthermore, β-glucan adapted AM also phagocytose quantitatively more *S. aureus* coated bioparticles. From an evolutionary perspective, the β-glucan-mediated increase in phagocytosis in AM could enhance subsequent clearance of fungal or bacterial species from the alveolar space and provide a benefit for host defence. Interestingly, flow cytometric analysis of the AM compartment post phagocytosis showed no difference between $ApoE^{+}CD11b^{+}$ AM and $CD11b^{-}$ AM for phagocytosis, indicating that trAM and moAM phagocytose equally well (data not shown), which is in line with previous results (12). In contrast, a previous publication showed a higher phagocytic capacity in β-glucan elicited monocyte-derived macrophage compared to their tissue-resident counterparts in the pancreas (126). This discrepancy in phagocytosis between monocyte-derived macrophages of different organs could be because pulmonary AM have a high phagocytic capacity per se, as they constantly clear mucus and sample pathogens in the alveolar space.

Previous data have shown that adaptation of pulmonary macrophages to acute viral infections or low grade inflammation by environmental factors confer to protection from secondary bacterial infections (12, 51, 127). In line with these findings, adaptation to β-glucan prior to infection significantly reduces the bacterial burden of *Legionella pneumophila* in the alveolar space. The elevated release of IL-6 in combination with enhanced phagocytosis by AM could explain the improved bacterial clearance as IL-6 has been proposed as one of the major cytokines promoting antibacterial protection via stimulation of adaptive immune responses (12). For chronic injuries, β-glucan exposure has been linked to reduced pulmonary fibrosis in rats, although moAM have been identified to exacerbate fibrosis outcome (42, 44, 128). We show that presence of β-glucan adapted AM limits fibrosis generation by decreased production of SMA by myofibroblasts in a broncho-alveolar lung organoid model. Previously, it has been shown that myofibroblast proliferation can be directly induced by AM via PDGFα (42), which suggests that β-glucan adaptation modulates fibrosis development through altered production of cytokines and growth factors.

IV.III. Apolipoprotein E controls survival of $ApoE^{+}CD11b^{+}$ AM by regulation of cholesterol storage and M-CSF secretion

Protein levels of secreted ApoE are low in the alveolar space during homeostasis, but β-glucan exposure triggers a fast release, which coincides with influx of monocytes and granulocytes one day post treatment, although a distinct source has not been identified by our experiments. Transcriptomic analysis reveals that *Apoe* expression is limited to β-glucan elicited moAM and absent in trAM seven days after exposure. To elucidate the functional effect of ApoE on moAM,

we crossed ApoE^{flox} to LysM^{Cre} mice to generate a cell specific ApoE knockout in monocytes, macrophages and granulocytes (129). Monocyte and macrophage-specific ablation of ApoE leads to the loss of ApoE^{+}CD11b^{+} AM in the alveolar space from day three to seven after β-glucan instillation, while influx of monocytes is unimpaired at day three. These results indicate that ApoE does not control the initial influx of monocytes, but is crucial for the maintenance of ApoE^{+}CD11b^{+} AM in the alveolar space. It has been previously described that local production of lipid free ApoE by macrophages is crucial for reverse cholesterol transport and cholesterol efflux ameliorating atherosclerosis, while lipoprotein bound plasma ApoE released by hepatocytes is not (130, 131). Further studies support the functional discrepancy between exogenous plasma ApoE and endogenously expressed ApoE in macrophages for cholesterol efflux (132). Loss of ApoE-deficient CD11b^{+} AM upon environmental adaptation could therefore be due to imbalance of cholesterol efflux, especially as moAM have to adapt to the lipid rich environment of the lung. Interestingly, monocyte and macrophage specific ablation of ApoE reduces Ly6c^{+} monocytes in the alveolar space and abrogates the effect in blood and bone marrow seven days after β-glucan. This raises the hypothesis that fewer monocytes are recruited to the alveolar space upon ApoE ablation, although the mechanism is poorly understood. Using a mixed chimera approach, we show that ApoE-deficient CD11b^{+} AM survive in the alveolar space past day three if neighbouring mononuclear phagocytes are proficient in ApoE production upon environmental adaptation. This suggests a paracrine mechanism by uptake of released ApoE by ApoE-deficient CD11b^{+} AM and restorage of intracellular protein function. It has been previously described that ApoE acts in both an autocrine and paracrine manner. While autocrine effects are constant, paracrine effects are dependent on the concentration of ApoE in the tissue environment and the proximity of the cells to each other (114). Recently, it has been shown that tumor-associated macrophages transfer ApoE to cancer cells via exosomes in a paracrine manner (133)., which could explain the rescue of ApoE-deficient CD11b^{+} AM by neighbouring ApoE proficient mononuclear phagocytes in our model.

Further experiments show that β-glucan elicited ApoE-deficient CD11b^{+} AM accumulate cholesterol in the ER due to impaired cholesterol efflux, which is in concordance with previous literature stating that endogenously expressed ApoE is crucial for this process in macrophages (132). A similar phenotype can be observed in Alzheimer's disease patients carrying the ApoE4 gene variant, which has been described as the largest genetic risk factor (90). It has been shown that ApoE4^{+} Alzheimer's patients suffer from lipid droplet accumulation in microglia and ER-specific cholesterol accumulation in oligodendrocytes causing stress (115, 134). In contrast, the majority of cholesterol in ApoE^{+}CD11b^{+} AM is present in endosomes and lysosomes in concordance with previous studies (135). Normally, ApoE-rich cholesterol-shuttling lipoproteins are taken up into endosomes, from where lipids are partially transported

into lysosomes, while ApoE is transported back to the surface and secreted to rebind to lipoproteins. This recycling process of ApoE is a major part of cholesterol efflux and impaired in cells carrying the ApoE4 gene variant (136). Impaired recycling of ApoE could therefore trigger mis-shuttling of excessive cholesterol to the ER and explain the cholesterol accumulation in ApoE-deficient $CD11b^+$ AM upon environmental adaptation.

Lipid accumulation in the ER has been linked to increased ER stress, which negatively affects the tightly regulated and correct biosynthesis of proteins and lipids (137). We further investigated if the cholesterol accumulation in β-glucan elicited ApoE-deficient $CD11b^+$ AM impairs the secretion of cytokines related to macrophage differentiation and maintenance, explaining their impeded survival. While GM-CSF, which has been linked to trAM development, is not secreted upon environmental adaptation (data not shown), M-CSF is rapidly released into the alveolar space one day after β-glucan coinciding with influx of monocytes and differentiation into moAM. Furthermore, we established a link between M-CSF and $ApoE^+CD11b^+$ AM, as they co-localize in histological evaluations of the lung tissue. Translation of the *Csf1* gene generates three different M-CSF variants, one membrane bound and two soluble isoforms, that share a core sequence of amino acids but differ in their biological activity (138). Ablation of ApoE significantly reduces M-CSF protein levels in the alveolar space and also particularly in ApoE-deficient $CD11b^+$ AM indicating that both soluble and membrane bound isoforms are affected. We therefore theorize that cholesterol accumulation in the ER upon ApoE ablation leads to improper folding of M-CSF inciting its degradation, as lipid accumulation triggers overloading of the ER with misfolded proteins, which are then degraded by the unfolded protein response (137). As a consequence, cholesterol accumulation and diminished M-CSF abundance increases apoptosis in ApoE-deficient $CD11b^+$ AM leading to the loss of the cells from day three to day seven post environmental adaptation. Mechanistically, upregulation of proapoptotic genes and Ca^{2+} release from the ER to the cytosol provoke mitochondria-mediated cell death (137). Lee *et al.* describe a similar mechanism for astrocytes, in which ApoE4-mediated cholesterol accumulation dysregulated mitochondrial respiration (139). Interestingly, effects were mitigated by depletion of intracellular cholesterol and restorage of mitochondrial homeostasis (139).

To establish a direct link between M-CSF and the maintenance of $ApoE^+CD11b^+$ AM in the alveolar space, we abrogated M-CSF signalling by blocking its receptor CSF-1R *in vivo* by a monoclonal antibody. While $CD11b^-$ AM and $Ly6c^+$ monocytes are not affected, $ApoE^+CD11b^+$ AM are significantly reduced in absence of functional M-CSF – CSF-1R signalling. These results are in concordance with recent publications that identify M-CSF as an important niche and maintenance factor in monocytes and moAM in the BM and lung (42, 140). In case of Joshi *et al.*, the authors showed depletion of $ApoE^+$ moAM upon administration of neutralizing anti-

M-CSF antibody demonstrating a similar mechanism for moAM emergence (42). Although our results suggest that ApoE$^+$CD11b$^+$ AM are maintained by autocrine M-CSF, paracrine secretion of M-CSF cannot be fully ruled out by our experiments, as both mechanisms have been described in literature (42, 140). As M-CSF does not only influence survival and differentiation, but also chemotaxis in monocytes and macrophages (reviewed in (138)), reduced chemotaxis of ApoE$^+$CD11b$^+$ AM to the alveolar space could explain diminished ApoE$^+$CD11b$^+$ AM numbers upon CSF-1R signalling blockade. However, we demonstrate in earlier experiments that M-CSF loss upon ApoE ablation does not influence monocyte migration to the alveolar space three days post β-glucan. These results indicate that M-CSF is crucial for for the survival and maintenance of ApoE$^+$CD11b$^+$ AM and not for chemotaxis of monocytes to the alveolar space.

IV.IV. Repetitive exposure to β-glucan increases the inflammatory amplitude and the emergence of ApoE$^+$CD11b$^+$ AM

Although aerial concentrations of β-glucan underlie seasonal differences, the fungal polysaccharide is present in ambient air throughout the year (59). Therefore, a model of repetitive administration mimics the daily exposure to β-glucan in a more precise fashion and allows investigation of long-term effects. Characterization of the pulmonary mononuclear phagocyte compartment after repetitive exposure to β-glucan demonstrate a boost in the emergence of ApoE$^+$CD11b$^+$ AM, while other myeloid cell populations are less affected. This indicates that adaptation to multiple doses of β-glucan increases the inflammatory amplitude by expanded emergence of ApoE$^+$CD11b$^+$ AM without inducing overshooting immune responses. Thus, this model shows that naïve specific pathogen free-housed mice do not accurately represent the mononuclear phagocyte composition in humans steadily exposed to environmental particles and pathogens. It has been previously demonstrated that β-glucan potentiates airway inflammation, allergy and asthma in mice and men (54–56, 141). However, it remains elusive, which factors determine the outcome of β-glucan exposure, as adaptation and resilience or maladaptation and pathologies have both been described. Nevertheless, daily exposure and adaptation to β-glucan is not restricted to inhaling airborne particles, but also occurs in the gastrointestinal tract as β-glucan or other immunomodulatory polysaccharides are present in oats, grains and yeast (reviewed in (142)). Lastly, this study shows that in addition to adaptive immunity reshaping throughout life, also innate immunity might be continuously reshaped with long-lasting consequences for immune cell composition of organs.

IV.V. Summary and future prospective

In this study, the fungal immunomodulatory polysaccharide β-glucan was utilized to model the effect of exposure to environmental stressors on mononuclear phagocytes in the murine lung. We demonstrate that a low-grade dose of β-glucan triggers influx of $Ly6c^+$ monocytes into the alveolar space, which subsequently differentiate into $ApoE^+CD11b^+$ AM in a Dectin-1 – CARD9 dependent manner. Furthermore, we identified ApoE and M-CSF as molecular determinants for the emergence of $ApoE^+CD11b^+$ AM by controlling their maintenance. Ablation of ApoE in monocytes and macrophages causes cholesterol accumulation in the ER, which impedes synthesis of M-CSF, an important maintenance factor for monocytes and moAM. Consequently, ApoE-deficient $CD11b^+$ AM undergo cell death, potentially via Ca^{2+} release into the cytosol and subsequent mitochondria-mediated apoptosis. Adaptation to β-glucan positively affects disease susceptibility by elevated release of IL-6 and phagocytosis leading to enhanced bacterial clearance and ameliorated fibrosis. Repeated exposure boosts the emergence of $ApoE^+CD11b^+$ AM without inducing overshooting immune responses. Altogether, we demonstrate that a macrophage-centric tissue-specific adaptation to low-grade inflammation inducing environmental factors improves the host fitness and resilience and links cellular cholesterol metabolism to monocyte to macrophage differentiation.

Although our experiments contribute to understanding, how a single tissue-specific exposure to environmental β-glucan positively shapes the host fitness and resilience, several questions remain open. In the present study, we focused on mononuclear phagocytes present in the alveolar space as β-glucan receptors are abundantly expressed on monocytes and macrophages. However, the effect of β-glucan on lymphoid cells and the immune cell composition in the interstitial space were not investigated. Our analyses have identified β-glucan specific signalling molecules crucial for the emergence of $ApoE^+CD11b^+$ AM, but cytokines and chemokines responsible for inflammation initiation and subsequent monocyte to macrophage differentiation remain unknown. Although we show that M-CSF is crucial for generation of β-glucan elicited moAM in the alveolar space, signals that further instruct their survival and longevity beyond their initial adaptation are unknown. Our results of CSF-1R-dependent depletion of moAM by antibodies provide insights into potential clinical applications, where moAM aggravate pathological conditions. Furthermore, investigating how repeated long-term exposure affects the cellular composition of the exposed tissue could help to understand β-glucan-induced maladaptation leading to enhanced allergies, asthma and airway inflammation.

References

1. Davies A., Moores C. Structure Of The Respiratory System, Related To Function. *The Respiratory System*, 11–28 (2010).

2. Aegerter H., Lambrecht B. N., Jakubzick C. V. Biology of lung macrophages in health and disease. *Immunity* **55**, 1564–80 (2022).

3. Dranoff G., Crawford A. D., Sadelain M. *et al.* Involvement of granulocyte-macrophage colony-stimulating factor in pulmonary homeostasis. *Science* **264**, 713–6 (1994).

4. Lloyd C. M., Marsland B. J. Lung Homeostasis: Influence of Age, Microbes, and the Immune System. *Immunity* **46**, 549–61 (2017).

5. Becher B., Schlitzer A., Chen J. *et al.* High-dimensional analysis of the murine myeloid cell system. *Nat Immunol* **12**, 1181–9 (2014).

6. Westphalen K., Gusarova G. A., Islam M. N. *et al.* Sessile alveolar macrophages communicate with alveolar epithelium to modulate immunity. *Nature* **506**, 503–6 (2014).

7. Standiford T. J., Kunkel S. L., Phan S. H. *et al.* Alveolar macrophage-derived cytokines induce monocyte chemoattractant protein-1 expression from human pulmonary type II-like epithelial cells. *Journal of Biological Chemistry* **266**, 9912–8 (1991).

8. Brieland J. K., Flory C. M., Jones M. L. *et al.* Regulation of monocyte chemoattractant protein-1 gene expression and secretion in rat pulmonary alveolar macrophages by lipopolysaccharide, tumor necrosis factor-alpha, and interleukin-1 beta. *Am J Respir Cell Mol Biol* **12**, 104–9 (1995).

9. Casanova-Acebes M., Nicolás-Ávila J. A., Li J. L. *et al.* Neutrophils instruct homeostatic and pathological states in naive tissues. *J Exp Med* **215**, 2778–95 (2018).

10. Schyns J., Bai Q., Ruscitti C. *et al.* Non-classical tissue monocytes and two functionally distinct populations of interstitial macrophages populate the mouse lung. *Nat Commun* **10**, 3964 (2019).

11. Jakubzick C. V., Randolph G. J., Henson P. M. Monocyte differentiation and antigen-presenting functions. *Nat Rev Immunol* **17**, 349–62 (2017).

12. Aegerter H., Kulikauskaite J., Crotta S. *et al.* Influenza-induced monocyte-derived alveolar macrophages confer prolonged antibacterial protection. *Nat Immunol* **21**, 145–57 (2020).

13. Liu Z., Gu Y., Chakarov S. *et al.* Fate Mapping via Ms4a3-Expression History Traces Monocyte-Derived Cells. *Cell* **178**, 1509-1525 (2019).

14. Chakarov S., Lim H. Y., Tan L. *et al.* Two distinct interstitial macrophage populations coexist across tissues in specific subtissular niches. *Science* **363** (2019).

15. Lyons-Cohen M. R., Thomas S. Y., Cook D. N. *et al.* Precision-cut Mouse Lung Slices to Visualize Live Pulmonary Dendritic Cells. *J Vis Exp* **122** (2017).

16. Guilliams M., Dutertre C.-A., Scott C. L. *et al.* Unsupervised High-Dimensional Analysis Aligns Dendritic Cells across Tissues and Species. *Immunity* **45**, 669–84 (2016).

17. Liu Z., Wang H., Li Z. *et al.* Dendritic cell type 3 arises from Ly6C+ monocyte-dendritic cell progenitors. *Immunity* **56**, 1761-1777 (2023).

18. Edelson B. T., Bradstreet T. R., Hildner K. *et al.* CD8α(+) dendritic cells are an obligate cellular entry point for productive infection by Listeria monocytogenes. *Immunity* **35**, 236–48 (2011).

19. Hildner K., Edelson B. T., Purtha W. E. *et al.* Batf3 Deficiency Reveals a Critical Role for CD8α+ in Cytotoxic T Cell Immunity. *Science* **322**, 1097–100 (2008).

20. Schlitzer A., McGovern N., Teo P. *et al.* IRF4 transcription factor-dependent CD11b+ dendritic cells in human and mouse control mucosal IL-17 cytokine responses. *Immunity* **38**, 970–83 (2013).

21. Mass E., Ballesteros I., Farlik M. *et al.* Specification of tissue-resident macrophages during organogenesis. *Science* **353** (2016).

22. Gomez Perdiguero E., Klapproth K., Schulz C. *et al.* Tissue-resident macrophages originate from yolk-sac-derived erythro-myeloid progenitors. *Nature* **518**, 547–51 (2015).

23. Mass E., Nimmerjahn F., Kierdorf K. *et al.* Tissue-specific macrophages: how they develop and choreograph tissue biology. *Nat Rev Immunol* **23**, 563–79 (2023).

24. Ginhoux F., Guilliams M. Tissue-Resident Macrophage Ontogeny and Homeostasis. *Immunity* **44**, 439–49 (2016).

25. Dick S. A., Wong A., Hamidzada H. *et al.* Three tissue resident macrophage subsets coexist across organs with conserved origins and life cycles. *Science Immunology* **7** (2022).

26. Neupane A. S., Willson M., Chojnacki A. K. *et al.* Patrolling Alveolar Macrophages Conceal Bacteria from the Immune System to Maintain Homeostasis. *Cell* **183**, 110-125 (2020).

27. Roberts A. W., Lee B. L., Deguine J. *et al.* Tissue-Resident Macrophages Are Locally Programmed for Silent Clearance of Apoptotic Cells. *Immunity* **47**, 913-927 (2017).

28. Fujimori T., Grabiec A. M., Kaur M. *et al.* The Axl receptor tyrosine kinase is a discriminator of macrophage function in the inflamed lung. *Mucosal Immunol* **8**, 1021–30 (2015).

29. Goritzka M., Makris S., Kausar F. *et al.* Alveolar macrophage-derived type I interferons orchestrate innate immunity to RSV through recruitment of antiviral monocytes. *J Exp Med* **212**, 699–714 (2015).

30. Mould K. J., Jackson N. D., Henson P. M. *et al.* Single cell RNA sequencing identifies unique inflammatory airspace macrophage subsets. *JCI Insight* **4** (2019).

31. Branchett W. J., Cook J., Oliver R. A. *et al.* Airway macrophage-intrinsic TGF-β1 regulates pulmonary immunity during early-life allergen exposure. *J Allergy Clin Immunol* **147**, 1892–906 (2021).

32. Todd E. M., Zhou J. Y., Szasz T. P. *et al.* Alveolar macrophage development in mice requires L-plastin for cellular localization in alveoli. *Blood* **128**, 2785–96 (2016).

33. Gschwend J., Sherman S. P. M., Ridder F. *et al.* Alveolar macrophages rely on GM-CSF from alveolar epithelial type 2 cells before and after birth. *J Exp Med* **218** (2021).

34. Guilliams M., Kleer I. de, Henri S. *et al.* Alveolar macrophages develop from fetal monocytes that differentiate into long-lived cells in the first week of life via GM-CSF. *J Exp Med* **210**, 1977–92 (2013).

35. Yu X., Buttgereit A., Lelios I. *et al.* The Cytokine TGF-β Promotes the Development and Homeostasis of Alveolar Macrophages. *Immunity* **47**, 903-912 (2017).

36. Schneider C., Nobs S. P., Kurrer M. *et al.* Induction of the nuclear receptor PPAR-γ by the cytokine GM-CSF is critical for the differentiation of fetal monocytes into alveolar macrophages. *Nat Immunol* **15**, 1026–37 (2014).

37. Daniel B., Czimmerer Z., Halasz L. *et al.* The transcription factor EGR2 is the molecular linchpin connecting STAT6 activation to the late, stable epigenomic program of alternative macrophage polarization. *Genes Dev* **34**, 1474–92 (2020).

38. Rauschmeier R., Gustafsson C., Reinhardt A. *et al.* Bhlhe40 and Bhlhe41 transcription factors regulate alveolar macrophage self-renewal and identity. *EMBO J* **38** (2019).

39. Minutti C. M., Jackson-Jones L. H., García-Fojeda B. *et al.* Local amplifiers of IL-4Rα-mediated macrophage activation promote repair in lung and liver. *Science* **356**, 1076–80 (2017).

40. Maus U. A., Janzen S., Wall G. *et al.* Resident alveolar macrophages are replaced by recruited monocytes in response to endotoxin-induced lung inflammation. *Am J Respir Cell Mol Biol* **35**, 227–35 (2006).

41. Li F., Piattini F., Pohlmeier L. *et al.* Monocyte-derived alveolar macrophages autonomously determine severe outcome of respiratory viral infection. *Science Immunology* **7** (2022).

42. Joshi N., Watanabe S., Verma R. *et al.* A spatially restricted fibrotic niche in pulmonary fibrosis is sustained by M-CSF/M-CSFR signalling in monocyte-derived alveolar macrophages. *Eur Respir J* **55** (2020).

43. Machiels B., Dourcy M., Xiao X. *et al.* A gammaherpesvirus provides protection against allergic asthma by inducing the replacement of resident alveolar macrophages with regulatory monocytes. *Nat Immunol* **18**, 1310–20 (2017).

44. Misharin A. V., Morales-Nebreda L., Reyfman P. A. *et al.* Monocyte-derived alveolar macrophages drive lung fibrosis and persist in the lung over the life span. *J Exp Med* **214**, 2387–404 (2017).

45. Gibbings S. L., Thomas S. M., Atif S. M. *et al.* Three Unique Interstitial Macrophages in the Murine Lung at Steady State. *Am J Respir Cell Mol Biol* **57**, 66–76 (2017).

46. Ural B. B., Yeung S. T., Damani-Yokota P. *et al.* Identification of a nerve-associated, lung-resident interstitial macrophage subset with distinct localization and immunoregulatory properties. *Science Immunology* **5** (2020).

47. Gangwar R. S., Vinayachandran V., Rengasamy P. *et al.* Differential contribution of bone marrow-derived infiltrating monocytes and resident macrophages to persistent lung inflammation in chronic air pollution exposure. *Sci Rep* **10** (2020).

48. Souza Xavier Costa N. de, Ribeiro Júnior G., Dos Santos Alemany A. A. *et al.* Air pollution impairs recovery and tissue remodeling in a murine model of acute lung injury. *Sci Rep* **10** (2020).

49. Hill W., Lim E. L., Weeden C. E. *et al.* Lung adenocarcinoma promotion by air pollutants. *Nature* **616**, 159–67 (2023).

50. Ege M. J., Mayer M., Normand A.-C. *et al.* Exposure to Environmental Microorganisms and Childhood Asthma. *The New England Journal of Medicine* **364**, 701–9 (2011).

51. Zahalka S., Starkl P., Watzenboeck M. L. *et al.* Trained immunity of alveolar macrophages requires metabolic rewiring and type 1 interferon signaling. *Mucosal Immunol* **15**, 896–907 (2022).

52. Marco Castro E. de, Calder P. C., Roche H. M. β-1,3/1,6-Glucans and Immunity: State of the Art and Future Directions. *Mol Nutr Food Res* **65** (2021).

53. McCann F., Carmona E., Puri V. *et al.* Macrophage internalization of fungal beta-glucans is not necessary for initiation of related inflammatory responses. *Infect Immun* **73**, 6340–9 (2005).

54. Fogelmark B., Thorn J., Rylander R. Inhalation of (1->3)-beta-D-glucan causes airway eosinophilia. *Mediators of Inflammation* **10**, 13–9 (2001).

55. Rylander R., Lin R.-H. (1->3)-beta-D-glucan — relationship to indoor air-related symptoms, allergy and asthma. *Toxicology* **152**, 47–52 (2000).

56. Thorn J., Beijer L., Rylander R. Airways inflammation and glucan exposure among household waste collectors. *Am. J. Ind. Med.* **33**, 463–70 (1998).

57. Netea M. G., Domínguez-Andrés J., Barreiro L. B. *et al.* Defining trained immunity and its role in health and disease. *Nat Rev Immunol* **20**, 375–88 (2020).

58. Iossifova Y., Reponen T., Sucharew H. *et al.* Use of (1-3)-beta-d-glucan concentrations in dust as a surrogate method for estimating specific fungal exposures. *Indoor Air* **18**, 225–32 (2008).

59. Madsen A. M., Frederiksen M. W., Allermann L. *et al.* (1 → 3)-β-d-glucan in different background environments and seasons. *Aerobiologia* **27**, 173–9 (2011).

60. Lee T., Grinshpun S. A., Kim K. Y. *et al.* Relationship between indoor and outdoor airborne fungal spores, pollen, and (1→3)-β-D-glucan in homes without visible mold growth. *Aerobiologia* **22**, 227–35 (2006).

61. Górny R. L., Reponen T., Willeke K. *et al.* Fungal fragments as indoor air biocontaminants. *Appl Environ Microbiol* **68**, 3522–31 (2002).

62. Geller A., Shrestha R., Yan J. Yeast-Derived β-Glucan in Cancer: Novel Uses of a Traditional Therapeutic. *Int J Mol Sci* **20** (2019).

63. Stuart L. M., Loi L., Fincher G. B. Immunological comparison of (1→3,1→4)-β-glucan endohydrolases in germinating cereals. *Journal of Cereal Science* **6**, 45–52 (1987).

64. Chen J., Seviour R. Medicinal importance of fungal beta-(1--3), (1--6)-glucans. *Mycol Res* **111**, 635–52 (2007).

65. Taylor P. R., Brown G. D., Reid D. M. *et al.* The beta-glucan receptor, dectin-1, is predominantly expressed on the surface of cells of the monocyte/macrophage and neutrophil lineages. *J Immunol* **169**, 3876–82 (2002).

66. Vetvicka V., Thornton B. P., Ross G. D. Soluble b-Glucan Polysaccharide Binding to the Lectin Site of Neutrophil or Natural Killer Cell Complement Receptor Type 3 (CD11b/CD18) Generates a Primed State of the Receptor Capable of Mediating Cytotoxicity of iC3b-Opsonized Target Cells. *Journal of Clinical Investigation* **98**, 60–1 (1996).

67. Brown G. D., Taylor P. R., Reid D. M. *et al.* Dectin-1 is a major beta-glucan receptor on macrophages. *J Exp Med* **196**, 407–12 (2002).

68. Ariizumi K., Shen G. L., Shikano S. *et al.* Identification of a novel, dendritic cell-associated molecule, dectin-1, by subtractive cDNA cloning. *J Biol Chem* **275**, 20157–67 (2000).

69. Brown G. D. Dectin-1: a signalling non-TLR pattern-recognition receptor. *Nat Rev Immunol* **6**, 33–43 (2006).

70. Mata-Martínez P., Bergón-Gutiérrez M., Del Fresno C. Dectin-1 Signaling Update: New Perspectives for Trained Immunity. *Front Immunol* **13** (2022).

71. Rogers N. C., Slack E. C., Edwards A. D. *et al.* Syk-dependent cytokine induction by Dectin-1 reveals a novel pattern recognition pathway for C type lectins. *Immunity* **22**, 507–17 (2005).

72. Gross O., Gewies A., Finger K. *et al.* Card9 controls a non-TLR signalling pathway for innate anti-fungal immunity. *Nature* **442**, 651–6 (2006).

73. Del Fresno C., Soulat D., Roth S. *et al.* Interferon-β production via Dectin-1-Syk-IRF5 signaling in dendritic cells is crucial for immunity to C. albicans. *Immunity* **38**, 1176–86 (2013).

74. Li X. J., Goodwin C. B., Nabinger S. C. *et al.* Protein-tyrosine phosphatase Shp2 positively regulates macrophage oxidative burst. *J Biol Chem* **290**, 3894–909 (2015).

75. Goodridge H. S., Simmons R. M., Underhill D. M. Dectin-1 stimulation by Candida albicans yeast or zymosan triggers NFAT activation in macrophages and dendritic cells. *J Immunol* **178**, 3107–15 (2007).

76. Kelly E. K., Wang L., Ivashkiv L. B. Calcium-activated pathways and oxidative burst mediate zymosan-induced signaling and IL-10 production in human macrophages. *J Immunol* **184**, 5545–52 (2010).

77. Rosas M., Liddiard K., Kimberg M. *et al.* The induction of inflammation by dectin-1 in vivo is dependent on myeloid cell programming and the progression of phagocytosis. *J Immunol* **181**, 3549–57 (2008).

78. Herre J., Marshall A. S. J., Caron E. *et al.* Dectin-1 uses novel mechanisms for yeast phagocytosis in macrophages. *Blood* **104**, 4038–45 (2004).

79. Gringhuis S. I., den Dunnen J., Litjens M. *et al.* Dectin-1 directs T helper cell differentiation by controlling noncanonical NF-kappaB activation through Raf-1 and Syk. *Nat Immunol* **10**, 203–13 (2009).

80. Quintin J., Saeed S., Martens J. H. A. *et al.* Candida albicans infection affords protection against reinfection via functional reprogramming of monocytes. *Cell Host Microbe* **12**, 223–32 (2012).

81. Ifrim D. C., Joosten L. A. B., Kullberg B.-J. *et al.* Candida albicans primes TLR cytokine responses through a Dectin-1/Raf-1-mediated pathway. *J Immunol* **190**, 4129–35 (2013).

82. Miao G., Zhuo D., Han X. *et al.* From degenerative disease to malignant tumors: Insight to the function of ApoE. *Biomed Pharmacother* **158**, 114127 (2023).

83. Marais A. D. Apolipoprotein E in lipoprotein metabolism, health and cardiovascular disease. *Pathology* **51**, 165–76 (2019).

84. Linton M. F., Gish R., Hubl S. T. *et al.* Phenotypes of apolipoprotein B and apolipoprotein E after liver transplantation. *J Clin Invest* **88**, 270–81 (1991).

85. Raffaï R. L., Hasty A. H., Wang Y. *et al.* Hepatocyte-derived ApoE is more effective than non-hepatocyte-derived ApoE in remnant lipoprotein clearance. *J Biol Chem* **278**, 11670–5 (2003).

86. Lafitte B. A., Repa J. J., Joseph S. B. *et al.* LXRs control lipid-inducible expression of the apolipoprotein E gene in macrophages and adipocytes. *PNAS* **98**, 507–12 (2001).

87. Getz G. S., Reardon C. A. Apoprotein E and Reverse Cholesterol Transport. *Int J Mol Sci* **19** (2018).

88. Plump A. S., Smith J. D., Hayek T. *et al.* Severe Hypercholesterolemia and Atherosclerosis in Apolipoprotein E-Deficient Mice Created by Homologous Recombination in ES Cells. *Cell* **71**, 343–53 (1992).

89. Bradley M. N., Hong C., Chen M. *et al.* Ligand activation of LXR beta reverses atherosclerosis and cellular cholesterol overload in mice lacking LXR alpha and apoE. *J Clin Invest* **117**, 2337–46 (2007).

90. Mahley R. W. Apolipoprotein E: from cardiovascular disease to neurodegenerative disorders. *J Mol Med (Berl)* **94**, 739–46 (2016).

91. Xu Q., Bernardo A., Walker D. *et al.* Profile and regulation of apolipoprotein E (ApoE) expression in the CNS in mice with targeting of green fluorescent protein gene to the ApoE locus. *J Neurosci* **26**, 4985–94 (2006).

92. Bont N. de, Netea M. G., Demacker P. N. *et al.* Apolipoprotein E knock-out mice are highly susceptible to endotoxemia and Klebsiella pneumoniae infection. *Journal of Lipid Research* **40**, 680–5 (1999).

93. Bont N. de, Netea M. G., Demacker P. N. *et al.* Apolipoprotein E-deficient mice have an impaired immune response to Klebsiella pneumoniae. *Eur J Clin Invest* **30**, 818–22 (2000).

94. Roselaar S. E., Daugherty A. Apolipoprotein E-deficient mice have impaired innate immune responses to Listeria monocytogenes in vivo. *Journal of Lipid Research* **39**, 1740–3 (1998).

95. Martens G. W., Arikan M. C., Lee J. *et al.* Hypercholesterolemia impairs immunity to tuberculosis. *Infect Immun* **76**, 3464–72 (2008).

96. Kemp S. B., Carpenter E. S., Steele N. G. *et al.* Apolipoprotein E Promotes Immune Suppression in Pancreatic Cancer through NF-κB-Mediated Production of CXCL1. *Cancer Res* **81**, 4305–18 (2021).

97. Pencheva N., Tran H., Buss C. *et al.* Convergent multi-miRNA targeting of ApoE drives LRP1/LRP8-dependent melanoma metastasis and angiogenesis. *Cell* **151**, 1068–82 (2012).

98. Tavazoie M. F., Pollack I., Tanqueco R. *et al.* LXR/ApoE Activation Restricts Innate Immune Suppression in Cancer. *Cell* **172**, 825-840.e18 (2018).

99. Jaitin D. A., Adlung L., Thaiss C. A. *et al.* Lipid-Associated Macrophages Control Metabolic Homeostasis in a Trem2-Dependent Manner. *Cell* **178**, 686-698.e14 (2019).

100. Vazquez-Armendariz A. I., Heiner M., El Agha E. *et al.* Multilineage murine stem cells generate complex organoids to model distal lung development and disease. *EMBO J* **39** (2020).

101. Du Z., Lin J.-R., Rashid R. *et al.* Qualifying antibodies for image-based immune profiling and multiplexed tissue imaging. *Nat Protoc* **14**, 2900–30 (2019).

102. Bankhead P., Loughrey M. B., Fernández J. A. *et al.* QuPath: Open source software for digital pathology image analysis. *Sci Rep* **7**, 16878 (2017).

103. Bolte S., Cordelières F. P. A guided tour into subcellular colocalization analysis in light microscopy. *J Microsc* **224**, 213–32 (2006).

104. Gierahn T. M., Wadsworth II M. H., Hughes T. K. *et al.* Seq-Well: portable, low-cost rna sequencing of single cells at high throughput. *Nature Methods* **14**, 395–8 (2017).

105. Macosko E. Z., Basu A., Satija R. *et al.* Highly Parallel Genome-wide Expression Profiling of Individual Cells Using Nanoliter Droplets. *Cell* **161**, 1202–14 (2015).

106. Hao Y., Hao S., Andersen-Nissen E. *et al.* Integrated analysis of multimodal single-cell data. *Cell* **184**, 3573-3587.e29 (2021).

107. Misharin A. V., Morales-Nebreda L., Mutlu G. M. *et al.* Flow cytometric analysis of macrophages and dendritic cell subsets in the mouse lung. *Am J Respir Cell Mol Biol* **49**, 503–10 (2013).

108. Becht E., McInnes L., Healy J. *et al.* Dimensionality reduction for visualizing single-cell data using UMAP. *Nat Biotechnol* **37**, 38–44 (2018).

109. Gautier E. L., Shay T., Miller J. *et al.* Gene-expression profiles and transcriptional regulatory pathways that underlie the identity and diversity of mouse tissue macrophages. *Nat Immunol* **13**, 1118–28 (2012).

110. Cohen M., Giladi A., Gorki A.-D. *et al.* Lung Single-Cell Signaling Interaction Map Reveals Basophil Role in Macrophage Imprinting. *Cell* **175**, 1031-1044 (2018).

111. Goltsev Y., Samusik N., Kennedy-Darling J. *et al.* Deep Profiling of Mouse Splenic Architecture with CODEX Multiplexed Imaging. *Cell* **174**, 968-981 (2018).

112. Serbina N. V., Pamer E. G. Monocyte emigration from bone marrow during bacterial infection requires signals mediated by chemokine receptor CCR2. *Nat Immunol* **7**, 311–7 (2006).

113. Werb Z., Chin J. R. Onset of Apoprotein E Secretion during Differentiation of Mouse Bone Marrow-derived Mononuclear Phagocytes. *The Journal of Cell Biology* **97**, 1113–8 (1983).

114. Dove D. E., Linton M. F., Fazio S. ApoE-mediated cholesterol efflux from macrophages: separation of autocrine and paracrine effects. *Am J Physiol Cell Physiol* **288**, 586-92 (2005).

115. Blanchard J. W., Akay L. A., Davila-Velderrain J. *et al.* APOE4 impairs myelination via cholesterol dysregulation in oligodendrocytes. *Nature* **611**, 769–79 (2022).

116. Probst H. C., Stoitzner P., Amon L. *et al.* Guidelines for DC preparation and flow cytometry analysis of mouse nonlymphoid tissues. *Eur J Immunol* **53**, 1-78 (2023).

117. McCubbrey A. L., Barthel L., Mohning M. P. *et al.* Deletion of c-FLIP from CD11bhi Macrophages Prevents Development of Bleomycin-induced Lung Fibrosis. *Am J Respir Cell Mol Biol* **58**, 66–78 (2018).

118. Mitroulis I., Ruppova K., Wang B. *et al.* Modulation of Myelopoiesis Progenitors Is an Integral Component of Trained Immunity. *Cell* **172**, 147-161 (2018).

119. Hohl T. M., Rivera A., Lipuma L. *et al.* Inflammatory monocytes facilitate adaptive CD4 T cell responses during respiratory fungal infection. *Cell Host Microbe* **6**, 470–81 (2009).

120. Serbina N. V., Cherny M., Shi C. *et al.* Distinct responses of human monocyte subsets to Aspergillus fumigatus conidia. *J Immunol* **183**, 2678–87 (2009).

121. Espinosa V., Jhingran A., Dutta O. *et al.* Inflammatory monocytes orchestrate innate antifungal immunity in the lung. *PLoS Pathog* **10** (2014).

122. Brown A. S., Yang C., Fung K. Y. *et al.* Cooperation between Monocyte-Derived Cells and Lymphoid Cells in the Acute Response to a Bacterial Lung Pathogen. *PLoS Pathog* **12** (2016).

123. Novakovic B., Habibi E., Wang S.-Y. *et al.* β-Glucan Reverses the Epigenetic State of LPS-Induced Immunological Tolerance. *Cell* **167**, 1354-1368 (2016).

124. Saeed S., Quintin J., Kerstens H. H. D. *et al.* Epigenetic programming of monocyte-to-macrophage differentiation and trained innate immunity. *Science* **345** (2014).

125. Kang S., Tanaka T., Narazaki M. *et al.* Targeting Interleukin-6 Signaling in Clinic. *Immunity* **50**, 1007–23 (2019).

126. Geller A. E., Shrestha R., Woeste M. R. *et al.* The induction of peripheral trained immunity in the pancreas incites anti-tumor activity to control pancreatic cancer progression. *Nat Commun* **13** (2022).

127. Chakraborty S., Singh A., Wang L. *et al.* Trained immunity of alveolar macrophages enhances injury resolution via KLF4-MERTK-mediated efferocytosis. *J Exp Med* **220** (2023).

128. Iraz M., Bilgic S., Samdanci E. *et al.* Preventive and early therapeutic effects of β-Glucan on the bleomycin-induced lung fibrosis in rats. *European Review for Medical and Pharmacological Sciences* **19**, 1505–16 (2015).

129. Clausen B. E., Burkhardt C., Reith W. *et al.* Conditional gene targeting in macrophages and granulocytes using LysMcre mice. *Transgenic Research* **8**, 265–77 (1999).

130. Linton M. F., Atkinson J. B., Fazio S. Prevention of Atherosclerosis in Apolipoprotein E-Deficient Mice by Bone Marrow Transplantation. *Science* **267**, 1034–7 (1995).

131. Fazio S., Babaev V. R., Murray A. B. *et al.* Increased atherosclerosis in mice reconstituted with apolipoprotein E null macrophages. *PNAS* **94**, 4647–52 (1997).

132. Ho Y. Y., Al-Haideri M., Mazzone T. *et al.* Endogenously expressed apolipoprotein E has different effects on cell lipid metabolism as compared to exogenous apolipoprotein E carried on triglyceride-rich particles. *Biochemistry* **39**, 4746–54 (2000).

133. Zheng P., Luo Q., Wang W. *et al.* Tumor-associated macrophages-derived exosomes promote the migration of gastric cancer cells by transfer of functional Apolipoprotein E. *Cell Death Dis* **9** (2018).

134. Haney M. S., Pálovics R., Munson C. N. *et al.* APOE4/4 is linked to damaging lipid droplets in Alzheimer's disease microglia. *Nature* **628**, 154–61 (2024).

135. Heeren J., Grewal T., Jäckle S. *et al.* Recycling of apolipoprotein E and lipoprotein lipase through endosomal compartments in vivo. *J Biol Chem* **276**, 42333–8 (2001).

136. Heeren J., Grewal T., Laatsch A. *et al.* Impaired recycling of apolipoprotein E4 is associated with intracellular cholesterol accumulation. *J Biol Chem* **279**, 55483–92 (2004).

137. Hapala I., Marza E., Ferreira T. Is fat so bad? Modulation of endoplasmic reticulum stress by lipid droplet formation. *Biol Cell* **103**, 271–85 (2011).

138. Stanley E. R., Chitu V. CSF-1 receptor signaling in myeloid cells. *Cold Spring Harb Perspect Biol* **6** (2014).

139. Lee H., Cho S., Kim M.-J. *et al.* ApoE4-dependent lysosomal cholesterol accumulation impairs mitochondrial homeostasis and oxidative phosphorylation in human astrocytes. *Cell Rep* **42** (2023).

140. Emoto T., Lu J., Sivasubramaniyam T. *et al.* Colony stimulating factor-1 producing endothelial cells and mesenchymal stromal cells maintain monocytes within a perivascular bone marrow niche. *Immunity* **55**, 862-878 (2022).

141. Inoue K.-i., Takano H., Koike E. *et al.* Candida soluble cell wall beta-glucan facilitates ovalbumin-induced allergic airway inflammation in mice: Possible role of antigen-presenting cells. *Respir Res* **10** (2009).

142. Han X., Luo R., Ye N. *et al.* Research progress on natural β-glucan in intestinal diseases. *Int J Biol Macromol* **219**, 1244–60 (2022).

Acknowledgements

First, I would like to thank my supervisor Prof. Dr. Andreas Schlitzer for the opportunity to work on this fascinating project. Andreas, you were not only a helpful supervisor during my PhD, but also a great mentor for my scientific career. I am glad I joined your lab and my time in Bonn could not have been better. I appreciated the endless insightful feedback to improve the project and to push it over the finish line, as well as all the crazy ideas you come up with. Despite the demanding and stressful episodes, especially during the publishing process of the paper, we always had a great and funny time together. Travelling to Banff, Berlin or Mallorca are for sure some of the best memories from PhD besides all the outings we did in Bonn. Thank you for all the support and thank you for bringing me together with people that quickly became some of my best friends.

I would also like to express my gratitude to the members of my doctoral committee. Thank you very much for evaluating my work. Thanks to PD Dr. Marc Beyer for being my second examiner, Prof. Dr. Irmgard Förster for being the chair of my committee and Prof. Dr. Natalio Garbi for being the external member.

Furthermore, I would like to thank the Bonn International Graduate School for Immunosciences and Infection and especially Dr. Alexandra Krämer for supporting my PhD journey with cool workshops and networking events. I am also very grateful for Prof. Dr. Eva Kiermaier, which has been a fantastic mentor over the last four years.

I also want to acknowledge all the members of the LIMES WiS that are actively trying to improve the situation of female scientists in academia. Thanks to Prof. Dr. Elvira Mass and Prof. Dr. Eva Kiermaier for leading our initiative, it was nice being part of this team.

Helping hands and collaborations are essential for successful experiments and fruitful science. I would like to thank all the members of the Schlitzer lab who contributed to the work shown here and highlight Dr. David Bejarano, Dr. Jessica Haub and Dr. Jiangyan Yu for the time and effort they invested. I also want to acknowledge the collaborations with scientists from the Schultze, Beyer, Kopf and Vazquez-Armendariz laboratories. Moreover, I thank the staff at the LIMES GRC animal facility for taking excellent care of the most essential component of this study. Last but not least, thanks to Dr. Jake Thomas, Dr. David Bejarano, Paul Maier and Tobias Beckröge for reading my thesis and proving feedback.

Science is always more fun when excellent people surround you and the people of the Schlitzer lab have been truly the best part of my PhD. David, one of my best friends, the Taurus to my Capricorn, always in my heart #TeamM. Sophie, my favourite Master student, Highschool musical enthusiast and Molchi. Marie, power mom, number one Frenchie and BM fanatic. Paul,

lives in symbiosis with Marie #MaPa, hates the things I love and vice versa, still owes me an apple cake. Jake, the most sarcastic person I know, still standing after six Hefeweizen, PS: toast is not bread. Jiangyan, Glühwein enthusiast and R queen. Miaomiao, pretty girl looking for a silver fox #okokok. Martina, Steffi and Maria, the backbone of our lab. Former members Sumit, Lili and Jessi and former students Hannah and Dave. You all made my time in the lab enjoyable, we shared so many funny and amazing memories inside and outside the lab, even travelled to other continents of the world. Working with you has been a beautiful dream!

Finally, I want to thank my favourite people in the world: Sarah, Ninfa and Tobi. Thank you for your endless support.